It is dangerous to put limits on wireless.

– Guglielmo Marconi, 1932.

University of Alberta

STATISTICAL ANALYSIS OF MULTIUSER AND NARROWBAND INTERFERENCE AND SUPERIOR SYSTEM DESIGNS FOR IMPULSE RADIO ULTRA-WIDE BANDWIDTH WIRELESS

by

Hua Shao

A thesis submitted to the Faculty of Graduate Studies and Research
in partial fulfillment of the requirements for the degree of

Doctor of Philosophy
in
Communications

Department of Electrical and Computer Engineering

Fall 2011
Edmonton, Alberta

Examining Committee

Norman C. Beaulieu, Electrical and Computer Engineering

Moe Z. Win, Aeronautics and Astronautics, Massachusetts Institute of Technology

Behrouz Nowrouzian, Electrical and Computer Engineering

Chintha Tellambura, Electrical and Computer Engineering

Hai Jiang, Electrical and Computer Engineering

Ioanis Nikolaidis, Computer Science

Dedicated to

my beloved parents.

Abstract

Ultra-wide bandwidth (UWB) wireless is a fast emerging technology which exploits major advances and offers unprecedented opportunity to impact wireless communications. In UWB systems, several users should coexist viably in the same coverage area. The multiuser interference (MUI) caused by asynchronous transmissions in UWB systems is difficult to eliminate, and becomes a limit to the system performance. It has been shown that the MUI in impulse radio (IR) UWB systems is impulse-like, and poorly approximated by a Gaussian distribution. Therefore, the performance of the conventional matched filter (CMF), which is the optimal receiver structure for signals embedded in additive white Gaussian noise (AWGN), degrades severely when the interference is significant, and alternative models for the MUI are thus motivated. Novel models which can provide more accurate descriptions of the UWB MUI than the Gaussian model are proposed, and new receiver structures are designed based on these novel models. It is shown that these new receiver designs can outperform the CMF receiver which is used extensively in UWB systems, and the performance gain is significant in interference-limited scenarios.

Channel coding is an effective method to overcome the effects of noise and interference encountered in the transmission of signals through channels, where some redundancy is introduced in a controlled manner in the information sequence. Early studies of IR UWB systems used the repetition code for signaling and considered the Gaussian distribution for modeling the total disturbance in the channel. However, the repetition code is a trivial channel coding scheme and not all the potentials are explored by this channel code. On the other hand, the Gaussian distribution is not necessarily valid for modeling the disturbance in UWB wireless with the presence of the MUI. A framework for evaluating the coding performance of IR UWB systems is constructed where a more accurate model for the disturbance is adopted. This framework represents valuable tools for evaluating the coding performance

of IR UWB wireless, especially when long codes are adopted or low data levels are of interest, cases where system performance evaluation based on simulation is time-consuming or impossible. More generally, these tools can also be applied to other communication systems where the ambient noise shares similar characteristics with the disturbance in IR UWB systems.

The huge bandwidth brings unique advantages to UWB, but it also brings challenges to UWB system deployment. The UWB band overlaps with several frequency bands already allocated to established narrowband (NB) services. Successful deployment of UWB systems requires that UWB devices contend and coexist with services operating within the dedicated bands. Therefore, the coexistence problem between UWB and narrowband systems and the effects of their mutual interference are topics that warrant investigation. Two effective UWB sequence designs are proposed to suppress the mutual interference between NB and UWB systems, which clears a crucial hurdle for UWB device deployment. These designs can adapt to the spectral occupancy state of current channels; this information can be provided by cognitive radio (CR) or by a priori knowledge of the spectrum usage in the network.

Acknowledgments

It would not have been possible to write this thesis without the help and support of the kind people around me. First and foremost, I owe my deepest gratitute to my supervisor, Dr. Norman C. Beaulieu, for his continuous encouragement and support during my Ph.D. program. This thesis would not be possible without his experience, knowledge and brilliant comments and suggestions, for which I am extremely grateful.

I would also like to thank the members of my defense committee, for taking their time to review my thesis and giving valuable suggestions for my research.

The financial support from Alberta Innovates Technology Futures during my program is also highly appreciated.

The *i*CORE Wireless Communications Laboratory (*i*WCL) has an open and friendly atmosphere. During my graduate studies, I have received tremendous help from my labmates. The years I spent at *i*WCL is an unforgettable period of learning and working experience. I would also like to offer my regards to Sharon Walker, Linda Abraham, and Suzanne Cunningham for their help during my Ph.D. program.

Last, but by no means least, my sincere thanks to my beloved parents for their great patience and unequivocal support and love throughout, for which mere words cannot express my gratitute.

Table of Contents

List of Tables

List of Figures

List of Symbols

$E_k(x)$	Incomplete exponent function	92
$E_{\mathrm{n,tot}}$	Total transmitted power of the NB interferers	116
$\mathcal{F}_g(f)$	Fourier transform of function $g(t)$	106
f_{H}	Higher emission frequency	12
f_{L}	Lower emission frequency	12
f_n	Carrier frequency of NB systems	105
$f_X(x)$	PDF of RV X	35
$\Gamma(x)$	Gamma function	64
$g_{\mathrm{pomatlr}}(\cdot)$	Transform function in the p-omatlr	70
g_{pomr}	Transform function in the p-omr	65
$g_{\mathrm{zonal}}(\cdot)$	Transform function in the zonal receiver	37
$\mathbf{h}$	Random vector of UWB multipath gains	104
$H_0(f)$	Transfer function of UWB MF for AWGN and flat-fading channels	107
$H_{\mathrm{u}}(f;\mathbf{h},\mathbf{t})$	Fourier transform of UWB channel impulse response	106
κ	Excess *kurtosis*	37
L_{f}	Number of fingers in the Rake receiver	41
L_{t}	Total number of UWB multipath components	40
$\mathcal{N}(\mu,\sigma^2)$	Normal distribution with mean μ and variance σ^2	90
$n(t)$	AWGN process	31
$N_0/2$	Power spectral density of AWGN	31
N_{h}	Number of hops per UWB frame	30
N_{n}	Number of NB interferers in the channel	105
n_{s}	Number of information bits conveyed by a codeword	85
N_{s}	Number of frames per UWB information bit	19
N_{u}	Number of UWB users in the system	31
Ω_0	Average power of the first arriving UWB multipath	86
p	Shape parameter of the generalized Gaussian distribution	64
$P(f)$	Fourier transform of UWB pulse $p(t)$	107
$p(t)$	UWB pulse	18
P_{BER}	Bit error rate	96
P_{CEP}	Codeword error probability	94
$P_{\mathrm{gb,BER}}$	Gallager bound for bit error rate	97

$P_{\mathrm{gb,CEP}}$	Gallager bound for codeword error probability	95
$P_{\mathrm{lb,BER}}$	Lower bound for bit error rate	97
$P_{\mathrm{lb,CEP}}$	Lower bound for codeword error probability	95
$P_{\mathrm{PEP}}(\cdot)$	Pairwise error probability	91
$P_{\mathrm{ub,BER}}$	Union bound for bit error rate	96
$P_{\mathrm{ub,CEP}}$	Union bound for codeword error probability	94
$\mathcal{Q}(\cdot)$	$\mathcal{Q}$-function	107
$R(t)$	Autocorrelation function of UWB pulse	18
$r(t)$	Received signal	31
$\mathrm{rank}(A)$	Rank of matrix A	111
R_c	Code rate	85
$\mathrm{sgn}(x)$	Sign function	72
$\mathrm{SINR}_{l,\mathrm{cmf}}$	SINR at the *l*th Finger of the CMF based Rake receiver	43
$\mathrm{SINR}_{l,\mathrm{pomr}}$	SINR at the *l*th Finger of the p-omr based Rake receiver	74
$\mathrm{SINR}_{l,\mathrm{zonal}}$	SINR at the *l*th Finger of the Zonal based Rake receiver	44
$\mathrm{SINR}_{\mathrm{MRC,cmf}}$	SINR after MRC for the CMF based Rake receiver	45
$\mathrm{SINR}_{\mathrm{MRC,zonal}}$	SINR after MRC for the zonal based Rake receiver	45
$\mathrm{SINR}_{\mathrm{MRC,pomr}}$	SINR after MRC for the p-omr based Rake receiver	75
$\mathbf{t}$	Random vector of UWB multipath delays	104
T_{b}	UWB bit duration	31
T_{c}	UWB chip duration	14
T_{cw}	UWB codeword duration	85
$T(D,N)$	Transfer function of a convolutional code	94
T_{f}	UWB frame duration	19
t_{h}	Upper bound of the zonal receiver	35
T_k	Delay of the *k*th user	31
t_{l}	Lower bound of the zonal receiver	35
τ_m	Normalization factor of the second derivative of a Gaussian monocycle	34
T_{opt}	The optimal threshold in the p-omatlr	70
τ_p	UWB pulse duration	14
T_{so}	Transfer function of superorthogonal codes	97
$\mathrm{var}(X)$	Variance of random variable X	33

List of Abbreviations

Chapter 1

Introduction

The wireless communications industry is enjoying its fast growing period in history. New emerging wireless methods and services have been enthusiatically adopted all around the world to provide opportunities for a better quality of life. However, virtually every wireless device depends on access to the radio frequency spectrum. With the tremendous growth of wireless technologies, spectrum scarcity becomes a primary problem encountered when trying to launch new wireless services.

Ultra-wide bandwidth (UWB) has emerged as an efficient solution to the spectrum scarcity problem. UWB radio technology distincts itself from other commercial technologies by its underlay philosophy, where it utilizes an enormous bandwidth by transmitting signals at the noise floor and underlaying legacy systems already operating within the band. Low-power, noise-like pulses, which appear as noise to legacy systems, are used for signal transmission. UWB radio technology comes with unique advantages that have been long appreciated by the radar and communication communities. However, the interests and applications of this technology were primarily limited to radar, sensing, military communications and niche applications before 2002 [5]. With the ever expanding demands for wireless services with higher data rates and improved quality, the potentials of UWB radio in other wireless applications, such as wireless communication, networking and localization systems, need to be explored. Prior to 2002, significant efforts had been made to convince radio regulatory authorities to release the UWB technology and allow license-free use of UWB products.

In 2002, the Federal Communications Committee (FCC) released the First Report and

Order (R&O) [1], where a huge bandwidth of 7.5 GHz in 3.1 GHz - 10.6 GHz at the noise floor is allocated to UWB radio. Three types of UWB devices, communication and measurement systems, imaging systems and vehicular radar systems, are defined in this UWB ruling. Spectral masks have also been given to UWB devices to strictly limit the power spectrum of the transmitted signals. With this ruling, UWB devices and services can benefit from the huge bandwidth without causing noticable interference to legacy systems already operating within the UWB frequency band, such as the global positioning system (GPS) , and the IEEE 802.11 wireless local area networks (WLANs) .

The enormous bandwidth enables UWB applications in an unprecedented number of bandwidth-demanding low-power low-cost systems. UWB holds great potentials for high-data-rate (HDR) communications over short distances. For example, it is an attractive candidate to replace Bluetooth as the wireless substitute for universal serier bus (USB) and cables. It can also be used to enable high-speed access to the Internet. Moreover, UWB can be used for low-data-rate (LDR) communications over medium to long distance as well. For example, UWB is a strong candidate for sensor networks which can be used for intelligent lightning and energy control within buildings, and asset and personnel tracking [6]. Major applications of UWB radio also include imaging systems (ground-penetrating radar (GPR), through-wall imaging, in-wall imaging and security perimeters [6]), and vehicular radar systems for collision avoidance, just to name a few.

1.1 Thesis Motivations and Contributions

Since the release of the first UWB ruling by the FCC in 2002, enormous efforts have been undertaken in both academia and industry to explore potentials of this technology in a variety of wireless applications. A great deal of research has been devoted to cope with challenges that limit the performance of UWB systems. Literatures can be found on the bit error rate (BER) performance evaluation of UWB systems [7]–[10], statistical analysis of UWB multiuser interference (MUI) and its effect on system performance [11]–[14], efficient receiver designs for multiple access (MA) UWB systems [15]–[17], coexistence problem between UWB and legacy narrowband (NB) systems [18]–[20]. However, there are still a number of challenges that should be addressed to make the UWB technology a more attractive candidate for practical applications. Motivations as well as contributions of this thesis are outlined as follows. It should be mentioned that UWB systems can be divided into two broad classes: those based on the multiband approach and those based on the impulse radio (IR) approach. This thesis focuses on the IR approach. The details of these two approaches for UWB radio are given in Chapter 2.

- **Statistical Analysis of Multiuser Interference and Receiver Designs for Impulse Radio UWB**

  In an UWB system, several users need to coexist viably in the same coverage area. To provide MA capability to IR UWB systems, several techniques, such as the direct sequence (DS) technique which has been used in code division multiple access (CDMA) systems, the time-hopping (TH) sequence technique [21] and a combination of both [22], have been proposed for UWB wireless. However, even with these techniques, the MUI caused by coexisting users due to asynchronous transmissions of different users as well as the multipath nature of UWB channels is difficult to eliminate. Note that ambient disturbance is one of the main factors affecting the performance of a wireless system which should be properly accounted for, and most UWB systems operate in the interference-limited scenario where the MUI is the main disturbance in the channel. Therefore, accurate models of the MUI give us a better understanding of practical UWB systems, and they are the foundations for system designs and performance analysis.

  Most of the earlier studies on the MUI in IR UWB systems were inspired by the legacy of literatures on spread spectrum (SS) communications, where the central limit theorem (CLT) was employed to approximate the sum of the MUI and the ubiquitous Gaussian distribution was adopted for modeling the MUI. However, IR UWB systems have substantially different MUI characteristics than traditional communication systems. Experimental evidences as well as theoretical considerations have suggested that the MUI in IR UWB systems deviates from those conformable to the Gaussian model [11]–[14], [23]. Therefore, the ubiquitous Gaussian distribution, which has been widely used for modeling the ambient noise in a variety of communication systems, is generally not accurate for modeling the MUI in IR UWB systems. Accordingly, the conventional matched filter (CMF), which is optimal for additive white Gaussian noise (AWGN) and has been widely used in IR UWB systems, is not necessarily optimal in this scenario. The tasks of accurate modeling of the MUI as well as better receiver designs in IR UWB present themselves as important and intriguing problems.

Modeling the MUI in UWB systems is a crucial while very challenging issue. A dilemma exists: the Gaussian interference model is generally inaccurate for modeling the MUI in IR UWB systems and the corresponding optimal receiver, the single-user CMF, is not optimal. Rigorous mathematical modeling of the UWB MUI is difficult and analytically intractable; the available partial and incomplete results are cumbersome and difficult to use to improve the design of UWB systems, especially in practical UWB multipath fading channels. In Chapter 3 of this thesis, we propose an intuitive and creative solution to this complicated issue. Simulations are carried out to give an intuitive insight into the problem, where some unique characteristics of the correlator output at the UWB receiver are observed. A novel UWB receiver structure, dubbed the "zonal" UWB receiver, was thus proposed based on the observation and the optimal, minimum probability of error, decision rule. Also in Chapter 3, a thorough mathemcatical analysis of this receiver design is provided, and implemention details of the zonal receiver in practical systems are covered. In general, this zonal UWB receiver structure can always outperform the CMF UWB receiver, and the performance gain is significant in interference-limited scenarios. Note that the robustness of UWB signals to multipath fading is due to their fine delay resolution, and high diversity order can be achieved with the adoption of a Rake receiver [24]. Therefore, in Chapter 3, a Rake receiver adopting zonal receiver structure in the fingers is also proposed for UWB signal detection in multipath fading channels. This new Rake structure is shown to outperform the traditional CMF based Rake receiver.

One of the most significant characteristics of the MUI in IR UWB systems is that the MUI exhibits impulsive nature and can be characterized by a probability density function (PDF) with "heavy tail", i.e., the tail of the PDF decays at a rate lower than that of the Gaussian distribution [3], [11], [12]. An intuitive implication of this heavy tail behavior is that the probability of observing large-magnitude impulsive noise samples in practice is higher than that would be predicted by the Gaussian noise model [25]. Therefore, another intuitive and effective method to study the MUI in IR UWB systems is to use a heavy-tailed distribution to model the MUI. In Chapter 4 of this thesis, a generalized Gaussian (GG) distribution is used to model the UWB MUI. The GG distribution is an effective and convenient model to describe the impulsive noise and interference encountered in real-world systems. It starts with the Gaussian distribution, but allows the exponential tail decay rate in the Gaussian distribution to become a free parameter [25], [26]. This free parameter, named the shape parameter of the GG distribution, can be used to control the heaviness of the tail. In particular, the ubiquitous Gaussian model, which has been used extensively for modeling the disturbance in a variety of communication systems, is a special case of the GG model. In Chapter 4, it is shown that the GG distribution can accurately model the MUI in almost all scenarios. Corresponding mathematical analysis is conducted thoroughly for this model, and a detailed method is provided to adapt this model to different UWB transmission scenarios. With properly chosen parameters, not only can the GG distribution model the MUI and predict the performance of UWB systems accurately, but it can also be easily applied to improve the UWB system design. Also in Chapter 4, a novel UWB receiver structure is proposed based on the GG model of the MUI. It is proved that, this novel receiver structure, dubbed the "p-order metric UWB receiver" (p-omr), can always outperform the CMF UWB receiver and other existing UWB receiver structures, and the performance gains are significant when the interference is strong in the channel. To utilize this structure for the UWB signal detection in multipath fading channels, a Rake receiver adopting the pomr structure in the fingers is also proposed in Chapter 4. This new Rake receiver structure is shown to outperform the conventional Rake receiver under all transmission scenarios, without complicating the system extensively.

- **Coding Performance Analysis in Multiple Access Impulse Radio UWB Systems** Early studies of IR UWB systems used the repetition code for signaling, where each information bit is transmitted using several repetitive pulses [21]. This repetition code structure is adopted to achieve a processing gain which may be used to combat interference and noise in the channel [5, Ch. 1]. However, it is known that the repetition code is a trival channel coding scheme; not all the system potentials are used by IR UWB systems adopting the repetition code structure [27]. Therefore, it is imperative to consider more sophisticated channel codes for UWB systems and provide reliable performance evaluation of such coded UWB systems.

Other channel codes besides the repetition code have been suggested for UWB systems, and corresponding performance evaluations have been provided in [12], [28], [29]. However, performance evaluations provided in these works either considered conditions that might not reflect practical transmission scenarios or have high computational complexity. Moreover, they only considered the performance of a particular channel code. In Chapter 5 of this thesis, we develop a framework to evaluate the coding performance of IR UWB systems in the presence of MUI. The analytical methods provided in Chapter 5 represent useful tools for predicting the performance of UWB systems when the dominant disturbance in the channel is caused by the coexisting UWB devices. This scenario is commom in practical systems since the interference caused by other sources can be greatly reduced by choosing the system parameters properly [30]–[33]. The analytical results provided in Chapter 5 can be easily calculated using commonplace computer resource; they are effective especially when long codes are adopted or low error rate levels are of interest, cases where system performance evaluation based on simulation is time-consuming or even impossible. More generally, these tools can also be applied to other communication systems where the ambient noise shares similar statistical characteristics as the MUI in IR UWB systems.

- **Sequence Code Designs for Narrowband Interference Mitigation in IR UWB Systems**

  As mentioned above, the huge bandwidth allocated to UWB brings unique advantages to this technology. However, it also brings challenges to the system deployment. The UWB band overlaps with several frequency bands already allocated to established NB services, such as the GPS and the 802.11 WLANs. Successful deployment of UWB systems requires that the devices contend and coexist with NB services operating within the dedicated bands. Therefore, the coexistence problem between UWB and legacy NB systems are topics that warrant investigation [18]–[20], [32]–[36]. It is well known that, as other SS systems [27], UWB radio has inherent resistance to the NB interference. However, despite the highly spread nature of UWB signals, there are scenarios where the interference rejection capability is not powerful enough and the performance is too deteriorated to provide required Quality-of-Service (QoS). Under such circumstances, suitable techniques should be provided to mitigate NB interference in UWB systems.

Narrowband interference suppression techniques for IR UWB systems can be borrowed from those used in CDMA SS systems [37]–[39]. For example, notch filter, nonlinear prediction filter and minimum mean-square-error (MMSE) Rake receiver, have all been suggested in UWB systems for NB interference mitigation [40]–[42]. However, these techniques are performed in UWB receivers to reduce the effect of NB interference on UWB systems, while the interference caused by UWB devices to NB services must also be mitigated. To suppress the mutual interference between UWB and NB systems, an effective approach is to shape the spectrum of UWB signals by designing the signal structure to create notch frequencies at the NB service dedicated bands. Therefore, the frequency bands occupied by legacy services can be avoided by UWB transmission.

The UWB spectrum can be shaped through pulse-shaping [30], [31]. However, greater spectrum shaping capability over greater dynamic signal range and greater frequency control can be attained through sequence code control [32], [33] [1]. In Chapter 6 of this thesis, we propose sequence designs for IR UWB systems to suppress the NB interference. It is shown that not only can these sequence designs mitigate the mutual interference between UWB and NB devices coexsiting in the same coverage area, but they can also preserve the desired properties of the sequence code such as the pseudorandomness. Note that, the sequence design problems considered in previous works (c.f. [32], [33]) are special cases of those examined by Chapter 6. Numerical results are provided to show that the sequence designs proposed in Chapter 6 can greatly suppress the mutual interference between NB and UWB systems, which clears a crucial hurdle for UWB device deployment. Moreover, these sequence designs can adapt to the spectral occupancy state of current channels; this information can be provided by cognitive radio (CR) or by prior knowledge of the spectrum usage in the network.

[1] The sequence code here refers to either direct sequence or time-hopping sequence, which is used in IR UWB systems to provide multiple access and spectrum randomization [2], [5], [43].

1.2 Thesis Outline

This thesis is organized as follows. In Chapter 2, the basic concepts of UWB radio are covered. Then we review previous works related to this thesis. The topics of these works include statistical analysis of the MUI in IR UWB systems, efficient receiver designs for MA IR UWB systems, performance evaluation of coded UWB systems, coexistence problem between UWB and legacy NB services, and system designs for suppressing mutual interference between UWB and NB devices. In Chapter 3, a detailed study of the MUI in IR UWB systems is provided; a novel receiver, dubbed the "zonal" receiver is proposed to enhance the BER performance of the traditional CMF receiver. In Chapter 4, we consider the generalized Gaussian distribution for modeling the MUI in IR UWB systems. Corresponding mathematical analysis is conducted thoroughly for this model, and a detailed method is provided to adapt the generalized Gaussian model to different UWB transmission scenarios. A receiver structure named the p-order metric UWB receiver is proposed based on the generalized Gaussian model, and the implementation details of this receiver in practical systems are also given in this chapter. In Chapter 5, we developed a general framework to evaluate the codeword and bit error rate performance of coded UWB systems in the presence of MUI. Chapter 6 provides sequence code designs for IR UWB systems to mitigate the mutual interference between UWB and legacy NB services already operating within the UWB band. Chapter 7 concludes the thesis and gives ideas for future research.

Chapter 2

Background and Literature Review

In this chapter, the basic concepts of UWB radio are described. A detailed review of previous works related to this thesis is also given.

2.1 UWB Basics

UWB communication radio is a fast emerging technology with uniquely attractive features which has an unprecedented impact on communication systems. Since its beginnings, UWB technology has traveled an interesting road from the lab, to the military, back to the lab, and finally to commercial implementation. The original idea of UWB technology can be traced back to more than a century ago when Guglielmo Marconi used enormous bandwidth to convey information using a spark-gap transmitter. Contributions to UWB industry which commenced in the late 1960s were made by a number of pioneering scientists, and Ross' U.S. patent is a landmark in the progress of UWB development [44]. Within the past 40 years, the merits of UWB communication systems have spurred a growing interest in both academia and industry. However, prior to 2002, UWB was relegated by regulatory bodies, such as the FCC in the United States, for a very long time; its applications were restricted to radar, sensing, military communications [2], [5].

Things changed substantially in 2002 when the FCC allocated 7.5 GHz bandwidth in 3.1 GHz - 10.6 GHz to UWB, allowing operation of UWB radio at the noise floor [1]. The applications of UWB radio defined in this ruling include data communication systems as well as radar and safety applications. Spectral masks have also been given in the R&O to strictly limit the power level transmitted by UWB devices. The basic principle of the UWB

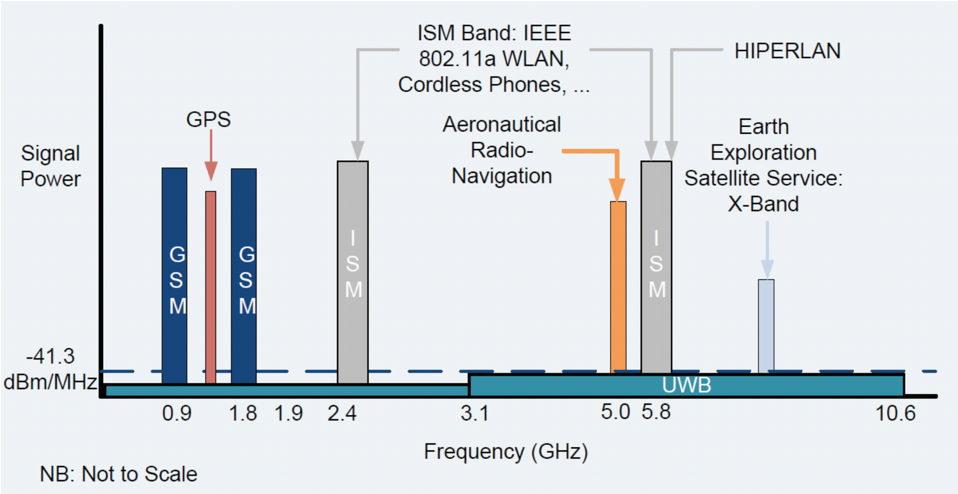

Fig. 2.1. Current exisiting services underlaid by UWB radio.

technology is that the transmitted signal power is being traded against the huge bandwidth to obtain satisfactory system performance where the low transmitted power allows UWB devices utilize the huge bandwidth using the underlaying philosophy [6]. Because of the low regulated power level (below -41.3 dBm), UWB radio underlays already available services such as the aeronautical radio-naviation system, the GPS and the IEEE 802.11 WLAN without causing noticeable interference (see Fig. 2.1). The huge bandwidth utilized by UWB makes it an attractive candidate for an unprecendented number of bandwidth-demanding low-power low-complexity wireless applications in communications, radar imaging, networking and localization systems [2], [45].

2.1.1 Definition of UWB Radio and Regulatory Issues

The definition of UWB radio was first given by the Defense Advanced Research Project Agency (DARPA) in 1989 [46]. In [46], a concept, the fractional bandwidth, is defined as

$$\text{Fractional Bandwidth} = \frac{\mathrm{BW}}{f_{\mathrm{c}}} = \frac{2\left(f_{\mathrm{H}} - f_{\mathrm{L}}\right)}{f_{\mathrm{H}} + f_{\mathrm{L}}} \tag{2.1}$$

where $\mathrm{BW} = f_{\mathrm{H}} - f_{\mathrm{L}}$ denotes the -20 dB bandwidth and $f_{\mathrm{c}} = \left(f_{\mathrm{H}} + f_{\mathrm{L}}\right)/2$ is the center frequency with f_{H} and f_{L} being the upper and lower -20 dB emission point. The term UWB coined in this assessment is for devices that occupy at least 1.5 GHz, or with a fractional bandwidth exceeding 25%.

In the first UWB ruling by the FCC, the R&O, a similar definition as that given by the

TABLE 2.1
THE FCC REGULATIONS OF $f_{\rm L}$, $f_{\rm H}$ AND $f_{\rm C}$ FOR UWB SYSTEMS[1]

Systems	Requirements of $f_{\rm L}$, $f_{\rm H}$ and $f_{\rm c}$
Vehicle radar systems	$f_{\rm c} > 24.075$ GHz, $f_{\rm L}$, $f_{\rm H} \in [22, 29]$ GHz
Indoor/Handheld UWB systems	$f_{\rm L}$, $f_{\rm H} \in [3.1, 10.6]$ GHz
Low-frequency imaging systems	$f_{\rm L}$, $f_{\rm H} <$ 960 MHz
Mid-frequency imaging systems	$f_{\rm L}$, $f_{\rm H} \in [1.99, 10.6]$ GHz
High-frequency imaging systems	$f_{\rm L}$, $f_{\rm H} \in [3.1, 10.6]$ GHz

TABLE 2.2
THE FCC SPECTRAL MASKS FOR UWB SYSTEMS [1], [2]

<table>
<tr><td></td><td colspan="6">Equivalent Isotropically Radiated Power (EIRP) (dBm)</td></tr>
<tr><td>Frequency (GHz)</td><td>Indoor</td><td>Handheld</td><td>Low-freq. imag.</td><td>Mid-freq. imag.</td><td>High-freq. imag.</td><td>Vehicular radar</td></tr>
<tr><td><0.96</td><td>Part 15 limit [a]</td><td>Part 15 limit</td><td>Part 15 limit</td><td>Part 15 limit</td><td>Part 15 limit</td><td>Part 15 limit</td></tr>
<tr><td>0.96-1.61</td><td>-75.3</td><td>-75.3</td><td>-65.3</td><td>-53.3</td><td>-65.3</td><td>-75.3</td></tr>
<tr><td>1.61-1.9</td><td rowspan="2">-53.3</td><td>-63.3</td><td rowspan="2">-53.3</td><td rowspan="2">-51.3</td><td rowspan="2">-53.3</td><td rowspan="5">-61.3</td></tr>
<tr><td>1.90-1.99</td><td rowspan="2">-61.3</td></tr>
<tr><td>1.99-3.10</td><td>-51.3</td><td rowspan="6">-51.3</td><td rowspan="2">-41.3</td><td>-51.3</td></tr>
<tr><td>3.10-10.60</td><td>-41.3</td><td>-41.3</td><td>-41.3</td></tr>
<tr><td>10.6-22.00</td><td rowspan="4">-51.3</td><td rowspan="4">-61.3</td><td rowspan="4">-51.3</td><td rowspan="4">-51.3</td></tr>
<tr><td>22.00-29.00</td><td>-41.3</td></tr>
<tr><td>20.00-31.00</td><td>-51.3</td></tr>
<tr><td>$>$ 31.00</td><td>-61.3</td></tr>
</table>

[a] The FCC Part 15 rules and regulates the operation of unlicensed transmissions to ensure unlicensed devices do not cause harful interference to other users within the frequency band. According to the FCC Part 15 rules, unintentional and intentional radiators are allowed to operate under some restrictions within certain frequency bands (Code of Federal Regulations, Title 47, Part 15 (47 CFR 15)).

DARPA is used for defining the this technology [1]. In this ruling, $f_{\rm H}$ and $f_{\rm L}$ are defined as the higher and lower -10 dB emission point, repectively, and UWB characterizes transmis-

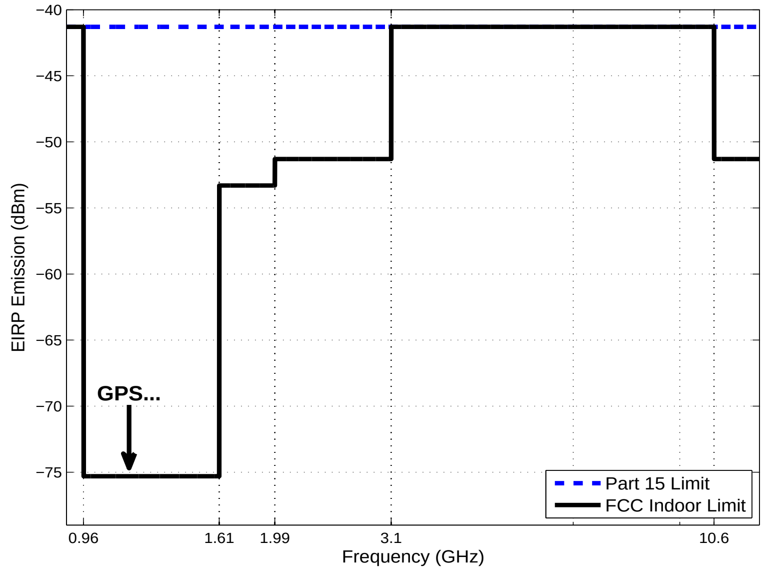

Fig. 2.2. The FCC spectral mask for indoor UWB communication systems [1].

sion systems with a -10 dB fractional bandwidth of at least 0.20, or a -10 dB bandwidth of at least 500 MHz. More specifically, for devices with center frequence $f_c > 2.5$ GHz, the -10 dB bandwidth should be at least 500 MHz, while for systems with $f_c < 2.5$ GHz, the fractional bandwidth should be at least 0.20. The UWB applications defined in [1] include imaging systems, vehicular radar systems, indoor UWB systems and handheld UWB systems. Moreover, the FCC determined that each proposed application had unique attributes and required different level of regulation. Detailed requirements of f_{L}, f_{H} and f_{C} for different sevices are listed in Table 2.1, and the spectral masks are given in Table 2.2 [1]. In particular, the spectral mask for indoor communication systems is illustrated in Fig. 2.2.

2.1.2 Major UWB Physical Layer Approaches

According to the spectral allocation and the definition of UWB radio given by the FCC, any physical layer approach meeting the FCC emission requirements can be used as a solution for UWB radio. The most popular approaches are the IR approach and the multiband orthogonal frequency division multiplexing (MB-OFDM) approach, where examples of the power spectral density (PSD) of these two approaches is shown in Fig. 2.3.

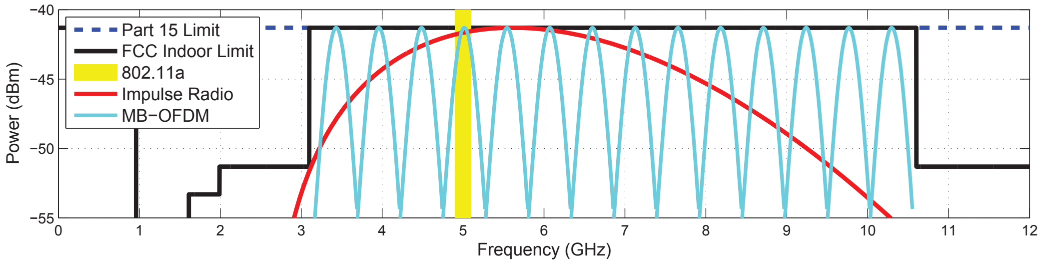

Fig. 2.3. Power spectral density of two major physical layer approaches for UWB radio.

Impulse Radio

The IR approach is a popular solution for UWB. In this approach, extremely narrow baseband pulses (on the order of nanosecond) are used for transmission (see Fig. 2.4). Note that in such systems, each of the transmission pulses occupies a huge bandwidth, and spans frequencies which are usually used as carrier frequency in traditional systems. Therefore, no carrier frequency is required since the pulses will propagate well through the radio channel. Observe that IR UWB systems share similarities with traditional SS systems, where one of the major differences is that IR UWB systems rely on discontinuous transmissions of extremely narrow pulses while traditional SS systems transmit signals continuously and the duty cycle of the pulse train is unity.

As any other physical layer solutions for UWB radio, the IR approach enjoys the benefit of the huge bandwidth. According to Shannon's well-known formula [47], one of the major advantages of UWB systems is the improved channel capacity. UWB systems can provide HDR transmission or equivalently support a large number of users with fixed data rate. As mentioned above, extremely narrow baseband pulses (on the order of nanosecond) are used for transmission in the IR approach. Therefore, IR UWB systems have potential to provide more time precision than the GPS. Moreover, the ability of IR UWB signals to penetrate through obstacles is also enhanced. Hence, this technology is an attractive candidate for short-range radar systems for security and rescue purposes. In addition, IR systems rely on baseband transmissions where sine-wave carrier is not required. Therefore, the radio frequency (RF) mixing stage, which translates signals to a desired frequency, is unnecessary. The reverse process of down-conversion is also not necessary at the receiver. Accordingly, a local oscillator is not needed at the receiver, and the complex delay and phase tracking

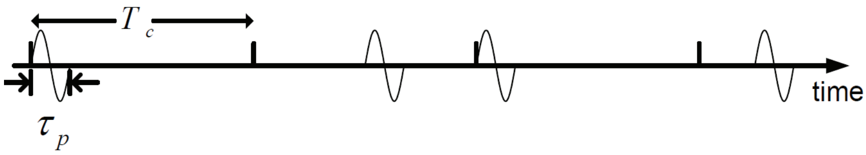

Fig. 2.4. Example of transmitted signals of IR UWB systems.

loops can be omitted. The absences of up-conversions and down-conversions in frequency make it possible to implement low-complexity, low-cost UWB devices. Furthermore, IR UWB radio is resistant to continuous jamming/interference signals. Note in Fig. 2.4 that, the pulse used in IR UWB systems does not accupy the whole chip duration ($\tau_p < T_\mathrm{c}$), and the duty cycle is extremely low. Therefore, the receiver only has to detect the signal during a small fraction of time and the effect of continuous jamming signals and interference can be highly reduced.

However, implementation challenges also arise due to the signal structure in IR UWB systems. The short duration of IR pulses imposes difficulty in time synchronization at the receiver. Moreover, since IR UWB signals spread the energy over a huge bandwidth, the propagation channel is highly frequency selective and the number of multipaths can be as high as a couple of hundred in practical environments. A relatively large number of Rake fingers are needed for collecting enough energy to achieve required performance. Meanwhile, channel estimation is difficult since the number of parameters to be estimated, i.e., amplitudes and delays of the multipath components, is large. Note also that channel estimation requires sampling at subpulse rate. Therefore, high-rate high-precision analog/digital conversion (ADC) is required for the IR approach. Furthermore, UWB devices underlay legacy systems, such as the GPS and the 802.11 WLANs, and the mutual interference between UWB and legacy services should be minimized so that they can coexist variably in the same coverage area. One efficient method for the mutual interference mitigation is to avoid the bands occupied by existing NB services in UWB transmission. However, the frequency bands occupied by NB services within the UWB spectrum might change over time and might be inconsistent in different regions throughout the world. Therefore, the band avoidance mechanism for IR UWB systems should be frequency agile. However, the implementation of such band avoidance mechanism might not be as easy as that for the multiband solution for UWB radio, as shown in the sequel [2].

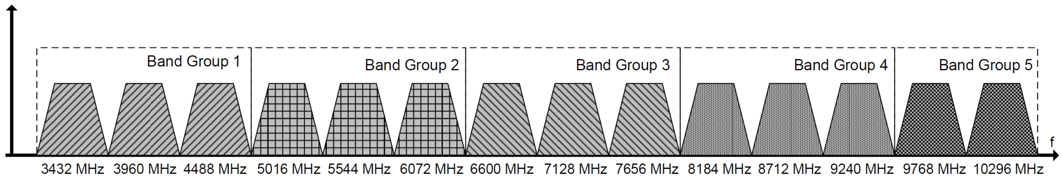

Fig. 2.5. MB-OFDM frequency band.

MB-OFDM

Another popular solution for UWB is the MB-OFDM approach. This approach is an OFDM solution for UWB proposed by the multiband OFDM alliance (MBOA), an alliance of industry and academic partners aiming to develop physical layer and medium access layer (MAC) technologies for OFDM based UWB systems. In the MB-OFDM approach, the whole available bandwidth for UWB is divided into sub-bands with smaller bandwidth, which is over 500 MHz in compliance with the FCC rules for UWB transmission. To be specific, in MB-OFDM systems, the whole bandwidth allocated to UWB is divided into 14 sub-bands with bandwidth 528 MHz, which are grouped into 5 band groups (see Fig. 2.5). Frequency hopping (FH) is introduced in the MB-OFDM approach to mitigate the interference between piconet [1] and obtain additional frequency diversity over different sub-bands. In MB-OFDM systems, a block of data form an OFDM symbol, and subsequent blocks of data might be transmitted by OFDM symbols over different sub-bands according to a pre-defined FH pattern [48].

One of the most significant benefits of the MB-OFDM approach is its spectral flexibility. The system designers are free to use a combination of sub-bands within the spectrum to optimize the system performance. Therefore, MB-OFDM technology is able to comply with local frequency regulations regardless of the spectral allocations and emissions restrictions in different regions of the world. Moreover, MB-OFDM systems can easily avoid legacy NB services within the UWB spectrum by turning off certain tones and channels in the systems (see Fig. 2.3).

On the other hand, the MB-OFDM approach also imposes difficulties in implementation. Since several carrier frequencies are used in MB-OFDM signals, the system faces

[1] A piconet represents a network with at least two devices, where one of them might act as a coordinator of the data transmission during the connection.

multiple carrier frequency offsets due to the mismatch of oscillators at the transmitter and receiver, which can cause severe performance degradation. Moreover, MA in such systems is provided by assigning user-specfic FH patterns to each device. The fast FH introduces challenges to the carrier frequency synchronization. Nonetheless, implementation difficulties for the MB-OFDM approach also arise in the time acquisition and channel estimation since they have to be performed for every subcarrier [2].

Note that the MB-OFDM approach has several advanatages over the IR approach, including the spectral flexibility to comply with frequency regulations, relaxed sampling rate, and enhanced ability to coexist with legacy narrowband systems. However, this approach requires more complex system structures and might not be an attractive candidate for UWB applications which require low-complexity, low-cost and power-efficient devices. Therefore, in this thesis, we will focus on the IR approach for UWB radio.

2.1.3 Motivating Applications of Impulse Radio UWB Systems

As mentioned above, the unique characteristics of IR UWB radio have brought a number of advantages. These advantages open up unprecedented opportunities for UWB in a variety of applications. We list here some of the applications where the performance of the devices can be highly enhanced by the unique features of IR UWB radio.

- *Wireless Personal Area Networks (WPANs):* It has been mentioned above that one of the most significant feature of UWB is its enhanced capacity. Therefore, UWB radio is an attractive candidate for HDR devices. For example, it is perfect for replacing cables and providing HDR connections between personal electronics in an in-home network, such as laptop, digital camera, camcorder, other storage devices, or even other home entertainment devices like TV, VCR or DVD player. It is a promising physical layer candidate for WPANs since the enormous bandwidth of UWB radio enables real-time video and audio distributions and fast file exchanges. Moreover, UWB can also provide high-speed Internet access for in-home or office environments.

- *Imaging Systems:* UWB enabled imaging systems operate across a broad range of frequncies, which allows imaging sensors to effectively penetrate a wide range of materials [1]. Therefore, the UWB technology can be implemented in GPR, wall, through-wall, surveillance, and medical imaging systems. It has also been pointed out in [2] that UWB imaging systems are different from conventional radar systems where targets are typically considered as point scatterers. Since the duration of signaling pulses used in UWB imaging systems is usually shorter than the obstacles, not only will the pulse amplitude and time shift be altered after the reflection, but there will also be changes in the pulse shape. Consequently, UWB imaging systems are more sensitive to scattering, thus more accurate compared to conventional radar systems.

- *Sensor Networks:* Sensor networks are typified by devices with low complexity. There are strict limitations on processing power and memory for such devices, and reliability of information exchange and sensors' battery life are major considerations in such networks. The low-complexity, low-cost, power-efficient features fit UWB technology right into this category of application. Moreover, the high achievable burst data rate for UWB radio means that sensors can transfer their payload data quickly and effectively [49].

- *Vehicular Radar Systems:* Due to the high sensitivity to scattering, UWB enabled vehicular radar systems can provide better resolution than conventional radar systems. Such vehicular radar systems have high ranging accuracy and are able to detect the location and movement of objects near a vehicle in order to provide collision avoidance. Improved airbag activation and adapt suspension systems which respond better to road conditions are also possible by using UWB enabled vehicle radar systems [1].

2.1.4 Signal Modulations

With baseband signals, frequency modulation and phase modulation are not feasible for IR UWB systems. Information symbols can be conveyed by either positions or amplitudes of signaling pulses. The most widely adopted modulation schemes in UWB systems include

- *Pulse Position Modulation (PPM)*

  In the PPM scheme, information bits are conveyed by positions of signaling pulses. Let $p(t)$ denote the pulse used for signal transmission. For M-ary PPM, M distinctly delayed pulses $p(t - m\delta),\ \ (m = 0, \cdots, M-1)$ are used to represent M symbols, where δ is termed the modulation index. The value of δ can be chosen according to the autocorrelation characteristics of the pulse, where the autocorrelator function of the pulse $p(t)$ is defined as [50]

$$R(t) = \int_{-\infty}^{+\infty} p(\tau)p(t+\tau)d\tau. \tag{2.2}$$

If orthogonal PPM is to be implemented, the optimum value for δ should satisfy the condtion

$$R(\delta_{\text{opt}}) = \int_{-\infty}^{+\infty} p(\tau)p(\delta_{\text{opt}}+\tau)d\tau = 0. \tag{2.3}$$

- *Pulse Amplitude Modulation (PAM)*
  In this modulation scheme, information bits are encoded on different levels of amplitude. In particular, for 2-ary PAM, antipodal pulses are used for transmission, and this scheme becomes the same as binary phase shift keying (BPSK).

PPM was almost exclusive in UWB communications since negating ultra-short pulses was difficult in the early days. However, as pulse negation of ultra-short pulses became easier, both PPM and PAM have been prevailing nowadays for IR UWB radio. Other modulation schemes, such as the on-off keying (OOK) and the pulse shape modulation, are also considered for IR UWB systems [5].

2.1.5 Multiple Access Schemes and Spectrum Randomization

In UWB applications, several transmitters coexist viably in the same coverage area. The received signal is the superposition of all signals in the same channel, with different attenuations and delays. To avoid catastrophic collisions between the desired user and interfering users, MA techniques are adopted. TH and DS are the two most popular MA schemes used in IR UWB systems.

- *Time-hopping scheme*
  In a TH-UWB system, each user is assigned a distinct pseudonoise (PN) TH sequence [21]. This PN sequence is used to randomize the time positions of the pulses so that the chance of collision between different users can be reduced. Specifically, the transmission time is divided into frames with duration T_{f}, where only one pulse is transmitted per frame. The frame duration is further divided into chips with duration T_{c}, and the position of the pulse within the frame is determined by the TH sequence assigned to this user. To be specific, assuming that the TH code assigned to the *k*th

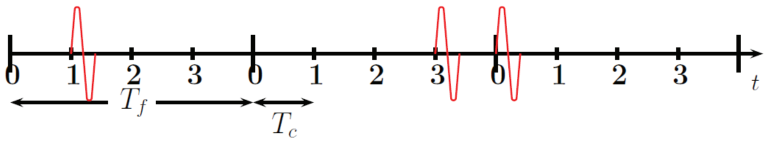

Fig. 2.6. An example of TH-UWB signals with the TH sequence (1,3,0).

user in the *j*th frame is $c_{\mathrm{TH},m}^{(k)}$, the *k*th user's pulse in the *m*th frame is then shifted by $c_{\mathrm{TH},m}^{(k)}T_{\mathrm{c}}$ (see Fig. 2.6).

In IR UWB systems, a repetition structure is adopted where each information-conveying symbol is represented by N_{s} pulses, one in each frame. This repetition structure is used to obtain a processing gain for combating interference and noise in the channel, a property essential for underlaying other radio systems. Let $d_n^{(k)} \in [0, M-1]$ denote the *n*th information symbol sent out by the *k*th user. A TH-UWB signal can be expressed as

$$s^{(k)}(t) = \sqrt{\frac{E_{\mathrm{b}}}{N_{\mathrm{s}}}} \sum_{n=-\infty}^{+\infty} a_n^{(k)} \sum_{m=0}^{N_{\mathrm{s}}-1} p\left(t - mT_{\mathrm{f}} - c_{\mathrm{TH},m}^{(k)}T_{\mathrm{c}} - b_n^{(k)}\delta - nT_{\mathrm{b}}\right) \tag{2.4}$$

where $s^{(k)}(t)$ is the signal the *k*th user, E_{b} is the energy per information bit, $c_{\mathrm{TH},m}^{(k)}$ is the TH sequence assigned to the *k*th user, and $p(t)$ is the transmitted UWB pulse. The chip and frame durations are denoted by T_{c} and T_{f} as mentioned above. Both PPM and PAM can be used with the TH scheme. For M-ary TH-PAM signals, we have $a_n^{(k)} = 2d_n^{(k)} + 1 - M$ and $b_n^{(k)} = 0$. For TH-PPM systems, we have $a_n^{(k)} = 1$ and $b_n^{(k)} = d_n^{(k)}$.

- *Direct sequence scheme*

  The MA scheme for UWB systems can be borrowed from DSSS systems, where a user-specific PN sequence is assigned to control the inversion of the UWB pulse train [51]. Let $d_n^{(k)} \in [0, M-1]$ denote the *n*th information symbol sent out by the *k*th user as above. In a DS-UWB system, the signal transmitted by the *k*th user is given by

$$s^{(k)}(t) = \sqrt{\frac{E_{\mathrm{b}}}{N_{\mathrm{s}}}} \sum_{n=-\infty}^{+\infty} a_n^{(k)} \sum_{m=0}^{N_{\mathrm{s}}-1} c_{\mathrm{DS},m}^{(k)} p\left(t - mT_{\mathrm{f}} - nT_{\mathrm{b}}\right) \tag{2.5}$$

where $c_{\mathrm{DS},m}^{(k)}$ is the user-specific DS code, and $a_n^{(k)} = 2d_n^{(k)} + 1 - M$ as defined above. Observe that DS-UWB signals have similar forms as conventional DS-CDMA signals, except that the duty-cycle of DS-UWB signals is much smaller than that of conventional DS-CDMA signals, and the carrier frequency is absent in UWB signals. The DS scheme can be used individually or combined with TH to provide MA to UWB systems.

Note that the repetitive use of the $N_{\rm s}$ pulses might lead to strong lines in the spectrum of transmitted signals [2], [5], [27]. These energy spikes can cause interference to NB services coexisting with UWB devices over short distances [27]. It has been shown in [5, Ch. 3] [2] that not only can the TH and DS schemes provide MA capability to IR UWB systems, but they can also smooth the transmitted PSD and make the UWB transmission more noise-like.

2.1.6 Propagation Channels for Impulse Radio UWB Signals

For communication systems, propagation channel is an important aspect for physical layer transmission, and it determines the ultimate performance limits [47], the performance of various transmission scheme and receiver algorithms. Therefore, understanding the channel is vital for UWB system designs and testings.

Since most of UWB applications are restricted to indoor communcations, indoor channel model should be considered. The well-known Saleh-Valenzuela (S-V) indoor channel model was proposed in 1987 based on measurements in a two-story office environment, using low power narrow pulses (of width 10 ns with center frequency 1.5 GHz) [52]. In the S-V model, multipaths arrive in clusters. Accordingly, double summations are used to describe the discrete time channel impulse response (CIR) as

$$\begin{aligned} h(t) &= \sum_{l=0}^{+\infty} \alpha_l \delta(t-\tau_l) \\ &= \sum_{m=0}^{\infty}\sum_{n=0}^{\infty} \alpha_{m,n} e^{j\theta_{m,n}} \delta(t - T_m - \tau_{m,n}) \end{aligned} \tag{2.6}$$

where $\alpha_{m,n}$ and $\theta_{m,n}$ are the amplitude attenuation and phase distortion of the *n*th ray within the *m*th cluster, respectively, and $\delta(\cdot)$ is the Dirac's delta function. The arrival time of the *m*th cluster is denoted by T_m, and that of the *n*th ray relative to the *m*th cluster is represented by $\tau_{m,n}$. The arrival times of clusters and rays are modeled by Poisson distributions, where the cluster and ray arrival rates are denoted by Λ and λ ($\lambda > \Lambda$),

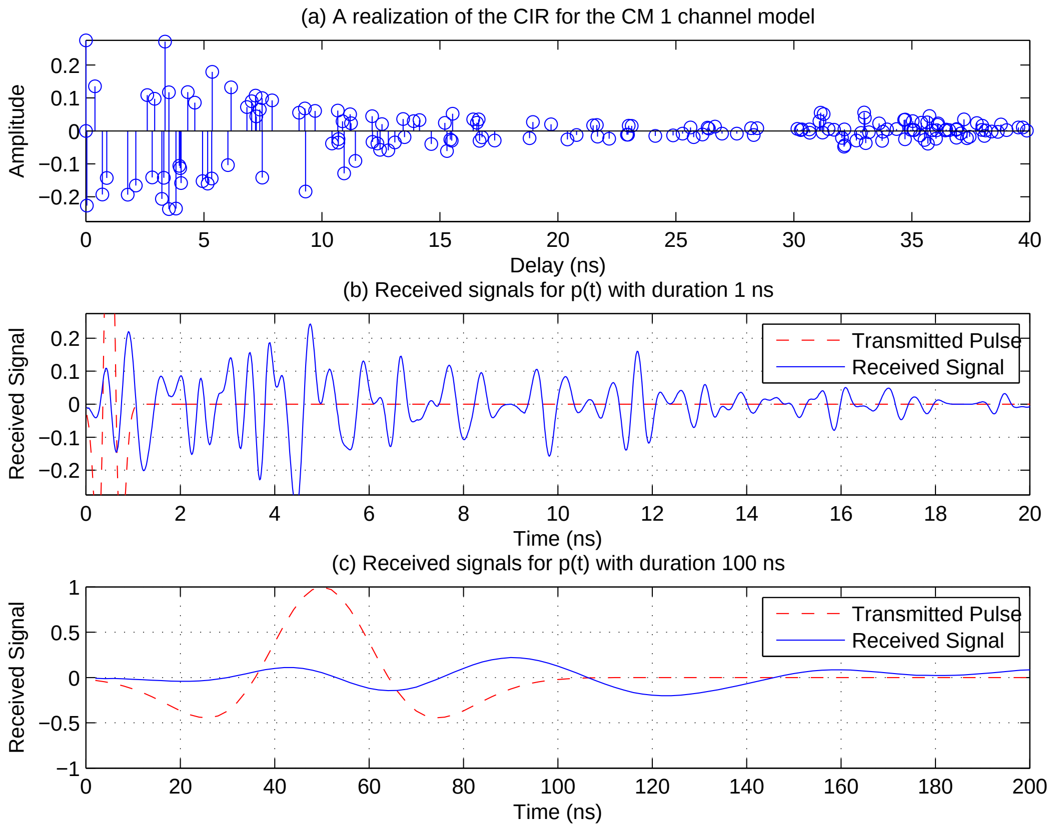

Fig. 2.7. A realization of the CIR of the CM 1 model in [4], which describes a LOS scenario for 0 m - 4 m transmission range; the received signals for pulses propagating through the channel are also plotted, the duration of the transmitted pulses is (a) τ_p = 1 ns and (b) τ_p = 100 ns.

respectively. Moreover, the multipath attenuations, $\alpha_{m,n}$, are independent Rayleigh RVs with power $\mathrm{E}\left(\alpha_{m,n}\right) = \Omega_0 e^{-T_m/\Gamma} e^{-\tau_{m,n}/\gamma}$, where Ω_0 is the expected value of power for the first arriving multipath. The phase distortion $\theta_{m,n}$ is assumed to be uniformly distributed in $[0, 2\pi)$.

To come up with a statistical model for IR UWB, channel realization should be identified. This can be done either by frequency sweeping in frequency domain or transmitting impulsive signal in time domain. In 2002, the IEEE 802.15.3a Task group recommended a channel model for UWB transmission, which is a modified version of the S-V model [4]. The cluster phenomenon has been experimentally confirmed, and the Rayleigh fading model is replaced by the lognormal fading model. Moreover, since no carrier frequency is used for signal transmission, the propagation channel is real and the phase distortion $\theta_{m,n}$ assumes values of $\{0, \pi\}$ with equal probability, accounting for random inversion of the signal due to reflection. To facilitate analysis using the channel model, instead of extending the multipath components to infinite time (c.f. eq. (2.6)), only the components within 10 dB from the strongest arrival are considered. In [4], parameters are provided for four channel models which cover line-of-sight (LOS) and non-line-of-sight (NLOS) scenarios for both 0 m - 4 m range and 4 m - 10 m range.

Fig. 2.7 shows a realization of the CIR in CM1 channels defined in [4]. Denote the tranmission pulse by $p(t)$ and its duration by τ_p. The received signal for $p(t)$ propagating through a channel with the CIR $h(t)$ can be expressed as $r(t) = p(t) * h(t) = \sum_{l=0}^{\infty} \alpha_l p(t - \tau_l)$, where α_l and τ_l represent the amplitude and delay of the lth multipath component (c.f. eq. (2.6)), respectively, and $*$ denotes convolution. Note in Fig. 2.7 (a) that the delays between adjacent multipaths are on the order of nanosecond. Therefore, whether the delayed copies of $p(t)$ are resolvable or not depends on the duration of the pulse (or equivalently the bandwidth of the signal) [27], [53] (c.f. Fig. 2.7 (b) and (c)). Note that IR signals span a huge bandwidth and durations of the pulses are on the order of nanoseconds. Hence, the propagation channel for IR UWB signals is highly frequency selective, i.e., IR UWB pulses propagate through a large number of resolvable paths, and a high multipath diversity can be expected at the receiver (c.f. Fig. 2.7 (b)).

2.2 Related Works

2.2.1 Signal Reception in Multiple Access UWB Systems

Ambient disturbance is one of the main factors affecting the performance of a wireless system, and it should be properly accounted for. In UWB applications, several users should coexist viably in the same coverage area. The MUI caused by asynchronous transmissions as well as the multipath fading nature of UWB channels is almost impossible to avoid and difficult to eliminate. Note that most UWB systems operate in an interference-limited scenario, where the MUI is the main disturbance in the channel [2].

Multiuser detection (MUD) is an effective method for rejecting MUI when several users

[2]As mentioned in Section 1.1, the interference-limited scenario is commom in UWB systems since the disturbance caused by other sources can be significantly reduced by choosing the system parameters properly (For the NB interference suppression, please refer to [30]–[33] and references therein. The NB suppression problem is also considered in Chapter 6 of this thesis. Furthermore, other interference, such as the intersymbol interference (ISI) and interchip interference (ICI) in IR-UWB systems, can also be significantly reduced by desiging the system parameters properly.

coexist in the same coverage area [54], and has been proposed for MA UWB systems [55]. Although MUD offers very attractive performance characteristics, it comes with the expense of complexity which increases exponentially with the number of users in the system. Most of the UWB applications are required to have low complexity and low cost, making the optimum MUD an unattractive candidate [43]. Moreover, the most common communication mode in UWB systems is peer-to-peer communication. Therefore, it is almost impossible for an UWB receiver to obtain accurate channel information and perform time synchronization for all the users in the same area in order to carry out such a detection. Thus, single-user CMF detection, which is optimal for signals embedded in AWGN, is widely adopted for signal recovery in UWB systems, even though it is suboptimal in the sense of minimizing the error probability [27].

2.2.2 Statistical Analysis of Multiuser Interference in Impulse Radio UWB Systems

Since the MUI is the main disturbance degrading the system performance in many UWB applications, accurate models of the MUI are critical for system designs and performance analysis. The most widely adopted approach for modeling the MUI in the early studies of IR UWB systems is inspired by the legacy of SS systems [56], [57]. This approach, dubbed the standard Gaussian approximation (GA), employs a CLT to approximate the sum of MUI as an AWGN additional to the background Gaussian noise process [58], [59]. Under this model, the tolerance of UWB systems to the impairment is easily calculated as a function of the signal-to-interference-plus-noise ratio (SINR). The GA is widely adopted because it is intuitive and easy to apply, and few system parameters are required to evaluate the system performance. However, it should be noted that there are substantial differences between conventional SS systems and IR UWB systems. First, traditional SS systems transmit signal continuously and the duty cycle of the pulse train is unity. Therefore, the receiver in such systems sees a superposition of signals from many independent users, and the MUI tends to a Gaussian process quickly with respect to the number of interferers (However, it should be noted that, for traditional SS systems with a small number of users, the PDF of the MUI cannot be well modeled by the Gaussian PDF [60].). In contrast, signals in IR UWB systems have very low duty cycles, i.e., off-time separation between adjacent pulses is allowed. Thus, a given pulse for the desired user sees interference from relatively few users compared to the total number of users simultaneously transmitting in the same coverage area. Moreover, in most applications of UWB radio (e.g. WPANs), the devices may be suited in a small area within a range of several meters. The number of coexisting interferers for an UWB device is usually much smaller than that in traditional SS systems where a larger coverage area with many contributing interfering users is considered (e.g. cellular systems).

All the properties mentioned above lead to the fact that the MUI in UWB system does not converge to the Gaussian distribution quickly, and the GA becomes inaccurate to model the UWB MUI [13], [61]. It has been shown that an interfering signal in IR UWB systems is impulsive due to the low duty cycle, the PN hopping sequence and random delays [3]. The characteristics of the MUI in UWB system were investigated in [62], where both oversimplified pulse models and practical pulse models were considered. Several key observations were made to explain the slow convergence of the PDF of the MUI to a Gaussian distribution. First, when considering the PDF of the MUI in IR UWB systems, there is a impulse with an amplitude $(1-2D)^{N_\mathrm{u}-1}$ at the origin, where D is the duty cycle and N_u is the number of coexisting users. Second, singularities caused by zeros in the derivative of the pulse autocorrelation function appear in the PDF (see [62] for details). It is noted that the PDF of a sum of independent random variables (RVs) is given by the convolution of the component PDFs. Thus, the PDF of the total interference sum over users and frames inherits singularities from the component PDF, resulting in the slow convergence of the MUI PDF to a Gaussian distribution.

As mentioned above, multipath fading propagation is abundant in UWB systems, and the IEEE standards group adopted a modified version of the S-V model [52] as the accepted standard for UWB channel modeling and investigation [4]. The channel models provided in this report depicted indoor environments with rich sets of reflection and refraction surfaces, forming hundreds of multipaths. Note that the multipath delay spread is usually much greater than the duration of the transmitting pulse. Thus, such channels are expected to improve the convergence of the MUI PDF to a Gaussian distribution, since they lower the duty cycle of UWB signals. In multipath fading channels, a Rake receiver is adopted for signal reception to exploit high diversity order [63]. However, it has been proven that an assumption that the MUI in each Rake finger is Gaussian distributed is still not valid.

2.2.3 Multiuser Interference Modeling and Receiver Structure Designs in Impulse Radio UWB Systems

As mentioned above, the derivation of an exact expression for the MUI in IR UWB systems is not straightforward. Even if the exact form of the PDF can be obtained, it does not have a compact and tractable expression. It is worth mentioning that the three key criteria in developing a suitable model of the MUI for performance evaluation and system design improvement are: the accuracy of the model, the extensibility of the MUI model to a model for MUI-plus-AWGN, and the utility of the model for synthesis of practical systems [3]. Therefore, it is necessary to model the MUI with distributions that are both accurate and tractable.

The Gaussian distribution, as mentioned above, is a tractable but not an accurate model. It has been shown that the MUI in IR UWB systems exhibits impulsive nature and deviates from the Gaussian distribution. It can be characterized by a PDF with "heavy tail", i.e., the tail of the PDF decays at a rate lower than that of the Gaussian distribution. An intuitive implication of this heavy tail behavior is that the probability of observing large-magnitude impulsive noise samples in practice is higher than that would be predicted by the Gaussian noise model [25]. Therefore, it is intuitive and reasonable to adopt heavy-tailed distributions with positive excess *kurtosis* for modeling the impulsive MUI [25, Ch.3] [26], [64]–[66]. In [67], a Laplace distribution was proposed to approximate the PDF of the MUI. In [16], a Gaussian-Laplacian noise-plus-MUI model was proposed to model the total disturbance which includes the AWGN and the MUI. In [68], the Middleton Class A (MCA) noise model was proposed to approximate the MUI in IR UWB systems. The Gaussian mixture (GM) distribution has also been proposed for modeling the UWB MUI, where the PDF of the distribution is given by a weighted mixture of Gaussian distributions [69].

These models can provide more accurate descriptions of the UWB MUI than the ubiquitous Gaussian model, which has been used widely in traditional communication systems for disturbance modeling. Assuming the MUI is independent of the desired signal component, the maximum-likelihood (ML) receiver structure design principle can be adopted to obtain improved receiver structures based on these models. UWB receiver structures based on the Laplacian model have been proposed in [15]. A Gaussian Laplacian mixture (GLM) receiver structure was proposed in [16] based on the Gaussian-Laplacian noise-plus-MUI model. The UWB receiver structure based on the GM model of the MUI has been derived in [69]. It was shown that these receiver structures can outperform the traditional CMF under certain operating conditions.

2.2.4 Coding Performance Evaluation of Multiple Access Impulse Radio UWB Systems

Early studies of IR UWB systems used the repetition code for signaling, where each information bit is transmitted using several repetitive pulses [21]. In [12], the authors proposed to use the superorthogonal code [70] in UWB systems. The performance analysis provided in [12] suggested that better performance can be expected by using more efficient channel coding scheme other than the repetition code. However, this work only considered the AWGN channel without multipath fading effects. In [28], the coding performance of UWB systems adopting repetition and superorthogonal codes was studied in multipath fading channels. However, the MUI was modeled by a Gaussian distribution in this work, which might not be accurate as mentioned above. In [29], the performance of coded IR UWB systems was studied where the channel coding scheme suggested by the IEEE 802.15.4a standard was used [71]. Nonetheless, this work only considered the single-user transmission case where the MUI is absent, and the performance evaluation relied on a semi-analytical method where error rates were calculated conditioned on channel fading coefficients and then averaged over channel realizations. It is worth mentioning that in order to provide reliable performance evaluation of coded UWB systems, several key criteria should be considered. The multipath fading nature of UWB propagation channels should be taken into consideration and the disturbance in the system should be properly accounted for. Furthermore, the analytical methods should be computational friendly and can be easily evaluated using commonplace computer resources.

2.2.5 Coexistence Between UWB and Narrowband Systems and Narrowband Interference Suppression Techniques in Impulse Radio UWB Systems

The huge bandwidth brings advantages to UWB radio, but also imposes challenges to UWB system deployment. The UWB band overlaps with several frequency bands already allocated to established NB services. Successful deployment of UWB systems requires that UWB devices contend and coexist with services operating within the dedicated bands.

Therefore, coexistence between UWB and NB devices is a critical problem for UWB system deployment [18]–[20], [36]. Recent results on this topic have been detailed in the survey paper [20] and references therein.

Despite the highly spread nature of the signals, in some scenarios, the aggregate effect of NB interference on UWB devices might be significant and the interference rejection capability of UWB might not guarantee satisfactory performance. Under such circumstances, suitable techniques should be provided to mitigate NB interference in UWB systems. NB suppression techniques for UWB systems can be borrowed from those used in CDMA systems (see [37]–[39] and references therein). In [40], the authors studied the use of a notch filter to suppress NB interference for TH-UWB systems. The authors of [41] studied the use of a nonlinear prediction filter in DS-UWB systems to reject NB interference. A NB suppression scheme based on MMSE Rake reception was examined for UWB systems in [42]. However, these techniques are performed in UWB receivers to reduce the effect of NB interference on the UWB signals, while the interference caused by UWB devices to NB services must also be mitigated. To suppress the mutual interference between UWB and NB systems, an effective approach is to shape the spectrum of UWB signals and create frequency nulls at NB service dedicated bands. Therefore, the interference caused by UWB signals to NB systems are suppressed since low signal powers are transmitted by the UWB devices in the NB service bands. On the other hand, since the UWB MF receiver is matched to the UWB signal waveform, the MF inherently acts as a notch filter that filters out undesired NB signals. Hence, the NB interference to UWB systems is also mitigated. References [30], [31] shaped the UWB spectrum through pulse-shaping. Greater spectrum shaping capability over greater dynamic signal range and greater frequency control can be attained by shaping the UWB spectrum through sequence code control. One promising and simple approach for shaping the UWB signal spectrum is by design of the DS or the TH sequence in UWB signals. In [32], the authors provided different methods for designing the TH sequence for TH-UWB signals to create notch frequencies where NB interferers operate. In [33], the authors revealed that a DS-UWB signal with a particular DS sequence can ostensibly mitigate NB interference in certain bands. In [72], the authors proposed two multiband UWB systems utilizing digital single- and multi-carrier spreading for baseband UWB to provide flexibility in handling MUI and NB interference. It has been shown that these NB mitigation techniques can reduce the mutual interference between NB and UWB systems.

Chapter 3

Zonal UWB Receiver[1]

In this chapter, we focus on the statistical analysis of the MUI in IR UWB systems and its effect on the UWB receiver designs. As mentioned earlier, in UWB applications, several users should coexist viably. The MUI is difficult to eliminate and is a main factor deteriorating the system performance. Therefore, to provide reliable performance analysis and improve system designs for IR UWB radio, the MUI should be carefully studied. The MUI in IR UWB systems and its effect on system performance have been studied and analyzed in [11], [13], [59], [61]. It was shown that the CLT is invalid for approximating the sum of interfering signals in a typical UWB system. Therefore, the Gaussian model, which follows the CLT, is not reliable for modeling the MUI in IR UWB systems [73], [27, Ch. 2]. The reasons for the slow convergence of the MUI to the Gaussian distribution were detailed in [3], [62], [74] and can be put as follows. The pulses used for transmission in IR UWB systems are extremely narrow, and the durations are usually on the order of one nanosecond. The IR UWB pulse train has a low duty cycle, viz., there is off-time separation between adjacent pulses. Hence, when the receiver detects a desired symbol, it can only see the interfering signals from a relatively small number of users compared to all the users transmitting simultaneously in the same coverage area. Moreover, most of UWB enabled devices are intented to operate within a small area where the number of coexisting interferers is usually small. Even for the case where the total number of interferers is relatively large, there are always some dominant interferers contributing most of the interference power in a typical UWB network [25], [74]–[77]. These factors cause the invalidity

[1] *A version of this chapter has been published in IEEE Transactions on Communications, 57: 1197-1206 (2009), and Proceedings of IEEE Global Communications Conference (GLOBECOM), 4118-4123 (2007).*

of the CLT and slow convergence of the distribution of the MUI to a Gaussian PDF.

Accurate and tractable descriptions of the MUI are required for performance analysis and system designs for IR UWB radio. In this chapter, we use an intuitive approach to study the MUI. A new receiver structure, named the zonal receiver, is then proposed for signal detection based on the results [78], [79]. In Section 3.1, we simply describe the system model to establish the operating conditions under which the zonal receiver is superior. In Section 3.2, the zonal receiver structure will be described. A new Rake receiver design based on the zonal receiver is proposed in Section 3.3 for UWB signal detection in multipath fading channels. Section 3.4 covers the implementation of the zonal receiver in practical systems. Example results for the error rate performance of the zonal UWB receiver and related discussions are provided in Section 3.5.

3.1 System Model

In this chapter, we consider a TH-BPSK signal. The analysis and results are similar for PPM signals. According to eq. (2.4), a TH-BPSK signal can be described as [58]

$$s^{(k)}(t) = \sqrt{\frac{E_{\mathrm{b}}}{N_{\mathrm{s}}}} \sum_{m=-\infty}^{+\infty} \left(2d^{(k)}_{\lfloor m/N_{\mathrm{s}} \rfloor} - 1\right) p(t - mT_{\mathrm{f}} - c^{(k)}_{\mathrm{TH},m} T_{\mathrm{c}}) \tag{3.1}$$

where $s^{(k)}(t)$ is the signal of the *k*th user. The parameters in eq. (3.1) are the same as defined in Section 2.1.5; E_{b} is the bit energy of UWB systems, N_{s} is the number of frames per information bit, the *j*th information bit of the *k*th user is represented by $d^{(k)}_j$ where $d^{(k)}_j \in \{0, 1\}$, and $p(t)$ with duration τ_p is the transmitted UWB pulse with unit energy satisfying the condition $\int_{-\infty}^{+\infty} p^2(t)\, dt = 1$. Each frame with duration T_{f} is divided into chips with duration T_{c}, the sequence $\left\{c^{(k)}_{\mathrm{TH},m}\right\}$ is the TH sequence for each frame of the *k*th user which takes integer values in the range $0 \leq c^{(k)}_{\mathrm{TH},m} < N_{\mathrm{h}}$, where N_{h} is the number of hops which should satisfy the condition $N_{\mathrm{h}} T_{\mathrm{c}} \leq T_{\mathrm{f}}$ [58]. Note that the product $c^{(k)}_{\mathrm{TH},m} T_{\mathrm{c}}$ adds an additional time shift to a user's TH pulses to reduce the chances of collisions with other users.

We digress here to explain the basis for improved UWB receiver designs. One might not expect that one can improve upon the conventional matched filter UWB receiver performance, especially in a static channel. In particular, any binary signaling scheme can be converted to an equivalent binary antipodal signaling scheme [80, Sec. V] and, therefore, the detection of one of two signals ultimately reduces to a threshold comparison. The reason that a better UWB receiver design is possible is due to the frame structure of the UWB signal, i.e., the repetition code. The repetition code structure represents an inherent diversity system within the conventional matched filter UWB receiver. It is important to note that adding together the outputs from the correlators of the different frames is a ML structure in AWGN, but is not an ML structure in the presence of MUI which is not Gaussian. As this chapter will show, simply adding the outputs of the correlators from all the frames is not an optimal processing of the frame correlator output signals.

To simplify the analysis, we first consider the free-space propagation scenario. Assuming that there are N_u transmitters coexisting in the same coverage area, the received signal can be expressed as

$$r(t) = \sum_{k=1}^{N_\mathrm{u}} A_k s^{(k)}\left(t - T_k\right) + n(t) \tag{3.2}$$

where $n(t)$ is a Gaussian random process with two-sided power spectral density $N_0/2$, and $\{A_k\}_{k=1}^{N_\mathrm{u}}$ and $\{T_k\}_{k=1}^{N_\mathrm{u}}$ are the attenuations and delays of the users, respectively. We assume that the first user is the desired user and $d_0^{(1)}$ is the transmitted symbol. Without loss of generality, the TH sequence for the desired user, $c_{\mathrm{TH},m}^{(1)}$, is set to be 0, for all m [11]. The delay for the desired user, T_1, is assumed known at the receiver side, while the delays of other users, $\{T_k\}_{k=2}^{N_\mathrm{u}}$ are RVs which can be assumed to be uniformly distributed on $[0, T_\mathrm{b})$, where $T_\mathrm{b} = N_\mathrm{s} T_\mathrm{f}$ is the bit duration [13], [14]. Assuming perfect time synchronization, the single-user CMF which adopts $p\left(t - T_1 - mT_\mathrm{f}\right)$ as the correlation waveform, is used to coherently detect the signal in the *m*th frame of the desired information bit. The final decision statistic for the CMF UWB receiver, R_cmf, can be expressed as

$$\begin{aligned} R_\mathrm{cmf} &= \sum_{m=0}^{N_\mathrm{s}-1} \int_{mT_\mathrm{f}+T_1}^{(m+1)T_\mathrm{f}+T_1} r(t) p(t - T_1 - mT_\mathrm{f}) dt \\ &= \sum_{m=0}^{N_\mathrm{s}-1} R_m = \sum_{m=0}^{N_\mathrm{s}-1} \left(S_m + I_m + N_m\right) \end{aligned} \tag{3.3}$$

where $S_m = A_1 \sqrt{E_\mathrm{b}/N_s}\left(2d_0^{(1)} - 1\right)$, I_m, and N_m are the desired signal component, the MUI, and the AWGN component in the *m*th frame, respectively. The RV $R_m = S_m + I_m + N_m$ is the statistic in the *m*th frame. Note that N_m is a Gaussian RV with variance $N_0/2$, and I_m can be expressed as

$$\begin{aligned} I_m &= \sum_{k=2}^{N_\mathrm{u}} \sqrt{\frac{E_\mathrm{b}}{N_\mathrm{s}}} A_k \sum_{j=-\infty}^{+\infty} \left(2d^{(k)}_{\lfloor j/N_\mathrm{s} \rfloor} - 1\right) \\ &\quad \times \int_{mT_\mathrm{f}+T_1}^{(m+1)T_\mathrm{f}+T_1} p(t - jT_\mathrm{f} - c^{(k)}_{\mathrm{TH},j} T_\mathrm{c} - T_k) p(t - T_1 - mT_\mathrm{f}) dt. \end{aligned} \tag{3.4}$$

We model the time shift difference between the desired user and the *k*th user as [58]

$$T_1 - T_k = m_k T_\mathrm{f} + \alpha_k \tag{3.5}$$

where m_k is the value of the time uncertainty rounded to the nearest integer, and a_k is the fractional part which is uniformly distributed in the interval $[-T_\mathrm{f}/2, T_\mathrm{f}/2)$. The assumption $N_\mathrm{h} T_\mathrm{c} < T_\mathrm{f}/2 - 2\tau_p$ [58] is adopted, which means that the pulse can only hop over an interval of one-half of a frame time. We use $R(x)$ defined in eq. (2.2) to denote the autocorrelation function of $p(t)$. Then, the MUI I_m in eq. (3.4) can be rewritten as

$$I_m = \sum_{k=2}^{N_\mathrm{u}} \sqrt{\frac{E_\mathrm{b}}{N_\mathrm{s}}} A_k \left(2d^{(k)}_{\lfloor (m+m_k)/N_\mathrm{s} \rfloor} - 1\right) R\left(a_k - c^{(k)}_{\mathrm{TH},m+m_k} T_\mathrm{c}\right). \tag{3.6}$$

In the sequel, $Y_m = I_m + N_m$ to used to denote the overall disturbance in the *m*th frame.

3.2 Zonal UWB Receiver Structure

As mentioned above, the MUI should be carefully studied to provide reliable performance evaluation and better system designs for UWB radio. Note in eq. (3.6) that the MUI is a function of $d^{(k)}_{\lfloor (m+m_k)/N_\mathrm{s} \rfloor}$, a_k, $c^{(k)}_{\mathrm{TH},m+m_k}$ and A_k. Therefore, the distribution of I_m can be determined by the distributions of these RVs according to the transformation theory for RVs [73, Ch. 5]. The exact distribution of the MUI in IR UWB systems has been studied in previous works [62], [74]. In [62], the PDF of the MUI in IR UWB systems was derived based on the assumption that the attenuations A_k are known, and rectangular pulses are used for transmission. In [74], the authors considered the interference in a network where the interfering nodes are spatially scattered according to a Poisson field. It has been proved in [74] that the aggregate interference belongs to the class of *Skewed stable* RVs [81]. Note that the rigorous expressions for the distribution of the MUI are important for studying IR

TABLE 3.1
SYSTEM PARAMETERS FOR CHAPTER 3

T_{f}	T_{c}	τ_p	T_{b}	N_{s}	N_{h}
20 ns	0.9 ns	0.575 ns	80 ns	4	8

UWB systems. However, there are some difficulties utilizing these expressions in practical scenarios. Note in eq. (3.6) that the distribution of the MUI depends on the form of the autocorrelation function $R(x)$. Therefore, the derivation of the rigirous distribution for MUI has to be done whenever a new pulse is adopted. Another problem of using the exact distribution is that the expression usually has a complicated form, especially in multipath fading scenarios. Therefore, it is usually unyielding and inconvenient to use such results for performance analysis and system design improvement in practice.

In this chapter, we use an intuitive approach to study the MUI. We first consider the ideal free-space propagation scenario. In order to emphasize the effect of the MUI, the AWGN term is ignored. Therefore, the statistic R_m in eq. (3.3) can be expressed as $S_m + I_m$. We define the signal-to-noise ratio (SNR) and signal-to-interference ratio (SIR) at the output of the correlator as

$$\mathrm{SNR} = \frac{E_{\mathrm{b}}}{N_0} \tag{3.7}$$

and

$$\mathrm{SIR} = \frac{A_1^2 E_{\mathrm{b}} N_{\mathrm{s}}}{\mathrm{var}(I)} = \frac{A_1^2 N_{\mathrm{s}}}{\sigma_I^2 \sum_{k=2}^{N_{\mathrm{u}}} A_k^2} \tag{3.8}$$

respectively, where $\mathrm{var}(X)$ denotes the variance of the RV X, and σ_I^2 is defined as [58]

$$\begin{aligned}\sigma_I^2 &= \frac{1}{T_f}\int_{-\infty}^{+\infty}\left[\int_{-\infty}^{+\infty} p(x-t)p(x)dx\right]^2 dt \\ &= \frac{1}{T_{\mathrm{f}}}\int_{-\infty}^{+\infty} R^2(t)dt. \end{aligned} \tag{3.9}$$

Simulations are carried out to generate the samples for I_m, where the parameters are given in Table 3.1. The second derivative of a Gaussian monocycle with unit energy given by

$$p(t) = \sqrt{\frac{8}{3\tau_m}}\left[1 - 4\pi\left(\frac{t}{\tau_m}\right)^2\right] e^{-2\pi(\frac{t}{\tau_m})^2} \tag{3.10}$$

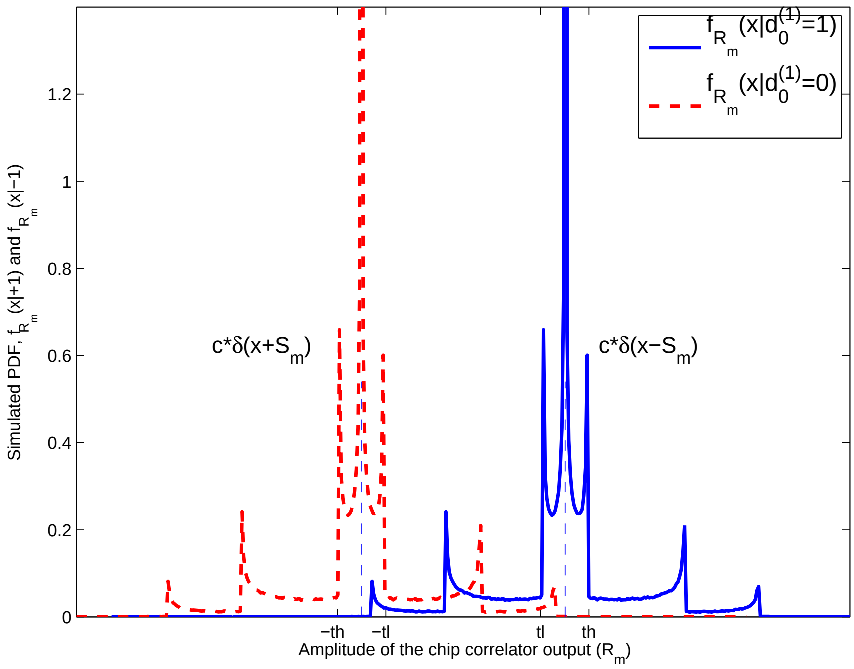

Fig. 3.1. The simulated conditional PDFs $f_{R_m}\left(x|d_0^{(1)}=1\right)$ and $f_{R_m}\left(x|d_0^{(1)}=0\right)$ of the amplitude of the chip correlator output $R_m = S_m + I_m$, where I_m is the MUI in the *m*th frame, c is a constant. The number of users in the system is $N_{\mathrm{u}} = 4$, and the SIR = 0 dB.

is considered for signal transmission, where τ_m is the normalization factor and related to the pulse duration τ_p. Equal power interferers are considered where the attenuations, A_k, are the same for all the users. We assume that there are $N_{\mathrm{u}} = 4$ users in the system and the value of the SIR defined by eq. (3.8) is 0 dB. Fig. 3.1 shows examples of the form of the conditional PDFs of the chip correlator output R_m when the information bit $d_0^{(1)} = 1$ and $d_0^{(1)} = 0$ are sent, $f_{R_m}\left(x|d_0^{(1)}=1\right)$ and $f_{R_m}\left(x|d_0^{(1)}=0\right)$, respectively. Considering the conditional pdf $f_{R_m}\left(x|d_0^{(1)}=1\right)$ first. Following observations can be made. There is an impulse at the point $R_m = S_m$. It was mentioned in [62] that the magnitude of this impulse is $(1-2D)^{N_{\mathrm{u}}-1}$, where D is the duty cycle of the UWB pulse train, roughly equal to the pulse duration divided by the frame duration. For IR UWB systems, the transmission pulse is extremely narrow (on the order of nanosecond) and the duty cycle is usually much smaller than unity. Therefore, the magnitude of this impulse could be significant for UWB systems with a relatively small number of users. Moreover, it was mentioned earlier that the MUI is a function of several RVs (c.f. eq. (3.6)). The zeros of the first derivative of the autocorrelation function, $dR(t)/dt$, becomes singularities in the PDF according to the transformation theory for RVs [73, Ch. 5], which can also be observed in Fig. 3.1. The impulse and singularities in the PDF result in the slow covergence of a CLT. Hence, the MUI cannot be approximated by a Gaussian distributed RV. Moreover, these characteristics indicate that it is difficult to provide the exact distribution of the MUI since the singularities are not easily accommodated in a closed form expression.

Let t_{l} and t_{h} denote the points where the singularity closest to S_m to the left and right side occur in Fig. 3.1, respectively. Observe that the probability that R_m assumes values in $(t_{\mathrm{l}}, t_{\mathrm{h}})$ is significant, as large or larger than the probability that R_m falls outside of $(t_{\mathrm{l}}, t_{\mathrm{h}})$ when the information bit 1 is sent. Similar observations can be noted considering the conditional PDF $f_{R_m}\left(x|d_0^{(1)}=0\right)$ when $d_0^{(1)}=0$ is sent. Consider now both conditional PDFs. Observe in Fig. 3.1 that if R_m falls outside $(-t_{\mathrm{h}}, -t_{\mathrm{l}})$ and $(t_{\mathrm{l}}, t_{\mathrm{h}})$, it is unreliable to decide the information bit as 1 or 0 because $f_{R_m}\left(x|d_0^{(1)}=1\right)$ and $f_{R_m}\left(x|d_0^{(1)}=0\right)$ are small and almost the same outside these regions. We here recall the optimal, minimum probability of error, decision rule which relies on the *(log-)likelihood ratio test* (LRT) [27], [82], and explore the possibilities to use this decision rule for UWB receiver design improvement even though the distribution of the MUI is unknown. Denote the sampled output of a generic binary communication system as $\{R_m\}_{m=0}^{N-1}$, where $R_m = (2d-1) + N_m$ with d being the symbol to be detected and N_m being the ambient noise, and assume that d can assume one of the two values in $\{0, 1\}$. The ML receiver structure makes the decision on the log-likelihood ratio which can be expressed as

$$\Lambda_R = \log \prod_{m=0}^{N-1} \frac{f_{R_m}(x|d=1)}{f_{R_m}(x|d=0)} = \sum_{m=0}^{N-1} \log \frac{f_{R_m}(x|d=1)}{f_{R_m}(x|d=0)}. \tag{3.11}$$

For equiprobable case where d assumes 1 and 0 with equal probability, the log-likelihood ratio is compared to 0 to make a decision, i.e.,

$$\begin{aligned} \Lambda > 0 \quad &\Rightarrow d = 1 \\ \Lambda < 0 \quad &\Rightarrow d = 0. \end{aligned} \tag{3.12}$$

If $\Lambda = 0$, the decision can be made by a fair coin toss. For our case, the sampled outputs of the UWB receiver are $R_m = S_m + Y_m = A_1\sqrt{E_{\mathrm{b}}/N_{\mathrm{s}}}\left(2d_0^{(1)}-1\right) + Y_m, (m = 0, \cdots, N_{\mathrm{s}}-1)$ (c.f. eq. (3.3)). Therefore, for a sample $R_m = x$ which gives the condi-

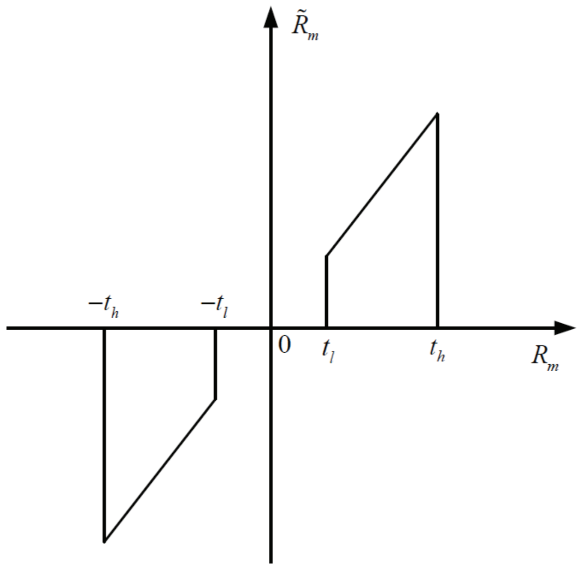

Fig. 3.2. The nonlinear transform in the zonal receiver structure.

tional PDFs $f_{R_m}\left(x|d_0^{(1)}=1\right)$ and $f_{R_m}\left(x|d_0^{(1)}=0\right)$ almost the same value, the summand $\log\frac{f_{R_m}(x|d_0^{(1)}=1)}{f_{R_m}(x|d_0^{(1)}=0)}$ on the right side of eq. (3.11) is close to zero, viz., this sample is unreliable and its effect on the final decision should be eliminated according to the optimal decision rule.

Based on the observations of the simulated PDF, and the optimal, minimum probability of error, decision rule, we propose a new UWB receiver structure. Unlike the CMF UWB receiver which make decisions based on the statistic

$$R_{\mathrm{cmf}} = \sum_{m=0}^{N_{\mathrm{s}}-1} R_m \tag{3.13}$$

the new receiver will detect the transmitted signal using the final decision statistic

$$R_{\mathrm{zonal}} = \sum_{m=0}^{N_{\mathrm{s}}-1} \tilde{R}_m \tag{3.14}$$

where the new partial statistics $\tilde{R}_m$ are obtained from R_m through the transform $g_{\mathrm{zonal}}(\cdot)$ given by

$$\tilde{R}_m = g_{\mathrm{zonal}}(R_m) = \begin{cases} R_m, & R_m \in (-t_{\mathrm{h}}, -t_{\mathrm{l}}) \text{ or } R_m \in (t_{\mathrm{l}}, t_{\mathrm{h}}) \\ 0, & \text{otherwise.} \end{cases} \tag{3.15}$$

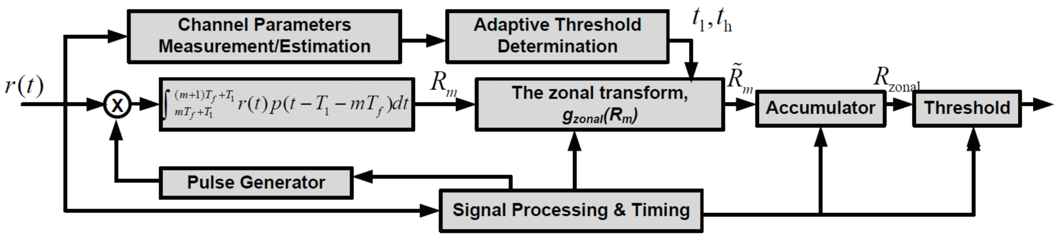

Fig. 3.3. The block diagram of the new UWB receiver.

The tranform function given by eq. (3.15) is plotted in Fig. 3.2. A block diagram showing the structure of the zonal UWB receiver is given in Fig. 3.3.

We emphasize that the design of the new UWB receiver structure is heuristic and based on observations of simulated data. If the chip correlator output R_m falls into the region $(t_\mathrm{l}, t_\mathrm{h})$, there is a relative large probability that the transmitted information bit is 1, and if R_m falls into $(-t_\mathrm{h}, -t_\mathrm{l})$, the information bit is more likely to be 0. Therefore, when R_m falls into $(t_\mathrm{l}, t_\mathrm{h})$ or $(-t_\mathrm{h}, -t_\mathrm{l})$, the zonal UWB receiver uses the received sample unaltered and lets it contribute to the final receiver decision statistic R_zonal. If R_m falls outside of these two regions, one can hardly discern which information bit was transmitted, intuitively motivating an erasure; in this case, the receiver discards the sample and adds 0 to R_zonal to eliminate R_m's effect on the final decision statistic. The zonal UWB receiver is not optimal. However, as mentioned earlier, characterizing mathematically the conditional PDFs in Fig. 3.1 seems difficult, and it is not tractable to derive rigorously an optimal receiver design using ML receiver design principles. The zonal receiver provides a simple and effective method for improving the system performance without complicating the receiver structure extensively.

It is also worth mentioning that, besides the qualitative nature, one of the most significant characteristics of the MUI distribution is the impulsive "heavy tail" behavior, i.e., the tail of the PDF decays at a rate lower than that of the Gaussian distribution (see Fig. (3.4)). An intuitive implication of this behavior is that the probability of observing noise samples with large amplitudes in practice is higher than that would be predicted by the Gaussian noise model [25], [83]–[86]. Note that the degree of non-Gaussianity or the heaviness of the distribution tail is typically measured by its excess *kurtosis* [26]. The excess *kurtosis* of a zero-mean RV X is defined as

$$\kappa = \frac{\mathbb{E}(X^4)}{\mathbb{E}^2(X)} - 3 \tag{3.16}$$

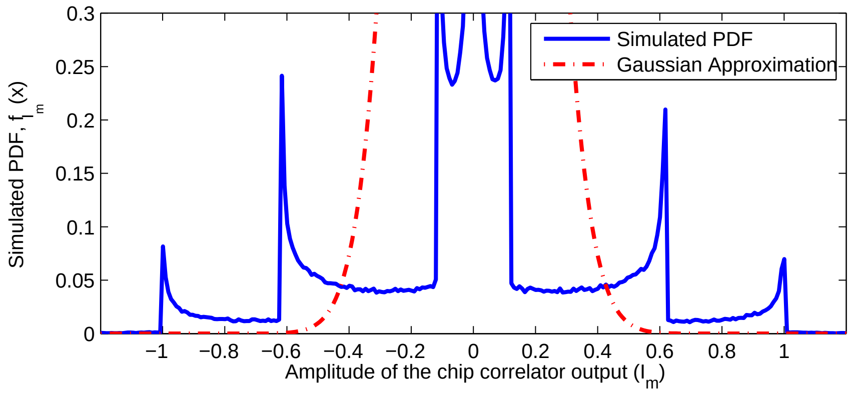

Fig. 3.4. The simulated PDF of the MUI in a frame, I_m, where there are $N_\mathrm{u} = 4$ users in the system; a zero-mean Gaussian distribution with the same variance is also plotted.

where $\mathbb{E}(\cdot)$ denotes the expectation operator. Note that the excess *kurtosis* for Gaussian distributed RVs is zero, while a heavy-tailed RV will have a positive excess *kurtosis*. Simulation is carried out to evaluate the excess *kurtosis* of I_m given by eq. (3.6) where the system parameters are given in Table 3.1 and the number of users in the systems are $N_\mathrm{u} = 4, 8, 16$ and 32. The simulated values of the excess *kurtosis* is given in Table 3.2. It is shown that even with $N_\mathrm{u} = 32$, the excess *kurtosis* of I_m is still positive. One should notice that UWB systems typically operate in indoor environments within a few meters. Hence, $N_\mathrm{u} = 32$ is not small for the number of significant interfering users, viz., for a typical UWB system, the distribution of the MUI usually has a heavy tail. Note that even though the zonal receiver is proposed based on the qualitative nature of the MUI distribution, the nonlinear transform in the receiver structure (c.f. eq. (3.15)) has inherent capability to enhance the performance of the CMF for signal detection in impulsive heavy-tailed noises. The phenomenon that the nonlinear correlator can compensate for the non-Gaussian behavior of the channel noise has been mentioned in [87]. For our case, the nonlinear transform in the zonal receiver structure is revealed by Fig. 3.2. It is observed that this transform is linear for correlator output samples with magnitude in $(t_\mathrm{l}, t_\mathrm{h})$ and $(-t_\mathrm{h}, -t_\mathrm{l})$, but generates zero for samples outside these two regions. As mentioned before, impulsive noise is more likely to produce large noise samples compared to Gaussian noise. Note that when a large-amplitude interference sample is present in the correlator output, the amplitude of the correlator output is far away from the desired signal component. In this case, the sample is not necessarily reliable due to the heavy-tailed distribution. Hence, the nonlinear transform assigns zero to such sample

TABLE 3.2
THE EXCESS *kurtosis* OF I_m GIVEN BY EQ. (3.6).

N_{u}	4	8	16	32
κ	23.0	9.8	4.6	2.2

to suppress its effect on the final decision (see Fig. 3.2). Therefore, for the signal detection in impulsive noise with a heavy-tailed distribution, the zonal receiver is expected to have better performance than the CMF.

Observe also that if we set the lower threshold t_{l} to 0 and the upper threshold t_{h} to infinity, the zonal receiver becomes exactly the CMF UWB receiver. This implies that if we make the thresholds t_{l} and t_{h} adaptive and always adopt the optimal thresholds, the zonal UWB receiver can always meet or outperform the CMF UWB receiver; this is not restricted to scenarios with implusive, heavy-tailed noises, but will be true for arbitrary additive signal disturbances, including MUI, AWGN, and MUI-plus-AWGN.

3.3 Zonal UWB Receiver in Multipath Fading Channels

3.3.1 Invalidity of the Gaussian Approximation for the MUI in a Particular Rake Finger

The previous sections have considered an ideal free-space propagation scenario. However, such a channel model does not reflect typical UWB transmission scenarios. In practical systems, IR UWB signals occupy a huge bandwidth and the propagation channel is highly frequency selective. Therefore, the multipath fading channel model given by eq. (2.6) should be considered, and it is imperative to design receiver structures for UWB signal detection in such channels. Since the delay spread is typically of much greater duration than the transmitted pulse, the assumptions based on the extremely narrow duration of the UWB pulse should be revisited, bearing in mind that the received signal might have a larger duration after propagating through a channel with a much longer channel response. Under such circumstances, one might expect that the CLT is valid and the total disturbance can be well approximated as a Gaussian RV since many multipath components are involved; the CMF should be the optimal receiver, and the benefits of the zonal UWB receiver should be vitiated. However, the assumption that the distribution of the MUI at a particular Rake finger converges to the Gaussian PDF still may not be accurate, and the superiority of the zonal receiver design exists even in highly dense multipath fading UWB channels, as subsequent results will show.

The UWB multipath channel model suggested by the IEEE 802.15.3a Task Group [4] was mathematically expressed by (2.6) in Section 2.1.6, where the CIR of the *k*th user can be expressed as

$$h^{(k)}(t) = \sum_{l=0}^{L_{\mathrm{t}}-1} \alpha_l^{(k)} \delta(t - \tau_l^{(k)}) \tag{3.17}$$

where l is the multipath index and L_{t} is the total number of multipath components[2]. The parameters $\alpha_l^{(k)}$ and $\tau_l^{(k)}$ are the amplitude and delay of the *l*th multipath component for the *k*th user, respectively. Assuming that there are N_{u} users transmitting asynchronously in the system, the received signal can be written as

$$\begin{aligned} r(t) &= h^{(1)}(t) * s^{(1)}(t - T_1) + \sum_{k=2}^{N_{\mathrm{u}}} h^{(k)}(t) * s^{(1)}(t - T_k) + n(t) \\ &= \sum_{l=0}^{L_{\mathrm{t}}-1} \alpha_l^{(1)} s^{(1)}(t - \tau_l^{(1)} - T_1) + \sum_{k=2}^{N_{\mathrm{u}}} \sum_{l=0}^{L_{\mathrm{t}}-1} \alpha_l^{(k)} s^{(k)}(t - \tau_l^{(k)} - T_k) + n(t) \end{aligned} \tag{3.18}$$

where $n(t)$ is zero-mean AWGN, T_k are the delays of the *k*th users in the system, and $*$ denotes convolution. For UWB signal detection in multipath fading channels, the Rake receiver and the autocorrelation receiver with transmitted-reference (TR) signaling are widely adopted. For the Rake reception, the receiver collects the signal energy from all, or a subset of, the received signal paths [27]. Combining schemes are used to combine the signals arriving in different paths to form a decision statistic [27], [88]. In the TR scheme, every information-bearing pulse is coupled with a unmodulated pilot pulse. The system is designed so that the propagation channel is unchanged during the transmission of the pilot pulse and its information-conveying pulse. Therefore, estimation of individual path delays and amplitudes is unnecessary, and the received signal for the pilot pulse can be used as a template for demodulating the information-bearing pulse. However, the TR scheme wastes half the energy in pilot signals, and the performance is degraded since the pilot signals are

[2] We assume that the numbers of paths are the same for all the users in the system. However, generalization to different path numbers for different users is straightforward.

contaminated by interference and noise. In this chapter, we focus on the Rake reception, and the maximal ratio combining (MRC) is considered for combining signals from different paths. As in the free-space propagation case, we assume that the TH sequence of the first user is 0 for all the frames [11] and the desired information bit is 1. Therefore, if the channel is perfectly known at the receiver, the zeroth information of the first user can be coherently detected and combined by employing the template

$$v(t) = \sum_{l=0}^{L_{\mathrm{f}}-1} \alpha_l^{(1)} \sum_{j=0}^{N_{\mathrm{s}}-1} p(t - mT_{\mathrm{f}} - T_1 - \tau_l^{(1)}) \tag{3.19}$$

where L_{f} is the number of Rake fingers. Letting $R_{l,m}$ denote the *m*th ($m = 0, \cdots, N_{\mathrm{s}} - 1$) sampled output in the *l*th Rake finger for the desired signal and R_{MRC} denote the output after the MRC, we have is considered

$$R_{\mathrm{MRC}} = \int r(t)v(t)dt = \sum_{l=1}^{L_{\mathrm{f}}} \alpha_l^{(1)} \sum_{m=0}^{N_{\mathrm{s}}-1} R_{l,m} = \sum_{l=1}^{L_{\mathrm{f}}} \alpha_l^{(1)} \sum_{m=0}^{N_{\mathrm{s}}-1} (S_{l,m} + I_{l,m} + N_{l,m}) \tag{3.20a}$$

where $S_{l,m}$, $I_{l,m}$ and $N_{l,m}$ represent the desired signal component, the MUI and the AWGN component in the *m*th frame of the *l*th Rake finger, respectively. Note that $S_{l,m}$ can be written as

$$S_{l,m} = \sqrt{\frac{E_{\mathrm{b}}}{N_{\mathrm{s}}}} (2d_0^{(1)} - 1)\alpha_l^{(1)}. \tag{3.20b}$$

The interference term, $I_{l,m}$, can be expressed as

$$\begin{aligned} I_{l,m} &= \sum_{k=2}^{N_{\mathrm{u}}} \sqrt{\frac{E_{\mathrm{b}}}{N_{\mathrm{s}}}} \sum_{j=-\infty}^{\infty} \sum_{l_1=0}^{L_{\mathrm{t}}-1} \alpha_{l_1}^{(k)} \left(2d_{\lfloor j/N_{\mathrm{s}} \rfloor}^{(k)} - 1\right) \\ &\quad \times \int_{mT_{\mathrm{f}}+\tau_l^{(1)}}^{mT_{\mathrm{f}}+\tau_{l+1}^{(1)}} p(t - jT_{\mathrm{f}} - c_{\mathrm{TH},j}^{(k)} T_{\mathrm{c}} - \tau_{l_1}^{(k)} - T_k) p(t - mT_{\mathrm{f}} - \tau_l^{(k)} - T_1) dt \\ &= \sqrt{\frac{E_{\mathrm{b}}}{N_{\mathrm{s}}}} \sum_{l_1=0}^{L_{\mathrm{t}}-1} \sum_{j=-\infty}^{\infty} \alpha_{l_1}^{(k)} \left(2d_{\lfloor j/N_{\mathrm{s}} \rfloor}^{(k)} - 1\right) \\ &\quad \times R\left((j-m)T_{\mathrm{f}} + c_{\mathrm{TH},j}^{(k)} T_{\mathrm{c}} + (\tau_{l_1}^{(k)} - \tau_l^{(1)}) + T_k - T_1\right) \end{aligned} \tag{3.20c}$$

where $R(t)$ is the autocorrelation function of the transmission pulse given by eq. (2.2). It is seen in eq. (3.20c) that the interfering pulses for a particular user is increased. We here use simulation to evaluate the excess *kurtosis* of $I_{l,m}$ given by eq. (3.20c) and the results are given in Table 3.3. Note that even with $N_{\mathrm{u}} = 32$, the excess *kurtosis* of $I_{l,m}$ is still

TABLE 3.3
THE EXCESS *kurtosis* OF $I_{l,m}$ GIVEN BY EQ. (3.20C).

N_{u}	4	8	16	32
κ	13.4	6.2	2.8	1.4

positive and the distribution of $I_{l,m}$ does not resemble the Gaussian PDF. As mentioned above, $N_{\mathrm{u}} = 32$ is not small for the number of significant interfering users. Therefore, for a typical UWB system operating in multipath fading channels, the Gaussian PDF is invalid for modeling the MUI in each frame of a Rake finger, and the zonal receiver structure is expected to improve the performance of Rake reception in this scenario. Hence, a new version of Rake receiver which employs MRC but adopts the zonal UWB receiver in each finger, is proposed for UWB signal detection in multipath fading channels. This new Rake receiver, which is shown in Fig. 3.5, can achieve larger SINR values than the CMF based Rake receiver as shown below, thus achieving better BER performance in multipath fading UWB channels.

3.3.2 Theoretical Proof of the Superiority of the Zonal Receiver in UWB Multipath Fading Channels

In this part, theoretical analysis is performed to show the superiority of the zonal based Rake receiver in UWB multipath fading channels. We let $Y_{l,m} = I_{l,m} + N_{l,m}$ denote the total disturbance in the *m*th frame of the *l*th Rake finger (c.f. eq. (3.20a)) and assume that the RVs $Y_{l,m}$ $(l = 0, \cdots L_{\mathrm{f}} - 1,\ m = 0, \cdots, N_{\mathrm{s}} - 1)$ are i.i.d. and independent of the signal component $S_{l,m}$. The *m*th chip correlator output in the *l*th finger, $R_{l,m} = S_{l,m} + Y_{l,m}$ is considered. The decision statistic, R_l, in the *l*th finger of the CMF based Rake receiver is

$$R_l = \sum_{m=0}^{N_{\mathrm{s}}-1} R_{l,m} \tag{3.21}$$

with mean $\mathbb{E}(R_l) = \mathbb{E}\left(\sum_{m=0}^{N_s-1} R_{l,m}\right) = N_s \mathbb{E}\left(R_{l,m}\right)$ and variance is $\mathrm{var}(R_l) = N_s \cdot \mathrm{var}\left(R_{l,m}\right)$. Note that the SINR of the decision statistic X in a transmission system is given by

$$\mathrm{SINR} = \frac{\mathbb{E}^2(X)}{\mathrm{var}(X)}. \tag{3.22}$$

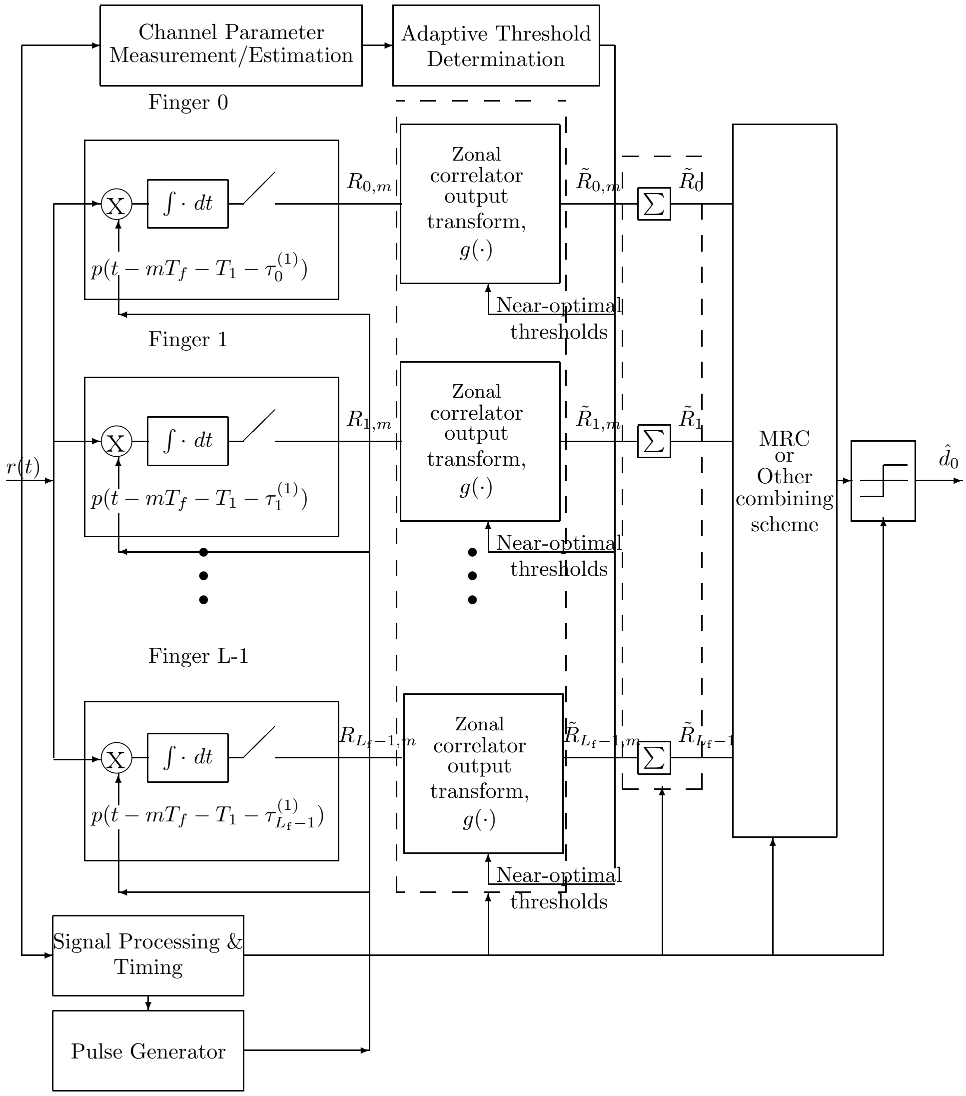

Fig. 3.5. The new Rake receiver based on the zonal UWB receiver structure.

Thus, the SINR in the *l*th finger of the CMF based Rake receiver is given by

$$\mathrm{SINR}_{l,\mathrm{cmf}} = \frac{\mathbb{E}^2(R_l)}{\mathrm{var}(R_l)} = N_\mathrm{s}\frac{\mathbb{E}^2(R_{l,m})}{\mathrm{var}(R_{l,m})}. \tag{3.23}$$

Consider now the new Rake receiver structure based on the zonal receiver design. The new *m*th chip correlator in the *l*th finger, $\tilde{R}_{l,m}$, is obtained from $R_{l,m}$ through the transformation

$$\tilde{R}_{l,m} = \begin{cases} R_{l,m}, & R_{l,m} \in (-t_h, -t_l) \text{ or } R_{l,m} \in (t_l, t_h) \\ 0, & \text{otherwise} \end{cases} \tag{3.24}$$

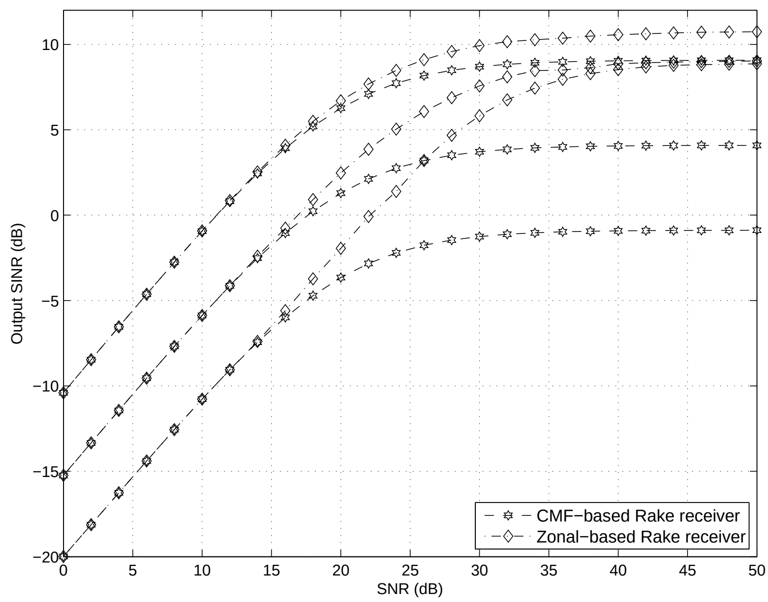

Fig. 3.6. The output SINR in each finger of the CMF based Rake receiver and the zonal based Rake receiver.

with mean $E(\tilde{R}_{l,m})$ and variance $\mathrm{var}(\tilde{R}_{l,m})$. The final decision statistic in the lth finger of the new Rake receiver $\tilde{R}_l$ is

$$\tilde{R}_l = \sum_{m=0}^{N_\mathrm{s}-1} \tilde{R}_{l,m} \tag{3.25}$$

with mean $\mathbb{E}(\tilde{R}_l) = \mathbb{E}(\sum_{m=0}^{N_\mathrm{s}-1} \tilde{R}_{l,m}) = N_\mathrm{s} \cdot \mathbb{E}(\tilde{R}_{l,m})$ and variance $\mathrm{var}(\tilde{R}_l) = N_\mathrm{s} \cdot \mathrm{var}(\tilde{R}_{l,m})$. Thus, the SINR in the lth finger of the new Rake receiver is

$$\mathrm{SINR}_{l,\mathrm{zonal}} = \frac{\mathbb{E}^2(\tilde{R}_l)}{\mathrm{var}(\tilde{R}_l)} = N_\mathrm{s} \frac{\mathbb{E}^2(\tilde{R}_{l,m})}{\mathrm{var}(\tilde{R}_{l,m})}. \tag{3.26}$$

Eq. (3.23) gives the SINR in each finger of the CMF based Rake receiver, while that of the new Rake receiver adopting the zonal receiver is given in eq. (3.26). Fig. 3.6 shows the output SINR in each finger of the CMF based, and the zonal UWB receiver based, Rake receiver. The factor N_s is omitted since it doesn't affect the result of the comparison. These results are obtained by simulation for SIR = 5 dB, 10 dB, and 15 dB in IEEE 802.15.3a CM1 channels [4]. Observe that, when the SNR is small, i.e. the total disturbance can be well approximated by a Gaussian RV and the CMF UWB receiver maximizes the SINR, the output SINRs of the CMF UWB receiver and the zonal UWB receiver are almost the same. However, the output SINR of the zonal UWB receiver with near-optimal thresholds (selection of near-optimal thresholds for the zonal receiver will be discussed in the sequel) grows rapidly with increasing SNR, and surpasses that of the CMF UWB receiver. The SINR gains for the zonal UWB receiver are significant for practical medium and large SNR values. Note also in Fig. 3.6 that, the SINR gains in each finger of the new Rake receiver over the standard matched filter Rake receiver are lower and upper bounded as

$$\gamma_{\text{min}} \cdot \text{SINR}_{l,\text{cmf}} \leq \text{SINR}_{l,\text{zonal}} \leq \gamma_{\text{max}} \cdot \text{SINR}_{l,\text{cmf}} \tag{3.27}$$

where γ_{min} = 1 = 0 dB for all three cases, and upper bound γ_{max} is 9.3 = 9.7 dB, 3.1 = 4.9 dB, and 1.4 = 1.6 dB for SIR = 5 dB, SIR = 10 dB, and SIR = 15 dB, respectively.

If MRC diversity is employed to combine the signals from each Rake finger, the instantaneous SINR for the final decision statistic is [88]

$$\text{SINR}_{\text{MRC}} = \sum_{l=0}^{L-1} \text{SINR}_l \tag{3.28}$$

where SINR_l is the value of SINR in the lth finger. Since the value of $\text{SINR}_{l,\text{zonal}}$ is between γ_{min} times, and γ_{max} times $\text{SINR}_{l,\text{mf}}$ for all values of l, we have

$$\gamma_{\text{min}} \cdot \text{SINR}_{\text{MRC,cmf}} \leq \text{SINR}_{\text{MRC,zonal}} \leq \gamma_{\text{max}} \cdot \text{SINR}_{\text{MRC,cmf}} \tag{3.29}$$

where $\text{SINR}_{\text{MRC,cmf}}$ and $\text{SINR}_{\text{MRC,zonal}}$ are the SINR after MRC for the CMF and zonal based Rake receivers, respectively. Thus, when measured in dB, the SINR gains of the final decision statistic of the new Rake receiver based on the design of the zonal UWB receiver over the standard matched filter UWB receiver are lower bounded by $10 \log_{10} \gamma_{\text{min}}$ and upper bounded by $10 \log_{10} \gamma_{\text{max}}$. For example, in Fig. 3.6, the SINR gain of the zonal based Rake receiver over the CMF based Rake receiver is upper bounded by 9.7 dB when the SIR = 5 dB, and the SNR ranges from [0 dB, 32 dB]. The value is 4.9 dB for SIR = 10 dB, and 1.6 dB for SIR =15 dB. Observe further that the zonal UWB receiver becomes exactly the CMF UWB receiver with proper thresholds selection. Hence, $\gamma_{\text{min}} \geq 1$ is a lower bound to the SINR gains, and the output SINRs of the zonal UWB receiver are as large or larger than those achieved by the CMF UWB receiver. Therefore, the new Rake receiver based on the zonal UWB receiver structure which collects the SINR gains from all the fingers can surely enhance the output SINR of the CMF based Rake receiver, achieving better BER performance in multipath fading UWB channels. Note also that the SINR gains of the zonal based Rake receiver over the standard CMF based Rake receiver are more significant when the input SIR value is smaller, i.e., the MUI component is relatively larger in the total disturbance. This fact makes the new Rake receiver more valuable in UWB channels where the multiple access interference is strong.

3.4 Zonal Receiver Implementation: Selection of Thresholds

In order to implement the zonal UWB receiver, the thresholds t_{h} and t_{l} should be selected. A look-up table can be constructed where the threshold can be selected according to certain system parameter(s). Therefore, in practical systems, the system parameter(s) can be estimated and the thresholds can be chosen according to the look-up table. Note that the values of the optimal thresholds are determined by several factors in the network, such as the network topology, the number of the interferers, the powers of interferers and the PSD of the AWGN. Therefore, for different transmission scenarios, the mechanism for threshold selection might be different. In this section, we will consider two typical scenarios for UWB transmission and discuss how the threshold selection can be performed in each scenario.

Scenario I

The first scenario we consider is a centralized UWB network where a device coordinates the data transfer for all the devices coexising in the same area. In such a network, there is a network coordinator acting as a "base station". This scenario can be seen in several UWB enabled indoor and outdoor networks. In this case, the receiver might have information of the number of users in the network, and power control could be performed to eliminate the near-far effect. In this case, A_k in eq. (3.8) are the same for all the interferers, and the SNR and SIR defined by eqs. (3.7) and (3.8) can fully characterize the relative values of AWGN and MUI, the relationship between them, and the shape of the distribution of the interference I_m in the system. Therefore, under such circumstances, we select the thresholds using the SNR and SIR values in the channel. However, it should be noted that other system parameters which can describe the interference and AWGN in the channel can also be used to choose the threshold [3].

[3]It has been mentioned earlier that the zonal receiver can outperform the CMF receiver in impulsive heavy-tailed noise, and such noise can be well described by the excess *kurtosis*. Therefore, the excess *kurtosis* of the disturbance in the channel can also be used as the system parameter based on which the thresholds are selected.

TABLE 3.4
OPTIMAL THRESHOLDS t_l AND t_h, NORMALIZED TO S_m, FOR DIFFERENT VALUES OF SIR AND SNR BASED ON CRITERION 1: MINIMIZING THE BER; SCENARIO I WITH $N_\mathrm{u} = 4$ USERS IS CONSIDERED.

SNR(dB)	$(t_\mathrm{l}, t_\mathrm{h})/S_m$	SIR = 5 dB	SIR = 10 dB	SIR = 15 dB
0	t_l	0.00	0.00	0.00
	t_h	20.10	24.31	30.12
4	t_l	0.00	0.00	0.00
	t_h	11.91	15.22	28.41
8	t_l	0.00	0.00	0.00
	t_h	10.22	11.14	14.92
12	t_l	0.00	0.00	0.00
	t_h	6.42	7.74	10.13
16	t_l	0.01	0.01	0.00
	t_h	2.21	3.24	3.47
20	t_l	0.03	0.02	0.00
	t_h	2.12	2.12	2.81
24	t_l	0.05	0.03	0.01
	t_h	1.41	1.83	2.15
28	t_l	0.10	0.03	0.02
	t_h	1.31	1.76	1.94
32	t_l	0.19	0.13	0.05
	t_h	1.12	1.43	1.72

For the table constructure under such circumstances, two criteria for determining the thresholds for the zonal UWB receiver will be investigated. The first criterion is to find the threshold which can minimize the BER of the UWB system with certain SNR and SIR values. Under this criterion, computer search is used to obtain the thresholds which give the zonal UWB receiver the best BER performance. The second criterion is to find the thresholds that maximize the SINR in each frame, which can be expressed as

$$\begin{aligned}\{t_\mathrm{l}, t_\mathrm{h}\} &= \arg\max_{t_\mathrm{l}, t_\mathrm{h}} \{\mathrm{SINR}_m(t_\mathrm{l}, t_\mathrm{h})\} \\ &= \arg\max_{t_\mathrm{l}, t_\mathrm{h}} \left\{ \frac{\mathbb{E}^2(\tilde{R}_m(t_\mathrm{l}, t_\mathrm{h}))}{\mathrm{var}(\tilde{R}_m(t_\mathrm{l}, t_\mathrm{h}))} \right\} \end{aligned} \tag{3.30}$$

where SINR_m is the SINR after the zonal transform in the *m*th frame, and $\tilde{R}_m$ is the transformed chip correlator output obtained from R_m based on the thresholds t_l and t_h. Tables 3.4 and 3.5 show examples of such look-up tables valid when equal power interferers are

TABLE 3.5
OPTIMAL THRESHOLDS $t_{\rm l}$ AND $t_{\rm h}$, NORMALIZED TO S_m, FOR DIFFERENT VALUES OF SIR AND SNR BASED ON CRITERION 2: MAXIMIZING THE SINR IN EACH FRAME; SCENARIO I WITH $N_{\rm u} = 4$ USERS IS CONSIDERED.

SNR(dB)	$(t_{\rm l}, t_{\rm h})/S_m$	SIR = 5 dB	SIR = 10 dB	SIR = 15 dB
0	$t_{\rm l}$	0.00	0.00	0.00
	$t_{\rm h}$	20.21	24.17	30.41
4	$t_{\rm l}$	0.00	0.00	0.00
	$t_{\rm h}$	12.15	15.32	28.18
8	$t_{\rm l}$	0.00	0.00	0.00
	$t_{\rm h}$	10.22	11.14	14.92
12	$t_{\rm l}$	0.00	0.00	0.00
	$t_{\rm h}$	6.42	7.54	10.23
16	$t_{\rm l}$	0.01	0.01	0.00
	$t_{\rm h}$	2.12	3.35	3.57
20	$t_{\rm l}$	0.03	0.02	0.00
	$t_{\rm h}$	2.12	2.32	2.81
24	$t_{\rm l}$	0.05	0.03	0.01
	$t_{\rm h}$	1.51	1.92	2.15
28	$t_{\rm l}$	0.10	0.03	0.02
	$t_{\rm h}$	1.21	1.76	1.94
32	$t_{\rm l}$	0.19	0.13	0.05
	$t_{\rm h}$	1.14	1.43	1.72

considered and $N_{\rm u} = 4$, for Criterion 1 and Criterion 2, respectively. It is noted that thresholds determined by Criterion 1 are almost the same as those determined by Criterion 2. This means that the thresholds which maximize the SINR in each frame of the transmission system give nearly the best BER performance at the same time. Since Criterion 2 is easy to implement in practical receivers, we will focus on the investigation of the zonal UWB receiver with thresholds determined by Criterion 2 in the remainder of the chapter.

SNR and SIR estimation for UWB systems has been studied in [89]–[91]. In [91], an algorithm which jointly estimates the SNR and SIR in a MUI environment was proposed for IR UWB systems. This algorithm can be used effectively to provide SNR and SIR estimation for the zonal threshold selection as shown in Section 3.5.

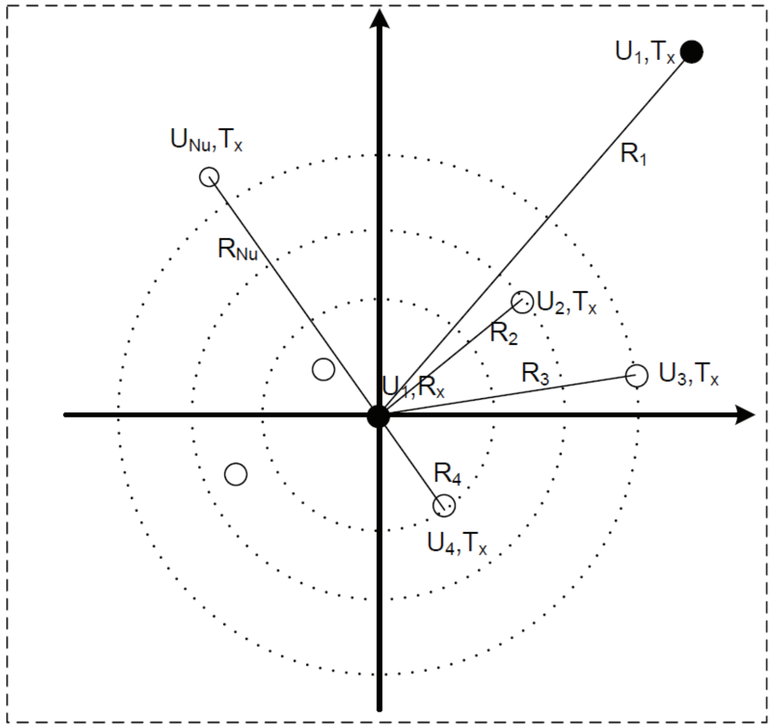

Fig. 3.7. The network topology where the interferers are scattered according to a homogeneous Poisson point process.

Scenario II

Scenario II describes the ad hoc UWB network where the transmission is peer-to-peer. Different from Scenario I mentioned above, this type of network is not centralized and there does not exist a single coordinator which controls the transmissions for all the nodes within the coverage area. An effective model for analyzing the interference for this scenario was provided in [18], [74] where the spatial locations of the interferers are unknown and treated as complete random according to a homogeneous Poisson point process in a two-dimensional space $\mathcal{R}^2$ with a density λ [18], [74], [92]. Without loss of generality, the intended receiver can be assumed to locate at the origin of the two-dimensional plane, and the transmitter of the desired user is located at a distance R_0 from the origin. The network topology is depicted by Fig. 3.7. Since the powers of the interferers decay with the distance r according to k/r^{ν} for some constant k and the path-loss exponent ν [4], the received powers A_k of the interferers at the intended receiver depend on their distances to the origin. In this

[4]The typical value for ν ranges from 1.8 - 6.5 [93, Table 2.2].

TABLE 3.6
OPTIMAL THRESHOLDS t_l AND t_h, NORMALIZED TO S_m, FOR DIFFERENT VALUES OF λ AND SNR BASED ON CRITERION 1: MINIMIZING THE BER; SCENARIO II IS CONSIDERED.

SNR(dB)	$(t_\mathrm{l}, t_\mathrm{h})/S_m$	$\lambda = 0.1$	$\lambda = 0.2$	$\lambda = 0.5$
0	t_l	0.00	0.00	0.00
	t_h	50.00	48.00	48.00
4	t_l	0.00	0.00	0.00
	t_h	19.50	19.50	19.50
8	t_l	0.00	0.00	0.00
	t_h	7.20	7.20	7.00
12	t_l	0.00	0.00	0.03
	t_h	2.80	2.80	3.60
16	t_l	0.00	0.01	0.03
	t_h	1.76	1.98	2.80
20	t_l	0.01	0.02	0.03
	t_h	1.68	1.98	2.80
24	t_l	0.02	0.06	0.03
	t_h	1.68	1.96	2.80
28	t_l	0.02	0.06	0.06
	t_h	1.68	1.96	2.80
32	t_l	0.02	0.06	0.08
	t_h	1.68	1.96	2.80

transmission scenario, the spatial density of interfering nodes and the path-loss exponent can fully describe the MUI, and the SNR can determine the AWGN component in the channel. Hence, for particular values of the spatial density of the interfering nodes λ and the path-loss exponent ν, a look-up table can be constructed where the thresholds can be selected according to the estimated SNR value. The criteria for constructing look-up tables in Scenario I can also be used here. Table 3.6 shows an example of such look-up table under Criterion 1, where the thresholds are searched to minimize the BER of the UWB system, while Table 3.7 is an example of such look-up table under Criterion 2 where the thresholds are selected to maximize the SINR in each frame (c.f. eq. (3.30)). The interfering nodes spatial densities are λ = 0.1, 0.2 and 0.5, and the path-loss exponent is 2. Noted that as in Scenario I, the thresholds determined by Criterion 1 are always almost the same as those determined by Criterion 2. This means that the thresholds which maximize the SINR in each frame of the transmission system give nearly the best BER performance at the

TABLE 3.7
OPTIMAL THRESHOLDS t_{l} AND t_{h}, NORMALIZED TO S_m, FOR DIFFERENT VALUES OF λ AND SNR BASED ON CRITERION 2: MAXIMIZING THE SINR IN EACH FRAME; SCENARIO II IS CONSIDERED.

SNR(dB)	$(t_{\mathrm{l}}, t_{\mathrm{h}})/S_m$	$\lambda = 0.1$	$\lambda = 0.2$	$\lambda = 0.5$
0	t_{l}	0.00	0.00	0.00
	t_{h}	50.00	48.00	48.00
4	t_{l}	0.00	0.00	0.00
	t_{h}	19.50	19.50	19.50
8	t_{l}	0.00	0.00	0.00
	t_{h}	7.20	7.10	6.90
12	t_{l}	0.00	0.00	0.03
	t_{h}	2.80	2.80	3.50
16	t_{l}	0.00	0.01	0.03
	t_{h}	1.76	1.98	2.80
20	t_{l}	0.01	0.02	0.03
	t_{h}	1.68	1.98	2.80
24	t_{l}	0.02	0.06	0.03
	t_{h}	1.68	1.97	2.80
28	t_{l}	0.02	0.06	0.06
	t_{h}	1.68	1.97	2.80
32	t_{l}	0.02	0.06	0.08
	t_{h}	1.68	1.96	2.80

same time. It has been mentioned above that Criterion 2 is easy to implement in practical receivers. Therefore, for Scenario II, the thresholds for the zonal receiver will be determined by Criterion 2 for the rest of the chapter.

3.5 Numerical Results and Discussion

Simulations are carried out for free-space propagation channels and multipath fading UWB channels to evaluate the average BER performance of the zonal UWB receiver and the zonal based Rake receiver. In the AWGN channel, the performance of the zonal receiver is compared with the CMF UWB receiver. In the UWB multipath fading channel, the BER performance of the zonal based Rake receiver is compared with the CMF based Rake receiver. The system parameters are given in Table 3.1.

3.5.1 Ideal Free-Space Propagation Scenario

Scenario I

We first examine the performance of the zonal receiver in a centralized network where a network coordinator acts as a "base station". In this case, the thresholds are selected according to Table 3.5, and the SIR and SNR estimations are necessary for the threshold selection. The estimator proposed in [91] is used to jointly estimate the SNR and SIR values under such circumstances.

Note in Table 3.5 that when the SNR is small, i.e. the AWGN is dominant in the total disturbance $Y_m = I_m + N_m$, and Y_m can be well approximated by a Gaussian RV. Note that the CMF UWB receiver works as an optimal receiver under such circumstances [27]. In this case, the zonal UWB receiver attains the CMF UWB receiver's performance by making its structure similar to the CMF receiver, i.e. by setting the optimal upper threshold t_h away from the desired signal component S_m, and the optimal lower threshold t_l close to 0. The upper and lower thresholds move towards S_m with increasing SNR. When the SNR is large enough to make the MUI the dominant term in the total disturbance, the near-optimal values for t_l and t_h are close to S_m. Then the zonal UWB receiver has exactly the same structure as first proposed for the case where only MUI is present, for all three cases. Moreover, the optimal value of the upper threshold gets larger with the increase of SIR values for a fixed value of SNR, while the optimal value of the lower threshold changes in the opposite manner (decreases) as the SIR increases. This happens because, for a fixed value of SNR, the MUI component in the total disturbance is relatively larger when the SIR value is smaller, and the zonal receiver becomes less like the CMF UWB receiver by setting both its near-optimal upper and lower thresholds closer to the desired signal component S_m, as the SIR decreases.

Fig. 3.8 shows BER curves of the CMF UWB receiver, the zonal UWB receiver with thresholds based on the estimated SNR and SIR, and the zonal UWB receiver with thresholds based on perfect knowledge of the SIR and SNR. The SIR is 5 dB, and the SNR ranges from 0 dB to 32 dB. Observe that when the SNR is small, i.e. the AWGN dominates the MUI and $Y_m = I_m + N_m$ can be approximated as a Gaussian distributed RV, the CMF UWB receiver is the optimal receiver [27]. Under such circumstances, the zonal UWB receiver adjusts the thresholds to meet the BER performance of the CMF UWB receiver. But when

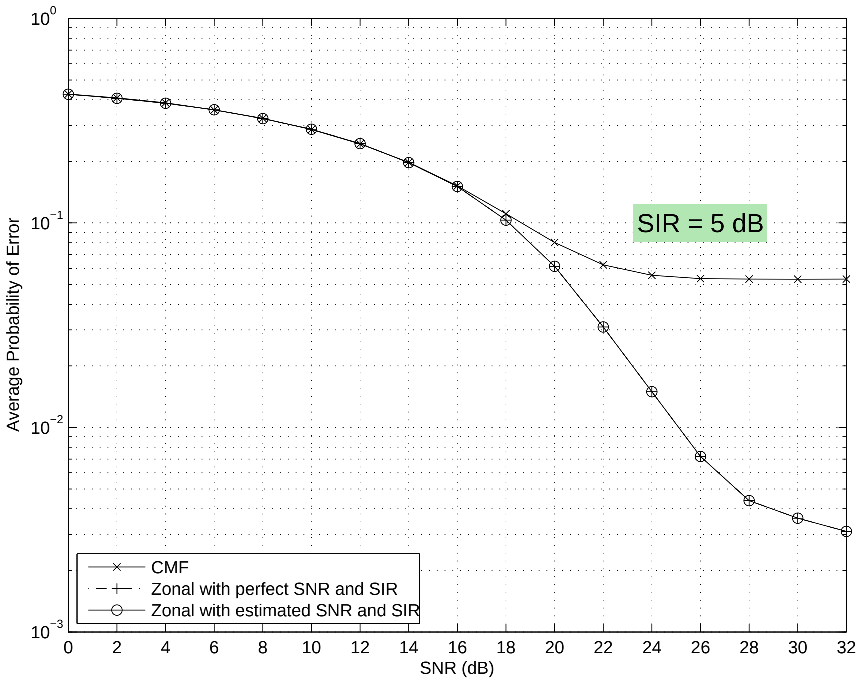

Fig. 3.8. The average BER versus SNR of the CMF and zonal UWB receivers in an ideal free-space propagation channel, where there are 3 equal-power interferers ($N_\mathrm{u} = 4$) and the SIR = 5 dB.

the SNR becomes large enough that the noise term does not dominate the MUI, the zonal UWB receiver with properly selected thresholds outperforms the CMF UWB receiver. It is found by simulation that the error rate floor of the zonal UWB receiver is around 2.2×10^{-3}, which is 23.2 times smaller than the error floor of the CMF UWB receiver (5.1×10^{-2}). The error rate floor of the zonal UWB receiver is not reached until the SNR exceeds 42 dB, which means that, in a practical sense, the zonal UWB receiver doesn't have an error rate floor for this value of SIR, because such large values of SNR cannot usually be achieved in practical wireless systems. Note also that the SNR and SIR estimation scheme proposed in [91] is very effective for our problem. The zonal receiver with this estimation scheme attains the performance of the zonal receiver with perfect knowledge of the SIR and SNR. This happens because the near-optimal thresholds for the zonal receiver are only weakly sensitive to SNR and SIR values. Although the estimator in [91] has errors in practical implementation, these errors do not cause noticeable degradation in the performance of the zonal UWB receiver.

Fig. 3.9 shows the BER curves of the CMF UWB receiver, the zonal UWB receiver with thresholds based on the estimated SNR and SIR, and the zonal UWB receiver with

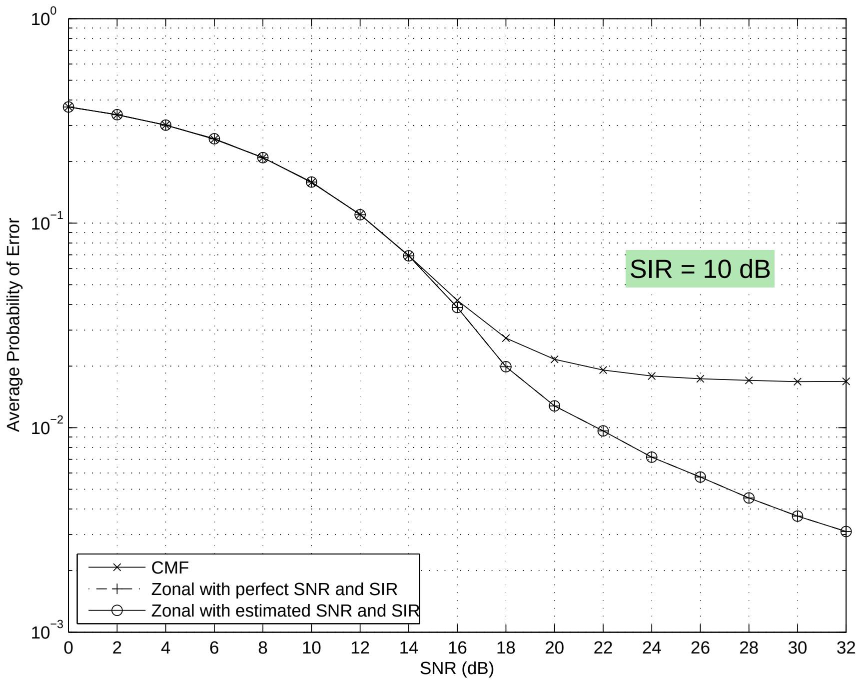

Fig. 3.9. The average BER versus SNR of the CMF and zonal UWB receivers in an ideal free-space propagation channel, where there are 3 equal-power interferers ($N_{\mathrm{u}} = 4$) and the SIR = 10 dB.

thresholds based on perfect knowledge of the SNR and SIR. The operating conditions are the same as Fig. 3.8, and the SIR is 10 dB. The BER curves under such circumstances change in the same manner as those in Fig. 3.8. However, the error rate floor of the zonal UWB receiver is around 2.0×10^{-3}, which is 9 times smaller than that of the CMF UWB receiver (1.8×10^{-2}). Comparison of the results in Figs. 3.8 and 3.9 shows that the BER performance gains of the zonal UWB receiver over the CMF UWB receiver are more significant when the value of SIR is smaller, i.e., the MUI term is relatively larger. This behaviour makes the zonal UWB receiver valuable in UWB systems with strong MUI. Moreover, it is noted that the SIR and SNR estimation scheme is also very effective under this operating condition, since the zonal receiver with thresholds based on estimated system parameters achieves almost the same BER performance as the zonal receiver with perfect knowledge of the SIR and SNR.

Scenario II

In this part, we examine the performance of the zonal receiver in an ad hoc network where the transmission is peer-to-peer. As mentioned above, in this case, the spatial locations of

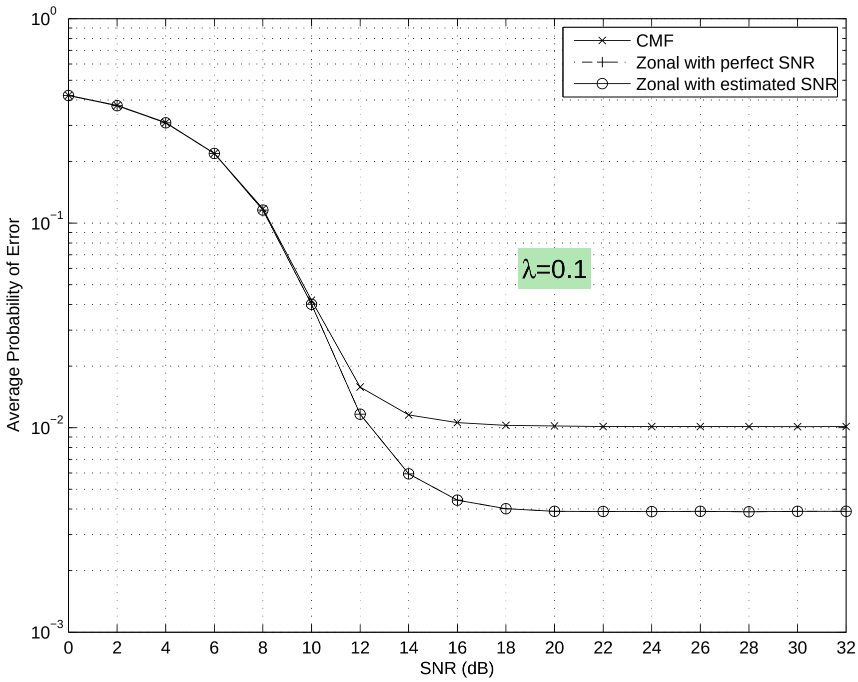

Fig. 3.10. The average BER versus SNR of the CMF and zonal UWB receivers in a network where the interfering nodes are scattered according to a homogeneous Poisson process in a two-dimensional space with density $\lambda = 0.1$; a free-space propagation channel with path-loss exponent $\nu = 2$ is considered.

the interferers are unknown and treated as complete random according to a homogeneous Poisson point process in a two-dimensional space $\mathcal{R}^2$ with a density λ. Under such circumstances, the zonal thresholds can be selected according to the estimated SNR value and Table 3.7.

Fig. 3.10 shows BER curves of the CMF UWB receiver and the zonal UWB receiver with thresholds based on the estimated SNR, and the zonal UWB receiver with thresholds based on perfect knowledge of the SNR in a network where the interfering nodes are scattered according to a homogeneous Poisson point process in a two-dimensional space $\mathcal{R}^2$ with a density $\lambda = 0.1$; a free-space propagation channel with path-loss exponent $\nu = 2$ is considered. The SNR ranges from 0 dB to 32 dB. Note that when the SNR values are small, the AWGN term is the dominant disturbance in the channel. In this case, the CMF is optimal and the zonal receiver adjusts the thresholds to meet the performance of the CMF. As the SNR increases, the total disturbance becomes impulsive due to the MUI component, and the zonal UWB receiver with adaptive thresholds lowers the error floor and outperforms the CMF UWB receiver. The same phenomenon can be observed in Fig. 3.11, where the spatial intensity of the interfering nodes is $\lambda = 0.2$. It is also worth mentioning that the

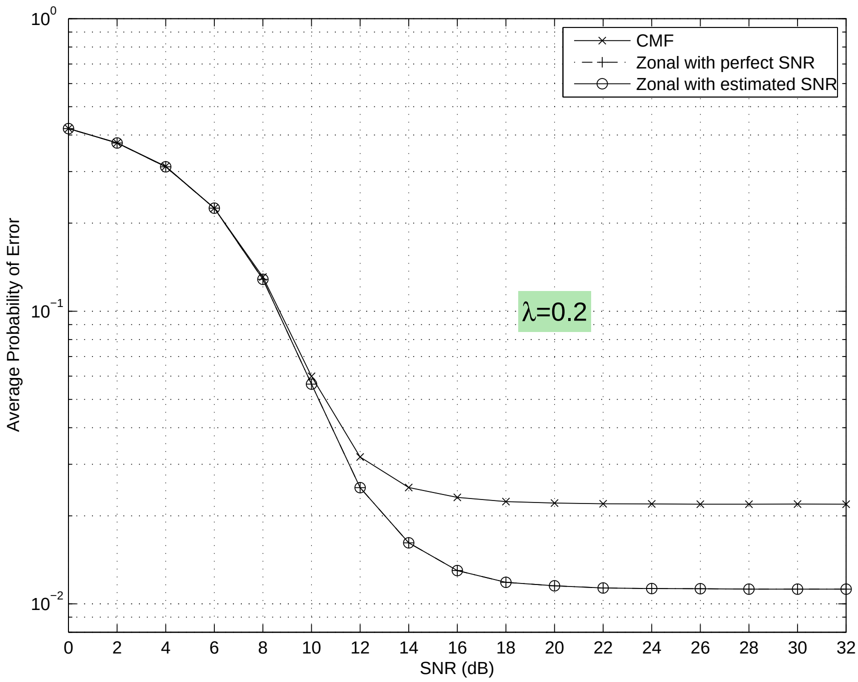

Fig. 3.11. The average BER versus SNR of the CMF and zonal UWB receivers in a network where the interfering nodes are scattered according to a homogeneous Poisson process in a two-dimensional space with density $\lambda = 0.2$; a free-space propagation channel with path-loss exponent $\nu = 2$ is considered.

SNR estimation scheme proposed in [91] is very effective for this scenario since the zonal receiver implemented with this estimation scheme attains the performance of the zonal receiver with a perfect knowledge of the SNR, viz., although the estimator in [91] has errors in practice, the performance of the zonal receiver is weakly sensitive to, and will not be affected by these estimation errors.

3.5.2 Multipath Fading Scenario

In this part, the BER performance of the zonal based Rake receiver in multipath fading UWB channels is evaluated and compared to that of the CMF based Rake receiver. We consider equal-power interferers where the thresholds can be selected according to the SNR and SIR values and Table 3.5. A partial Rake (PRake) receiver [7] which collects first L_{f} arriving paths is considered. The MRC structure is used to combine the outputs of the taps. We consider the CM1 channel model proposed in [4]. The system parameters are the same as those in the ideal free-space propagation scenario given in Table 3.1. For the PRake receiver, the number of Rake fingers, L_{f}, is set to be 1, 5, 10 and 20.

Fig. 3.12 shows the BER curves of the zonal based Rake receiver and the CMF based

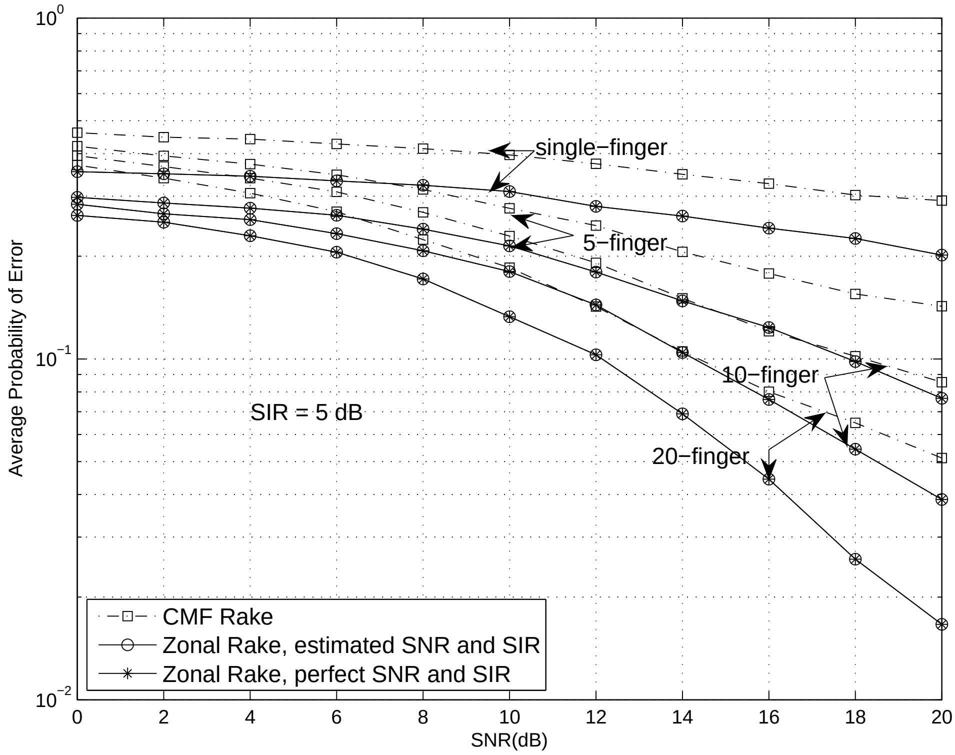

Fig. 3.12. The average BER versus SNR of the CMF and zonal based Rake receivers in CM1 channels, where there are 3 equal-power interferers ($N_\mathrm{u} = 4$) and the SIR = 5 dB.

Rake receiver where there are 3 equal-power interferers ($N_\mathrm{u} = 4$) in the system, the SIR = 5 dB and the values of SNR range from 0 dB to 20 dB in CM1 UWB channels [4]. It is shown in Fig. 3.12 that the zonal based Rake receiver always outperforms the CMF based Rake receiver, and the performance gain grows with increasing SNR. Note also that the performance gain of the zonal based Rake receiver becomes more significant if more paths are combined. For example, for the PRake receiver with $L_\mathrm{f} = 5$ and $L_\mathrm{f} = 10$, the BER of the zonal based Rake receiver is as much as 1.87 times and 2.20 times smaller than that of the CMF based Rake receiver, respectively. As for $L_\mathrm{f} = 20$, the BER of the zonal based structure is as much as 3.08 times smaller than that of the CMF based Rake receiver structure. Note also that the threshold selection of the zonal Rake receiver based on the proposed SNR and SIR estimation scheme works effectively, since the zonal based Rake receiver with thresholds based on the estimated SNR and SIR values can achieve almost the same BER performance as the zonal based Rake receiver with thresholds based on perfect knowledge of these parameters.

Fig. 3.13 shows BER curves for the zonal based Rake receiver and the CMF based Rake

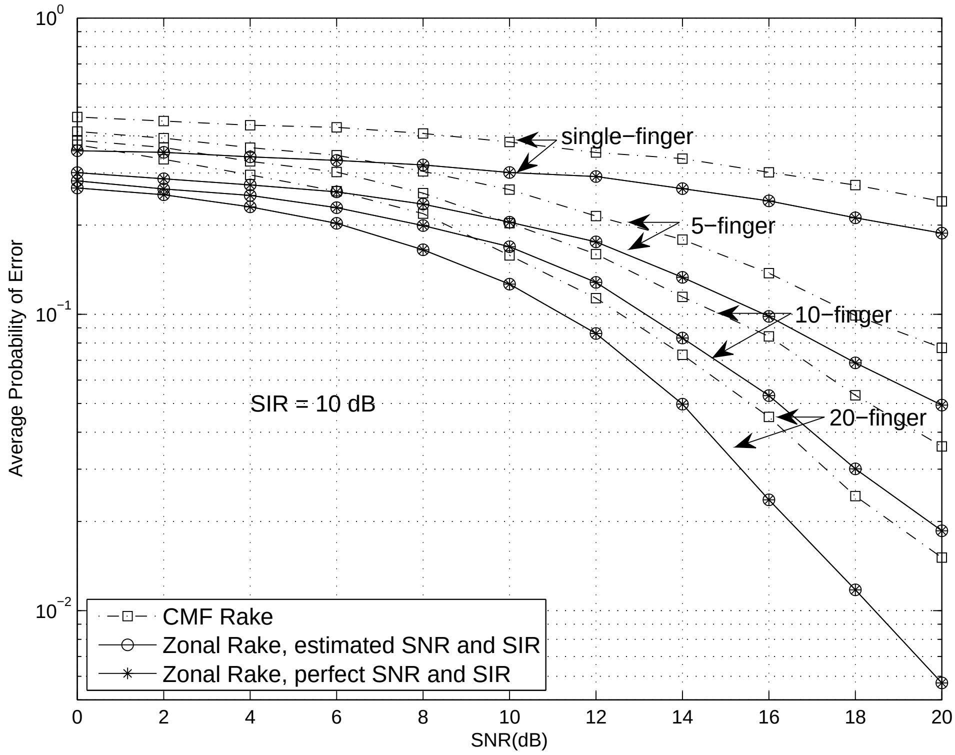

Fig. 3.13. The average BER versus SNR of the CMF and zonal based Rake receivers in CM1 channels, where there are 3 equal-power interferers ($N_{\rm u} = 4$) and the SIR = 10 dB.

receiver for the same operating conditions as in Fig. 3.12 when the SIR is 10 dB. Observe that the BER curves change in the same manner as those in Fig. 3.12. However, it is noted in Fig. 3.13 that, although the zonal based Rake receiver can always achieve better BER performance than the CMF based Rake receiver, the performance gain is not as significant as that seen in Fig. 3.12 with SIR = 5 dB. This is because the MUI component becomes less significant compared to the AWGN term when the value of SNR in the system is fixed and the SIR value gets larger. This behavior of the zonal based Rake receiver makes this novel structure valuable in multipath fading UWB channels when the MUI is strong, as in the free-space propagation scenario.

3.6 Chapter Conclusion

In this chapter, the statistical characteristics of the MUI in IR UWB systems was studied. Simulation results revealed that the UWB correlator output amplitudes can be divided into zones where the transmitted bit can be distinguished with high reliability and zones where the bit is indistinguishable. Based on this qualitative nature of the MUI PDF, a novel UWB receiver structure, the zonal UWB receiver, was proposed using the optimal, minimum probability of error, decision rule. It was shown that this zonal receiver can always outperform the CMF UWB receiver used extensively for signal detection in UWB systems, since the CMF receiver is the zonal receiver with certain parameters. Moreover, it was pointed out that one of the most important characteristics of the UWB MUI is its impulsiveness, and such impulsive noise can be well modeled by a heavy-tailed distribution. It was revealed that the zonal receiver with a nonlinear transform has inherent capability to suppress the impulsive noise. Hence, the superiority of the zonal receiver over the CMF receiver is guaranteed. The implementation of the zonal receiver in pratical systems was also detailed in this chapter, where several effective methods were proposed to choose the parameters for the zonal receiver.

A Rake structure based on the zonal receiver was proposed for UWB signal detection in multipath fading channels. Theoretical analysis and simulation results were used to show the superiority of the zonal based Rake receiver over the conventional Rake receiver based on the CMF structure. It was shown in this chapter that the performance gain of the zonal receiver over the CMF receiver is more significant in interference-limited scenarios where the MUI is the dominant disturbance. This is true for both free-space propagation and multipath fading channels.

Chapter 4

P-Order Metric UWB Receiver[1]

It has been mentioned earlier that the MUI in IR UWB systems deviates from the ubiquitous Gaussian model and has substantially different characteristics than the disturbances in traditional communication systems. Therefore, the CMF, which is the optimal receiver structure for signal recovery in AWGN, is not necessary optimal for detecting signals in IR UWB systems. Better receiver designs for UWB systems can be expected based on more accurate models for the MUI. In Chapter 3, a zonal receiver is proposed heuristically based on simulation data of the MUI. It was also revealed in Chapter 3 that one of the most important characteristics of the MUI is the heavy tail behavior. Therefore, another effective way for studying the MUI in IR UWB systems is to use a heavy-tailed distribution to approximate the MUI. Several heavy-tailed distributions have been used for modeling the MUI in IR UWB systems, and it was shown that these models can described the UWB MUI more accurately than the Gaussian model under certain operating conditions. Based on these models and the optimal, minimum probability of error, decision rule, an ML receiver can be derived to surpass the performance of the CMF [15], [16], [68], [69]. For example, an UWB receiver named the soft-limiting UWB receiver was proposed based on the Laplacian approximation for the UWB MUI [15]. It is worthy mentioning that among all the heavy-tailed distributions, the generalized Gaussian (GG) distribution is an effective and convenient candidate. It starts with the ubiquitous Gaussian distribution, but allows the exponential tail decay rate to be controlled by a free parameter. The superiority of this model is its flexibility to adapt to different channel conditions by properly choosing the

[1] *A version of this chapter has been published in IEEE Transactions on Communications, 56: 1666-1676 (2008), and Proceedings of IEEE Global Communications Conference (GLOBECOM), 4112-4117 (2007).*

shape controlling parameter.

In this chapter, an UWB receiver structure dubbed the "p-order metric" receiver (p-omr) is proposed based on the GG model for the total disturbance (MUI-plus-AWGN) and a p-order metric receiver decision statistic [94], [95]. It is shown that the performance of this UWB receiver structure always exceeds those of the CMF UWB receiver and the soft-limiting UWB receiver [67]. An enhanced version of the p-omr, the p-order metric adaptive threshold limiting receiver (p-omatlr), is proposed by introducing an extra degree of freedom to the p-omr structure. It will be shown that the p-omatlr UWB receiver design meets or surpasses the performance of all of, the CMF UWB receiver, the soft-limiting UWB receiver, and the p-order metric UWB receiver. To exploit the value of the new receiver structures in multipath channels, a new version of the Rake receiver which adopts the p-omr or p-omatlr in each finger is proposed for signal detection when the multipath components are resolvable. It is shown theoretically that this new Rake receiver can achieve larger SINR than the standard CMF based Rake receiver, thus achieving better BER performance in multipath UWB channels. The simulation results also confirm the superiority of the p-omr (p-omatlr) based Rake receiver.

The remainder of this chapter is organized as follows. In Section 4.1 we recall the system model to establish the operating conditions under which the p-omr and p-omatlr are superior. The p-omr structure is described in Section 4.2, while estimation of the shape controlling parameter is discussed in Section 4.3. The enhanced version of the p-omr, the p-omatlr, is proposed in Section 4.4, and Section 4.5 proposes a new Rake receiver based on the p-omr (p-omatlr) for multipath channels. Numerical results for the error rate performances of the p-omr and p-omatlr are discussed in Section 4.6.

4.1 System Model

For simplicity of analysis, the ideal free-space propagation scenario will be investigated first, while a discussion of multipath UWB channels is given in Section 4.5. In an ideal free-space propagation scenario with N_{u} users in the same coverage area, the received signal is given by eq. (3.18) as

$$r\left(t\right)=\sum_{k=1}^{N_{\mathrm{u}}}A_{k}s^{(k)}\left(t-T_{k}\right)+n\left(t\right) \tag{4.1}$$

where $s^{(k)}(t)$ and T_k are the signal and the delay of the *k*th user, respectively. We consider the TH-BPSK UWB signal structure where the mathematical expression for the signal $s^{(k)}(t)$ is given by in eq. (3.1) of Section 3.1. At the receiver side, assuming perfect time synchronization, the conventional single-user matched filter, which adopts $p\left(t - T_1 - mT_f\right)$ as the correlation waveform, is used to coherently detect the signal to be recovered. Adopting the same assumptions as in Section 3.1 and following a similar procedure as eqs. (3.3) - (3.6), the correlator output for the desired information bit can be expressed as (c.f. eq.(3.3))

$$R_{\mathrm{cmf}} = \sum_{m=0}^{N_{\mathrm{s}}-1} R_m = \sum_{m=0}^{N_{\mathrm{s}}-1} \left(S_m + I_m + N_m\right) = \sum_{m=0}^{N_{\mathrm{s}}-1} \left(S_m + Y_m\right) \tag{4.2}$$

where R_m is the chip correlator output in the *m*th frame, $S_m = A_1\sqrt{E_{\mathrm{b}}/N_s}\left(2d_0^{(1)} - 1\right)$ is desired signal component in the *m*th frame, and N_m is a Gaussian RV with variance $N_0/2$. The expression for the interference term I_m was given by eq. (3.6) in Section 3.1 as

$$I_m = \sum_{k=2}^{N_{\mathrm{u}}} \sqrt{\frac{E_{\mathrm{b}}}{N_{\mathrm{s}}}} A_k \left(2d^{(k)}_{\lfloor (m+m_k)/N_{\mathrm{s}} \rfloor} - 1\right) R\left(a_k - c^{(k)}_{m+m_k} T_{\mathrm{c}}\right). \tag{4.3}$$

The RV Y_m in eq. (4.2) is the overall disturbance in the *m*th frame which can be writted as $Y_m = I_m + N_m$. The definitions of other system parameters in eq. (4.3) can be found in Section 3.1.

4.2 P-Order Metric Receiver Structure (P-omr)

Instead of considering the MUI separately as in Chapter 3, we consider the total disturbance in the *m*th frame, Y_m. Fig. 4.1 shows an example of the form of the PDF of the overall disturbance in a single frame, $f_{Y_m}(x)$, with SIR = 10 dB for different SNR values. These results are obtained by simulation where the second derivative of a Gaussian monocycle given by eq. (3.10) is used for signal transmission [58]. The system parameters are given in Table 3.1, and we assume that there are 3 equal-power interferers in the area ($N_{\mathrm{u}} = 4$). The same definitions for the SNR and SIR as in Chapter 3 (c.f. eqs. (3.7) and (3.8)) are adopted. We note that the overall disturbance in a single frame Y_m cannot be simply described as a Gaussian RV or a Laplacian RV. Observe in Fig. 4.1 that when the SNR is small, i.e., the AWGN dominates the MUI, the overall disturbance in a single frame Y_m can be approxi-

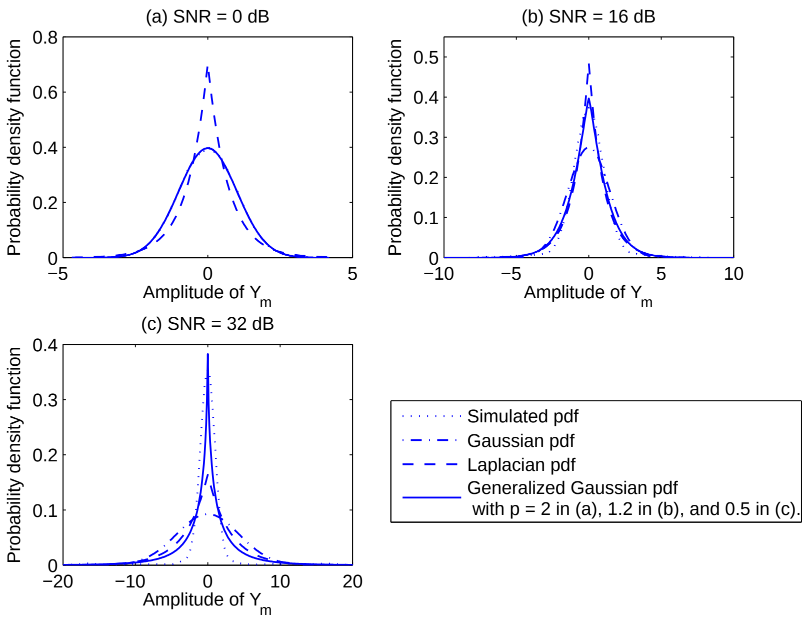

Fig. 4.1. The simulated PDF, $f_{Y_m}(x)$, of the amplitude of the total disturbance sample in each frame; the Gaussian PDF, the Laplacian PDF, and the generalized Gaussian PDF for different values of p are also plotted.

mated as a Gaussian RV. In this case, the CMF UWB receiver works almost as an optimal receiver. As the SNR grows larger, the MUI term I_m becomes more and more significant in $Y_m = I_m + N_m$. Therefore, the distribution of the total disturbance started to show the heavy tail behavior and starts to resemble the Laplacian distribution. This is the reason why the soft-limiting UWB receiver [15], which is the optimal structure for a signal embedded in additive Laplacian noise [96], outperforms the CMF UWB receiver even though the overall disturbance Y_m in this SNR region is not exactly Laplacian distributed. In the SNR region where the SNR is large enough that the MUI dominates the AWGN, neither the Gaussian approximation nor the Laplacian approximation is good model. Observe that the distribution of the total disturbance Y_m changes with the relative powers of the interference and the AWGN, and the Gaussian and Laplacian distribution can only model the ambient noise under certain circumstances. Introducing a new approximation which is flexible for modeling the UWB MUI in different channel conditions is thus motivated.

The GG distribution is effective model to fulfill this expectation, where its PDF is given by [26]

$$f_{\mathrm{gg}}(x; S, \sigma, p) = \frac{1}{2\Gamma(1+1/p)A(p,\sigma)} e^{-|\frac{x-S}{A(p,\sigma)}|^p} \tag{4.4}$$

where S is the mean of the RV, the function $A(p, \sigma) = \left[\frac{\sigma^2 \Gamma(1/p)}{\Gamma(3/p)}\right]^{\frac{1}{2}}$ is a scaling factor which ensures that $\mathrm{var}(x) = \sigma^2$, $\Gamma(x)$ is the gamma function defined as $\Gamma(x) = \int_0^{+\infty} t^{x-1} e^{-t} dt$, and p is the parameter controlling the shape of the distribution. Observe that the PDFs of the Gaussian and Laplacian distributions are special cases of the GG distribution, the Gaussian PDF having $p = 2$ and the Laplacian PDF having $p = 1$. Therefore, the GG distribution is more general than the Gaussian approximation and the Laplacian approximation, and expect to outperform the latters for modeling the disturbance in UWB systems.

Different values of p can be selected to best approximate the PDF of Y_m for different operating conditions. Within the region where the SNR is small and the RV Y_m is approximately Gaussian distributed, $f_{\mathrm{gg}}(x; S, \sigma, p)$ fits the PDF of Y_m by setting p close to 2, while in the region where the SNR values are moderate and the PDF can be approximated by the PDF of the Laplacian distribution, $f_{\mathrm{gg}}(x; S, \sigma, p)$ with $p = 1$ becomes a good approximation of the PDF of the RV Y_m. Note from Fig. 4.1 that the approximate PDF $f_{\mathrm{gg}}(x)$ changes in the same manner with decreasing p as the PDF of Y_m changes with increasing values of the SNR. When the SNR is large, neither the Gaussian nor Laplacian distribution is a good approximation of the PDF of Y_m, and $f_{\mathrm{gg}}(x; S, \sigma, p)$ with p less than 1 approximates the true PDF of Y_m better as indicated in Fig. 4.1 (c).

Recall the optimal, minimum probability of error, decision rule given by eq. (3.11) [82]. For our case, the sampled outputs of the UWB receiver are $R_m = S_m + Y_m = A_1 \sqrt{E_{\mathrm{b}}/N_s}\left(2d_0^{(1)} - 1\right) + Y_m, (m = 0, \cdots, N_{\mathrm{s}} - 1)$ (c.f. eq. (4.2)). Therefore, when the GG distribution is used to model the ambient noise Y_m in UWB systems, the log-likelihood ratio given by eq. (3.11) can be expressed as

$$\begin{aligned} \Lambda_{\mathrm{pomr}} &= \sum_{m=0}^{N_{\mathrm{s}}-1} \log \frac{f_{R_m}(x|d_0^{(1)} = 1)}{f_{R_m}(x|d_0^{(1)} = 0)} \\ &= \sum_{m=0}^{N_{\mathrm{s}}-1} \log \frac{f_{\mathrm{gg}}(R_m; S_m, \sigma, p)}{f_{\mathrm{gg}}(R_m; -S_m, \sigma, p)} = \sum_{m=0}^{N_{\mathrm{s}}-1} g_{\mathrm{pomr}}(R_m) \end{aligned} \tag{4.5a}$$

where $f_{\mathrm{gg}}(x; S, \sigma, p)$ is given by eq. (4.4), and $g_{\mathrm{pomr}}(R_m)$ transforms the single chip correlator output, R_m, into the single sample log-likelihood ratio as [82]

$$\tilde{R}_m = g_{\mathrm{pomr}}(R_m) = \log \left\{ \frac{f_{\mathrm{gg}}\left(R_m; S_m, \sigma, p | d_0^{(1)} = 1\right)}{f_{\mathrm{gg}}\left(R_m; S_m, \sigma, p | d_0^{(1)} = 0\right)} \right\} = |R_m + S_m|^p - |R_m - S_m|^p. \tag{4.5b}$$

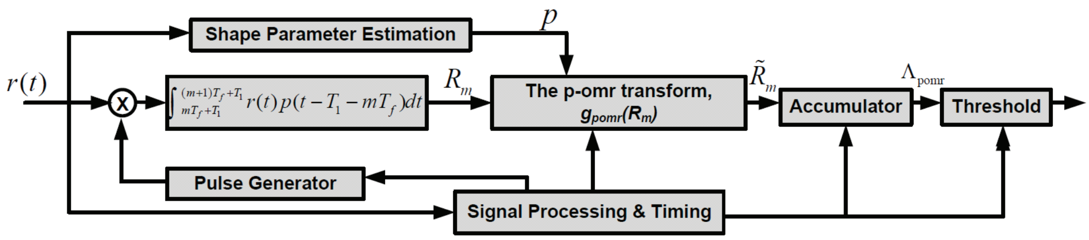

Fig. 4.2. The block diagram for the p-order metric UWB receiver.

The decision rule given by eq. (3.12) is used for making detection decisions. The structure of the p-omr is shown in Fig. 4.2. Note that if $p = 2$, the p-omr becomes exactly the same as the CMF UWB receiver, and if p assumes the value of 1, the p-omr becomes the same as the soft-limiting UWB receiver [67].

We digress here to discuss the transform function $g_{\text{pomr}}(\cdot)$ for the p-omr given by eq. (4.5b). The transform function is plotted in Fig. 4.3 for $p = 0.5$, $p = 1$ and $p = 2$. Note that the transform function takes the correlator outputs R_m $(m = 0, \cdots, N_{\text{s}} - 1)$ and transform them into partial decision statistics $\tilde{R}_m$ $(m = 0, \cdots, N_{\text{s}} - 1)$ which are summed to make the final decision. Note that with $p = 2$, the GG distribution becomes the Gaussian distribution and the corresponding transform function in the ML receiver, $g_{\text{pomr}}(\cdot)$, is linear as shown in Fig. 4.2. However, as the shape parameter decreases, the distribution of Y_m becomes impulsive and heavy-tailed. As mentioned in Chapter 3, an intuitive implication of the heavy tail behavior is that the probability of observing noise samples with large amplitudes in practice is higher than that would be predicted by the Gaussian noise model. Therefore, with such noises, the correlator output samples with amplitudes far away from S_m and $-S_m$ are not reliable since they might be caused by the impulsive noise. Under such circumstances, $g_{\text{pomr}}(\cdot)$ becomes nonlinear and has a tendency to suppress these samples; small weights are put to them to decrease their effects on the final decision statistic, as shown in Fig. 4.3.

We emphasize that the design of the p-omr structure is based on an approximation of the true PDF. That is, as the zonal receiver proposed in Chapter 3, the p-omr is not optimal. However, the p-omr becomes exactly the same as the CMF UWB receiver or the the soft-limiting UWB receiver for certain values of p, which implies that if the shape parameter p is properly chosen, the p-omr can always meet or outperform both the CMF UWB receiver

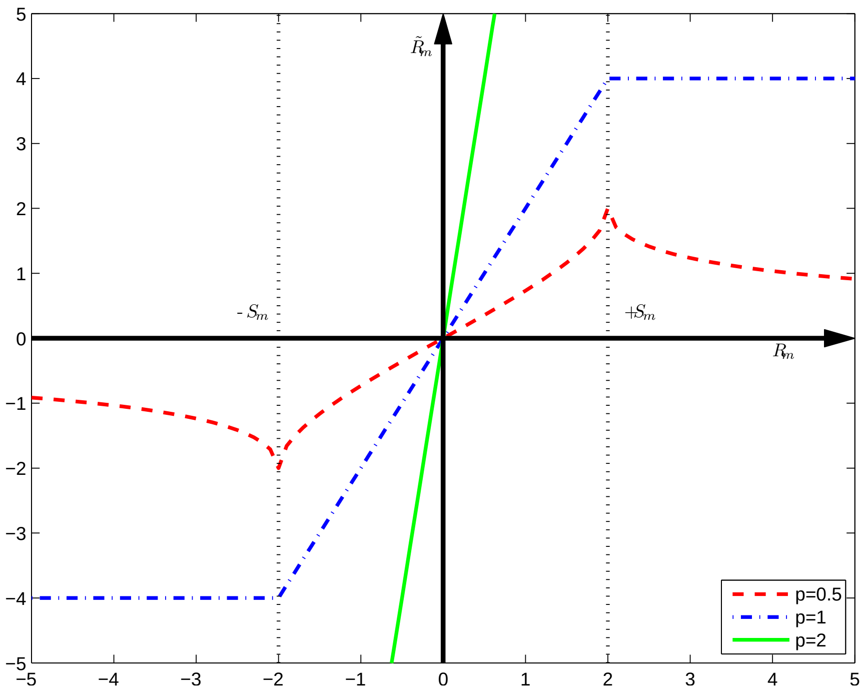

Fig. 4.3. The transform function $g_{\mathrm{pomr}}(\cdot)$ in the p-omr.

and the soft-limiting UWB receiver.

4.3 P-omr Implementation: Estimation of the Shape Parameter

In order to implement the p-omr for signal detection, the shape parameter p in the transform function needs to be chosen properly (c.f. eq. (4.5)). Note that p should be selected so that the generalized Gaussian PDF can best describe the essential characteristics of the total disturbance in UWB systems, and the most significant difference between the distribution of the ambient noise in UWB systems and the Gaussian PDF is the heaviness of the distribution tail. Moreover, it has been mentioned in Chapter 3 that, for a zero mean RV X, the heaviness of its distribution tail can be well measured by its excess *kurtosis*, which is given by (c.f. eq. (3.16))

$$\kappa = \frac{\mathbb{E}(X^4)}{\mathbb{E}^2(X^2)} - 3. \tag{4.6}$$

Therefore, we use a *kurtosis* matching method to find the shape parameter p.

Note that the odd central moments of a RV X with PDF $f_{\mathrm{gg}}(x; 0, \sigma, p)$ are all zeros, and the even central moments of X are given by [97]

$$\mathbb{E}(X^n) = \left[\frac{\sigma^2\Gamma(1/p)}{\Gamma(3/p)}\right]^{n/2} \frac{\Gamma((n+1)/p)}{\Gamma(1/p)}. \tag{4.7}$$

Thus, the excess *kurtosis* of a zero mean GG distributed RV X can be expressed as

$$\kappa = \frac{\mathbb{E}(X^4)}{\mathbb{E}^2(X^2)} - 3 = \frac{\Gamma(1/p)\Gamma(5/p)}{\Gamma^2(3/p)} - 3. \tag{4.8}$$

Note that, the shape parameter p is the only argument on the right side of eq. (4.8). Moreover, as a function of p, the kurtosis given by eq. (4.8) is monotonically decreasing. Therefore, once the excess *kurtosis* is obtained, the shape parameter p can be solely determined.

The excess *kurtosis* of the disturbance in an UWB system can be determined theoretically based on prior knowledge of the system. It can also be estimated at the receiver. The latter method can be used conveniently for signal detection in practial UWB systems since no prior knowledge of the operating scenario is required, and the estimation can be done periodically to adapt the shape parameter p to the current channel condition. However, the former method is important for system designs since it can be used to obtain the shape parameter and predict the system performance without setting up the network. We here briefly describe the former method, while the latter method is used in Section 4.6 to implement the p-omr and perform the signal detection. For simplicity of analysis, the free-space propagation scenario is considered. Note that the expression for the UWB MUI is given by eq. (4.3). Therefore, assuming that the signals from different users are independent, the second and fourth moments of I_m are given by

$$\mathbb{E}(I_m^2) = \frac{E_\mathrm{b}\sum_{k=2}^{N_\mathrm{u}-1} A_k^2}{N_\mathrm{s}T_\mathrm{f}} \int_{-\infty}^{\infty} R^2(x)dx \tag{4.9}$$

and

$$\begin{aligned}\mathbb{E}(I_m^4) \;=\; & \left(\frac{E_\mathrm{b}}{N_\mathrm{s}}\right)^2 \left[\left(\frac{1}{T_f}\int_{-\infty}^{\infty} R^4(x)dx\right)\sum_{k=2}^{N_\mathrm{u}-1} A_k^4\right. \\ & \left. +6\left(\frac{1}{T_f}\int_{-\infty}^{\infty} R^2(x)dx\right)^2 \sum_{k=2}^{N_\mathrm{u}-1}\sum_{k_1=k+1}^{N_\mathrm{u}} A_k^2 A_{k_1}^2\right]\end{aligned} \tag{4.10}$$

respectively. A proof for eqs. (4.9) and (4.10) is given in Appendix A. Assuming that the AWGN and MUI component both have zero means and are independent, the mean of the total disturbance term $Y_m = I_m + N_m$ is also zero, and its second and fourth moments can be expressed

$$\mathbb{E}(Y_m^2) = \mathbb{E}(I_m^2) + \mathbb{E}(N_m^2) \tag{4.11}$$

and

$$\mathbb{E}(Y_m^4) = \mathbb{E}(I_m^4) + 6\mathbb{E}(I_m^2)\mathbb{E}(N_m^2) + \mathbb{E}(N_m^4) \tag{4.12}$$

respectively. Hence, the excess *kurtosis* of Y_m is given as

$$\kappa = \frac{\mathbb{E}(Y_m^4)}{\mathbb{E}^2(Y_m^2)} - 3 = \frac{\mathbb{E}(I_m^4) + 6\mathbb{E}(I_m^2)\mathbb{E}(N_m^2) + \mathbb{E}(N_m^4)}{[\mathbb{E}(I_m^2) + \mathbb{E}(N_m^2)]^2} - 3 \tag{4.13}$$

where $\mathbb{E}(I_m^2)$ and $\mathbb{E}(I_m^4)$ are the second and fourth moments of I_m given by eqs. (4.9) and (4.10), respectively, and $\mathbb{E}(N_m^2) = N_0/2$ and $\mathbb{E}(N_m^4) = 3(N_0/2)^2$ are the variance and the fourth moment of the AWGN component in the *m*th frame. Therefore, if the system parameters on the right sides of eqs. (4.9) and (4.10) and the PSD of the AWGN component are known, the shape parameter p can be calculated by matching eq. (4.13) with eq. (4.8) as

$$\frac{\Gamma(1/p)\Gamma(5/p)}{\Gamma^2(3/p)} = \frac{\mathbb{E}(I_m^4) + 6\mathbb{E}(I_m^2)\mathbb{E}(N_m^2) + \mathbb{E}(N_m^4)}{[\mathbb{E}(I_m^2) + \mathbb{E}(N_m^2)]^2}. \tag{4.14}$$

Fig. 4.4 shows the excess *kurtosis* of Y_m based on simulation and theoretical analysis when both MUI and AWGN are present in the channel. Equal-power interferers are considered and we assume that there are $N_\mathrm{u} = 4$ users in the system. The SIR is fixed to be 10 dB while the SNR ranges from 0 dB to 36 dB. Note that when the SNR value is small and the AWGN is significant, the total disturbance resembles a Gaussian RV with excess *kurtosis* 0. However, as the SNR value increases, the MUI component becomes the dominant disturbance. Under such circumstances, the distribution of the total disturbance becomes impulsive and heavy-tailed, and the excess *kurtosis* is shown to be much larger than 0. Note that in this case, the GG distribution can adjust the shape parameter p and provide a better approximation for the total disturbance than the Gaussian and Laplacian distributions. Therefore, the p-omr and p-omaltr based on the GG approximation should have a significant improvement over the receivers based on the Gaussian and Laplacian approximations for the disturbance in this SNR regime.

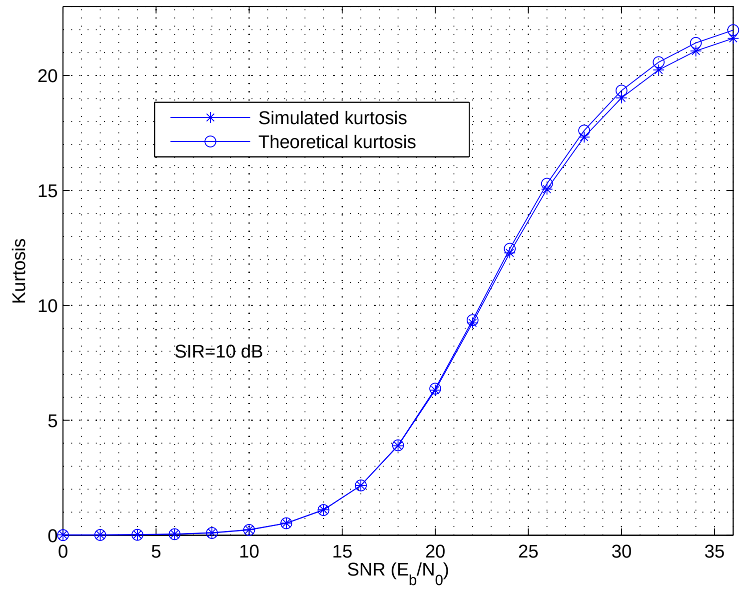

Fig. 4.4. The simulated and theoretical values of the excess *kurtosis*, when there are 3 equal-power interferers in the systems ($N_{\mathrm{u}} = 4$) and the SIR = 10 dB.

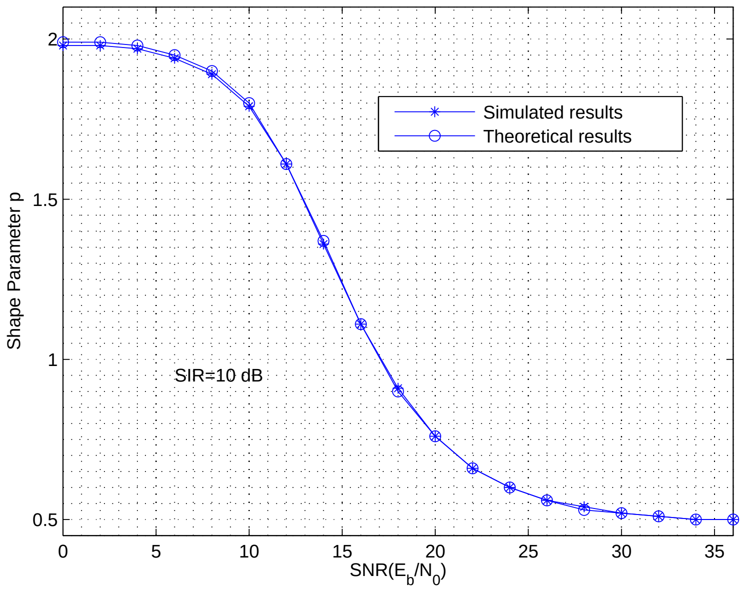

Fig. 4.5. The shape parameter p obtained by the simulated and theoretical values of the excess *kurtosis*, when there are 3 equal-power interferers in the systems ($N_{\mathrm{u}} = 4$) and the SIR = 10 dB.

Fig. 4.5 shows the estimates of the shape parameter p obtained from the simulated and theoretical estimates of the excess *kurtosis* for the example of Fig. 4.4. It is seen that, the theoretical method can provide accurate prediction of the shape parameter p.

4.4 P-Order Metric Adaptive Threshold Limiting Receiver (P-omatlr)

Recall the p-omr structure given by eq. (4.5). Observe that not all the system potentials are exploited by this structure. An extra degree of freedom can be introduced by replacing the desired signal component S_m in eq. (4.5) with an adaptive threshold, i.e., the transform $g_{\mathrm{pomr}}(x)$ in the receiver can be improved as

$$g_{\mathrm{pomatlr}}\left(R_m\right) = |R_m + T_{\mathrm{opt}}|^p - |R_m - T_{\mathrm{opt}}|^p. \tag{4.15}$$

The final decision statistic of the this receiver is the same as that of the p-omr given by eq. (4.5a), except that $g_{\mathrm{pomr}}(\cdot)$ is replaced by $g_{\mathrm{pomatlr}}(\cdot)$ in eq. (4.15). We name this receiver structure the p-order metric adaptive threshold limiting receiver (p-omatlr). To implement this receiver, two steps should be taken; the shape parameter p is determined either by theoretical calculation or estimation as described in Section 4.3, and the threshold T_{opt} is selected by empirical search to obtain the best performance according to certain criterion. Theoretically, the new receiver must always meet or outperform the CMF UWB receiver, the soft-limiting UWB receiver and the p-omr, since all these receivers are special cases of the p-omatlr. This will be true for arbitrary additive signal disturbances, including MUI, AWGN, and MUI-plus-AWGN.

4.5 P-omr (P-omatlr) in Multipath Fading Channels

We proposed the p-omr and p-omatlr in free-space propagation channels. It has been mentioned in Section 3.3 that the ideal free-space propagation channel model does not reflect a typical UWB transmission scenario. In practical systems, IR UWB signals propagate through multipath fading channels where the Rake receiver or the autocorrelation receiver with TR signaling are widely adopted. As in Chapter 3, we consider the Rake reception for UWB signal recovery. Since it has been shown in Section 3.3 that the total disturbance

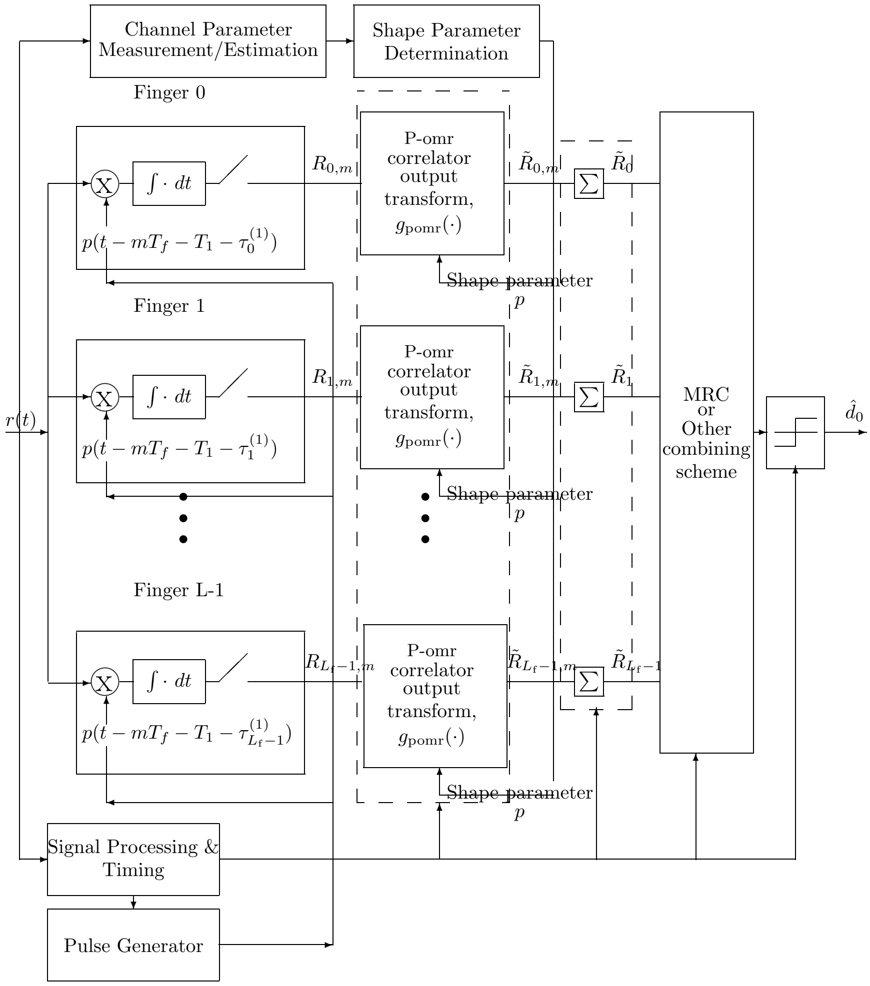

Fig. 4.6. The structure of the new Rake receiver adopting p-omr or p-omatlr in each finger.

in a particular Rake finger does not necessarily resemble the Gaussian distribution even in highly dense multipath fading channels, the p-omr (p-omatlr) is expected to enhance the performance of the CMF under such circumstances.

The structure of the p-omr (p-omatlr) based Rake receiver is shown in Fig. 4.12, where the p-omr (p-omatlr) transform is performed in each Rake finger. This new Rake receiver can achieve larger SINR than the CMF based Rake receiver, as shown in the sequel.

4.5.1 Theoretical Proof of the Superiority of the P-omr (P-omatlr) in UWB Multipath Fading Channels

We consider a special case and proof the superiority of the p-omr (p-omatlr) in UWB multipath fading channels. Let $R_{l,m} = S_{l,m} + Y_{l,m}$ $(m = 0, \cdots, N_{\text{s}} - 1;\ l = 0, \cdots, L_{\text{f}} - 1)$

denote the correlator output of the *m*th frame in the *l*th finger, where N_s is the length of the repetition code for each information bit and L_f is the number of fingers in the Rake receiver. The parameters $S_{l,m}$ and $Y_{l,m}$ are the desired signal component and the total disturbance in $R_{l,m}$. Assume that $Y_{l,m}$ can be well modeled by a Laplacian distribution (the generalized Gaussian distribution with $p = 1$), the disturbance terms in different frames are i.i.d. and independent of the desired signal. Therefore, the PDF of $R_{l,m}$ can be expressed as

$$f_{R_{l,m}}(x) = \frac{1}{2b}\exp\left(-\frac{|x - S_{l,m}|}{b}\right) \tag{4.16}$$

and the cumulative density function (CDF) can be written as

$$F_{R_{l,m}}(x) = \frac{1}{2}\left[1 + \mathrm{sgn}(x - S_{l,m})\left(1 - e^{-|x-S_{l,m}|/b}\right)\right] \tag{4.17}$$

where $\mathrm{sgn}(x)$ is the sign function defined as

$$\mathrm{sgn}(x) = \begin{cases} -1, & \text{if } x < 0 \\ 0, & \text{if } x = 0 \\ 1, & \text{if } x > 0 \end{cases} . \tag{4.18}$$

The mean of $R_{l,m}$ is $\mathbb{E}\left(R_{l,m}\right) = S_{l,m}$, and the variance is $\mathrm{var}(R_{l,m}) = 2b^2$. For CMF based Rake receiver, the decision statistic in the *l*th Rake finger can be represented as

$$R_l = \sum_{m=0}^{N_\mathrm{s}-1} R_{l,m}. \tag{4.19}$$

The mean of R_l is

$$\mathbb{E}(R_l) = \mathbb{E}\left(\sum_{m=0}^{N_\mathrm{s}-1} R_{l,m}\right) = N_\mathrm{s}\mathbb{E}(R_{l,m}) = N_\mathrm{s}S_{l,m} \tag{4.20}$$

and the variance is

$$\mathrm{var}(R_l) = N_\mathrm{s} \cdot \mathrm{var}\left(R_{l,m}\right) = 2N_\mathrm{s}b^2. \tag{4.21}$$

Note that the SINR of the decision statistic X in a transmission system is given by $\mathrm{SINR} = \mathbb{E}^2(X)/\mathrm{var}(X)$, the SINR in *l*th finger of the CMF based Rake receiver can be expressed as

$$\mathrm{SINR}_{l,\mathrm{CMF}} = \frac{\mathbb{E}^2(R_l)}{\mathrm{var}(R_l)} = N_\mathrm{s} \cdot \frac{S_{l,m}^2}{2b^2}. \tag{4.22}$$

Consider now the p-omr Rake receiver structure in Fig. 4.12. Based on the assumption that the shape parameter is 1, the new correlator output $\tilde{R}_{l,m}$ after the p-omr is obtained from $R_{l,m}$ through the transform

$$\tilde{R}_{l,m} = \begin{cases} S_{l,m}, & \text{if} \quad R_{l,m} \geq S_{l,m} \\ R_{l,m}, & \text{if} \quad -S_{l,m} < R_{l,m} < S_{l,m} \\ -S_{l,m}, & \text{if} \quad R_{l,m} \leq -S_{l,m} \end{cases}. \tag{4.23}$$

Let $f_{\tilde{R}_{l,m}}(x)$ denote the PDF of $\tilde{R}_{l,m}$, which can be obtained by the transformation theory for RVs [73, Ch. 5]. The mean of $\tilde{R}_{l,m}$ can be given as

$$\mathbb{E}(\tilde{R}_{l,m}) = \int_{-\infty}^{+\infty} x f_{\tilde{R}_{l,m}}(x) dx = S_{l,m} - \frac{b}{2}\left(1 - e^{-2S_{l,m}/b}\right) \tag{4.24}$$

and its variance is

$$\begin{aligned} \mathrm{var}(\tilde{R}_{l,m}) &= \mathbb{E}(\tilde{R}_{l,m}^2) - \mathbb{E}^2(\tilde{R}_{l,m}) \\ &= \frac{3}{4}b^2 - \left(2bS_{l,m} + \frac{b^2}{2}\right) e^{-2S_{l,m}/b} - \frac{b^2}{4} e^{-4S_{l,m}/b}. \end{aligned} \tag{4.25}$$

The decision statistic in *l*th finger of the new Rake receiver can be represented as

$$\tilde{R}_l = \sum_{m=0}^{N_\mathrm{s}-1} \tilde{R}_{l,m}. \tag{4.26}$$

with mean

$$\mathbb{E}(\tilde{R}_l) = \mathbb{E}(\sum_{m=0}^{N_\mathrm{s}-1} \tilde{R}_{l,m}) = N_\mathrm{s} \cdot \mathbb{E}(\tilde{R}_{l,m}) \tag{4.27}$$

and variance

$$\mathrm{var}(\tilde{R}_l) = N_\mathrm{s} \cdot \mathrm{var}(\tilde{R}_{l,m}) \tag{4.28}$$

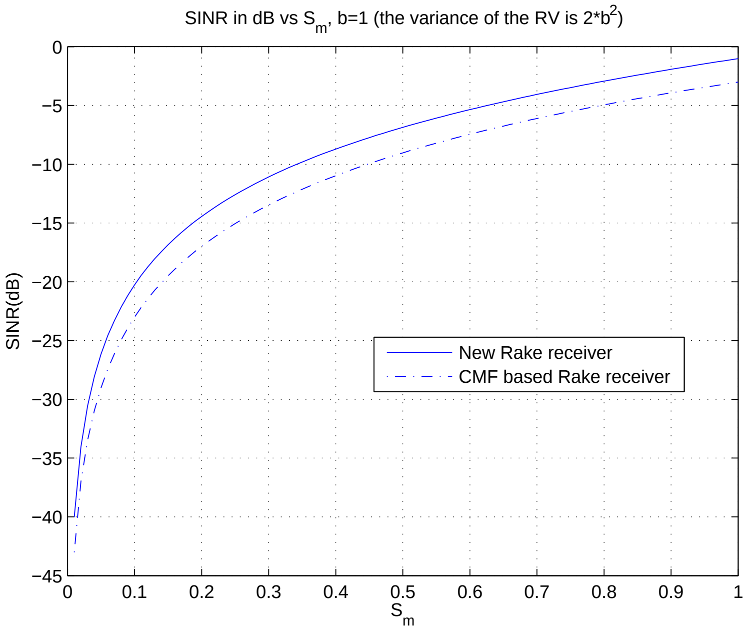

Fig. 4.7. Comparison of the SINR (the factor N_s is omitted) in each finger of the CMF and p-omr based Rake receivers, when the ambient noise is Laplacian distributed and the shape parameter for the p-omr is $p = 1$.

where $\mathbb{E}(\tilde{R}_{l,m})$ and $\mathrm{var}(\tilde{R}_{l,m})$ are given by eqs. (4.24) and (4.25), respectively. The SINR in the lth finger of the new Rake receiver can, thus, be expressed as

$$\mathrm{SINR}_{l,\mathrm{pomr}} = \frac{\mathbb{E}^2(\tilde{R}_l)}{\mathrm{var}(\tilde{R}_l)} = N_\mathrm{s} \cdot \frac{S_m^2 - S_m b(1 - e^{-2S_m/b}) + \frac{b^2}{4}(1 - e^{-4S_m/b})}{\frac{3}{4}b^2 - \left(2bS_m + \frac{b^2}{2}\right) e^{-2S_m/b} - \frac{b^2}{4} e^{-4S_m/b}}. \tag{4.29}$$

Eq. (4.22) gives the SINR in each finger of the CMF based Rake receiver, while that of the new Rake receiver adopting the p-omr is given in eq. (4.29). The SINR values are compared in Fig. 4.7. The factor N_s is omitted since it doesn't affect the results of the comparison. Observe that the p-omr based Rake receiver has substantial SINR gain, more than 3 dB, over the CMF based Rake receiver for all values of $S_{l,m}$, and that the SINR gain is monotonically increasing with SINR. Using asymptotic analysis and compare the SINRs given by eqs. (4.22) and (4.29), the SINR gain of the p-omr based Rake receiver over the CMF based Rake receiver is $2 = 3.01$ dB for small values of SINR, and $8/3 = 4.26$ dB for large values of SINR. It has been mentioned in Section 3.3 that when MRC is used to combining signals from different paths, the SINR for the statistic R after combining is $\mathrm{SINR}_\mathrm{MRC} = \sum_{l=0}^{L_\mathrm{f}-1} \mathrm{SINR}_l$ (c.f. eq. (3.28)), where SINR_l and $\mathrm{SINR}_\mathrm{MRC}$ are the SINR values in the lth Rake finger and after combining, respectively [88]. Since the value of

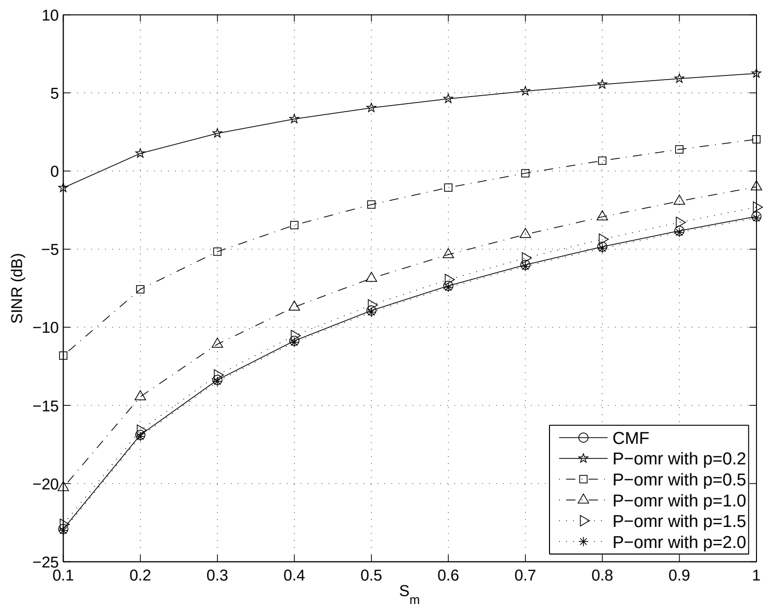

Fig. 4.8. Comparison of the SINR (the factor N_{s} is omitted) in each finger of the CMF based and the p-omr based Rake receiver, when the shape parameter p assumes different values.

$\mathrm{SINR}_{l,\mathrm{pomr}}$ is between 2 times and 8/3 times $\mathrm{SINR}_{l,\mathrm{cmf}}$ for all values of l, we have

$$2 \cdot \mathrm{SINR}_{\mathrm{MRC,cmf}} \leq \mathrm{SINR}_{\mathrm{MRC,pomr}} \leq \frac{8}{3} \cdot \mathrm{SINR}_{\mathrm{MRC,cmf}} \tag{4.30}$$

where $\mathrm{SINR}_{\mathrm{MRC,cmf}}$ and $\mathrm{SINR}_{\mathrm{MRC,pomr}}$ denote the SINR of the statistics after diversity combining for the CMF and p-omr based Rake receiver, respectively.

The preceding discussion for p = 1 clarifies the mechanism of the SINR improvement. To show that there is also a SINR gain for the p-omr over the CMF for other values of p, we present the results in Fig. 4.8. Fig. 4.8 shows the output SINRs in each finger of the CMF based Rake receiver, and those of the p-omr based Rake receiver, when the shape parameter p in the system equals 0.2, 0.5, 1.0, 1.5 and 2.0. The results in Fig. 4.8 are obtained numerically. It is seen that the SINR gains of the p-omr based Rake receiver are significant when p is small, and decrease as p gets close to 2 where the GG distribution becomes the Gaussian distribution and the p-omr has the same structure as the CMF receiver. It is seen in Fig. 4.8 that the gain for the p-omr with $p = 0.2$ over the CMF is as much as 20 dB. As for systems with $p = 0.5$, the largest SINR gain decreases to 11 dB. The SINR curves for the p-omr based and the CMF based Rake receivers agree perfectly when $p = 2$, and the SINR gains are 0 in this case.

Note that, as long as the multipath components in UWB channels are resolvable so that the Rake receiver is viable, the p-omr based Rake receiver always performs at least as well the CMF based Rake receiver (with $p = 2$, the SINR gain is 0 dB, and the p-omr based Rake receiver becomes exactly the same as the CMF based Rake receiver). The fact that the new Rake receiver adopting the p-omr or p-omatlr in each Rake finger can achieve larger SINR values than the CMF based Rake receiver makes the designs of the p-omr and p-omaltr valuable not only in ideal free-space propagation (AWGN) channels, but also in multipath UWB channels.

4.6 Numerical Results and Discussion

4.6.1 Ideal Free-Space Propagation Scenario

We first evaluate the average BER performances of the p-omr and the p-omatlr in an ideal free-space propagation channel, and compare them with those of the CMF UWB receiver and the soft-limiting UWB receiver [67]. The signal waveform is the second derivative of a Gaussian monocycle given by eq. (3.10) and the system parameters are the same as given in Table 3.1. We consider equal-power interferers and assume that there are $N_{\mathrm{u}} = 4$ users in the system. It has been mentioned above that, for the p-omr and p-omatlr, the shape parameter p can be calculated based on the theoretical analysis provided in Section 4.3 if all the required system parameters are already known, or it can be obtained by estimating the excess *kurtosis* and matching it with the right side of eq. (4.8). In this section, we refer to the latter method. As for the p-omatlr, we first estimate the shape parameter p, and then optimize the threshold T_{opt} to maximize the SINR value in a single frame through a empirical search.

Fig. 4.9 shows the BER curves of the CMF UWB receiver, the soft-limiting UWB receiver, the p-omr and the p-omatlr operating in free-space propagation channels. For comparison, the BER curves for the p-omr and the p-omatlr with perfect knowledge of the excess *kurtosis* of the total disturbance in the channel are also plotted. The SIR value is 10 dB and the SNR ranges from 0 to 36 dB. Equal-power interferers are considered where the number of users in the same coverage is $N_{\mathrm{u}} = 4$. The optimal values for T_{opt} is plotted in Fig. 4.10. Theoretically, since the p-omr becomes the CMF UWB receiver by setting p to equal 2 and the soft-limiting UWB receiver by setting p to equal 1, the p-

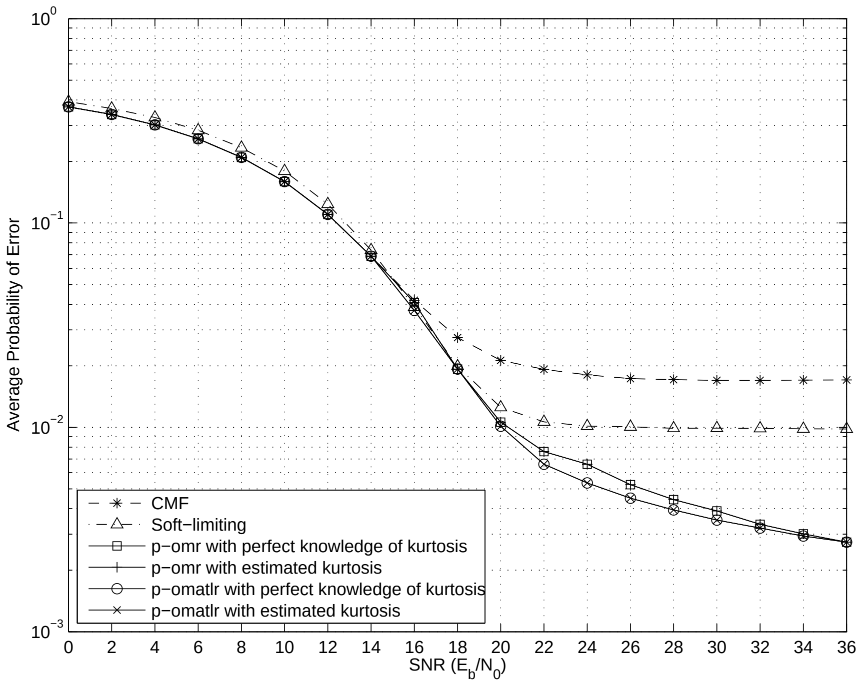

Fig. 4.9. The average BER versus SNR of the CMF UWB receiver, the soft-limiting UWB receiver, the p-omr and the p-omatlr in an ideal free-space propagation channel, where there are 3 equal-power interferers ($N_{\mathrm{u}} = 4$) and the SIR = 10 dB.

omr can always meet or outperform the CMF UWB receiver and the soft-limiting UWB receiver. Furthermore, since the p-omatlr with $T_{\mathrm{opt}} = S_m$ becomes the p-omr, the p-omatlr must always perform as well as or better than all the other receivers. Observe that when the SNR is small, i.e. the AWGN dominates the MUI, the overall disturbance in a single frame $Y_m = I_m + N_m$ can be approximated as a Gaussian distributed RV, and the CMF UWB receiver works essentially as well as an optimal receiver [27]. Under such circumstances, the p-omr and the p-omatlr can adjust the parameter p to meet the BER performance of the CMF UWB receiver. As the SNR gets large to the point where the background noise stops dominating the MUI, the BER performance of the soft-limiting UWB receiver begins to surpass that of the CMF UWB receiver. The p-omr and the p-omatlr attain the BER performance of the soft-limiting UWB receiver in this SNR region by changing the parameter p from 2 to values close to 1. Note also that when the SNR exceeds 20 dB, the BER curves of the CMF UWB receiver and the soft-limiting UWB receiver both reach error rate floors while the BER curves of the p-omr and the p-omatlr keep decreasing, attaining significantly smaller BERs for large values of SNR. For example, when SNR = 36 dB, the BER of the p-omr and the p-omatlr is 2.7×10^{-3}, which is 6.31 times smaller

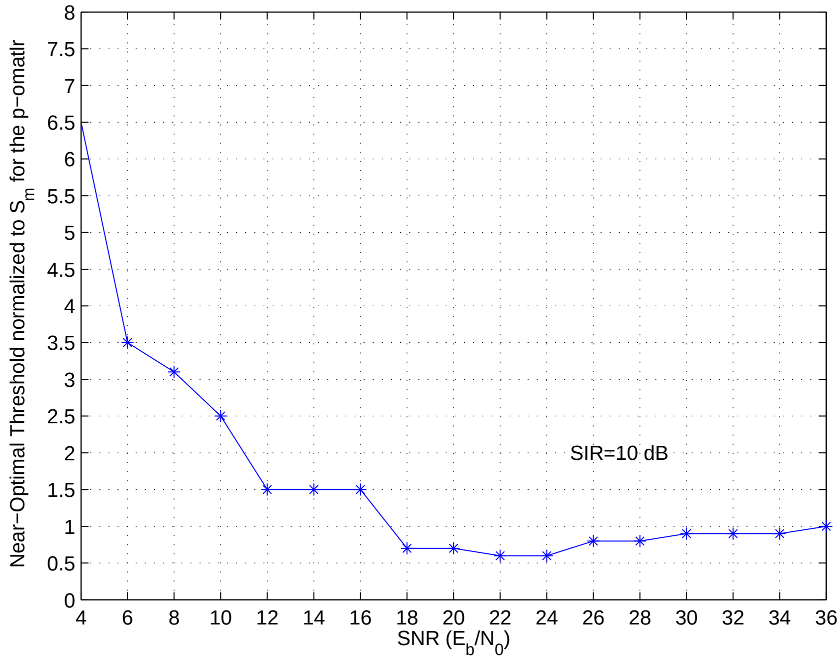

Fig. 4.10. The optimal threshold $T_{\rm opt}$, normalized to S_m, of the p-omatlr for the operating condition in Fig. 4.9.

than the BER of the CMF UWB receiver (1.71×10^{-2}) and 3.62 times smaller than the BER of the soft-limiting UWB receiver (9.8×10^{-3}). The p-omr and the p-omatlr do reach error rate floors, but not until values of SNR above 45 dB in this operating condition. In a practical scenario, the p-omr and the p-omatlr do not have error rate floors for this value of SIR, because such large values of SNR cannot usually be achieved in practical wireless systems. Observe that the p-omatlr with adaptive threshold T_{opt} always achieves the best performance in all operating conditions. It is seen in Fig. 4.9 that the p-omatlr improves the BER performance of the p-omr for all values of SNR. Of particular interest, observe that there is a reduction in BER achieved by the p-omatlr over the p-omr in the SNR region from 18 dB to 35 dB. The improvement is as much as 2.95 dB in SNR, achieved at a BER of 5×10^{-3}.

Fig. 4.11 shows the BER curves of the CMF UWB receiver, the soft-limiting UWB receiver, the p-omr and the p-omatlr for the same operating conditions as in Fig. 4.9, where the SIR = 5 dB. The BER curves under such circumstances change in the same manner as those in Fig. 4.9. Comparison of the results in Figs. 4.11 and 4.9 shows that the BER performance gains of the p-omr and p-omatlr receivers over the CMF UWB receiver are more

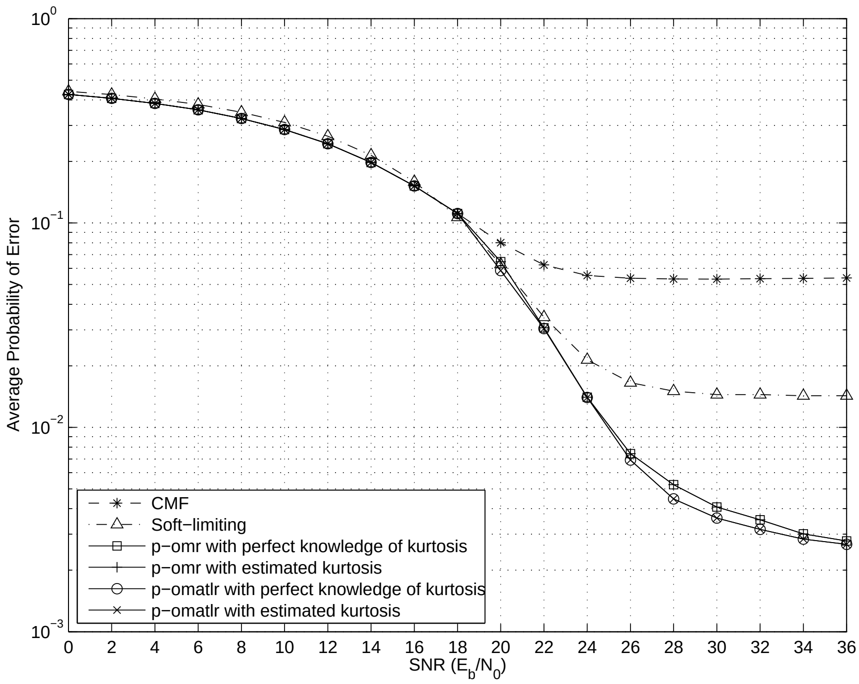

Fig. 4.11. The average BER versus SNR of the CMF UWB receiver, the soft-limiting UWB receiver, the p-omr and the p-omatlr when there are 3 equal-power interferers in the system and the SIR = 5 dB.

significant when the value of SIR is smaller, i.e., the MUI term is relatively stronger. This makes the p-omr and p-omatlr designs valuable in interference-limited scenarios. Moreover, it is worth mentioning that the shape parameter obtained by excess *kurtosis* estimation is quite accurate since the p-omr (p-omatlr) with shape parameter obtained by this estimation scheme achieves almost the same BER performance as the p-omr (p-omatlr) with perfect knowledge of the excess *kurtosis* as seen in Figs. 4.9 and 4.11.

4.6.2 Multipath Fading Scenario

We here examine the superiority of the p-omr in UWB multipath fading channels. We assume that there are 3 equal-power interferers in the system and the SIR = 10 dB. The number of Rake fingers is $L_{\mathrm{f}} = 10$. The BER curve of the p-omr based Rake receiver in a CM1 multipath fading channel [4] is shown in Fig. 4.12. The BER curve for the CMF based Rake receiver, which has been widely used for UWB signal detection in multipath fading channels, is also plotted for comparison. Observe that, as in free-space propagation channels, the p-omr can highly enhance the BER performance of the CMF receiver. Fig. 4.12 shows that at the error level of 10^{-1}, the reduction in BER achieved by the p-omr

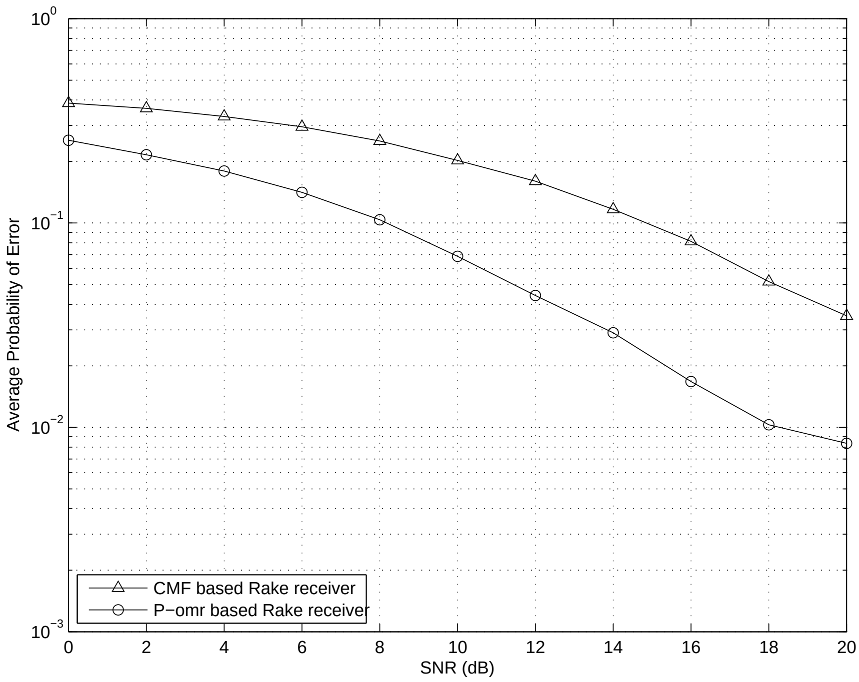

Fig. 4.12. The average BER versus SNR of the CMF based and the p-omr based Rake receivers in a CM1 channel [4], when there are 3 equal-power interferers ($N_\mathrm{u} = 4$), the SIR = 10 dB and the number of Rake fingers is $L_\mathrm{f} = 10$.

based Rake receiver over the CMF based Rake receiver is as much as 4.6 dB. Therefore, the p-omr is an effective receiver structure for UWB signal detection since it can highly enhance the system performance of the CMF receiver without complicating the receiver structure extensively, for both free-space propagation or multipath fading scenarios.

4.7 Overview of Novel UWB Receiver Designs

Up to this point, three novel UWB receivers have been proposed. We here briefly compare different receiver structures. Fig. 4.13 compares the BER performances of the zonal and the p-omr under the same operating condition as in Fig. 4.9. Observe that the p-omr and the zonal receiver have almost the same BER performance for the case we are examining, and both outperform the CMF UWB receiver[2]. However, it is worth mentioning that the implementation of p-omr is easier since the shape parameter in the receiver structure can be obtained by theoretical calculations or by the excess *kurtosis* matching at the receiver, while for the zonal UWB receiver, adapted thresholds based on presimulated results should

[2]The p-omr usually has a slightly better performance than the zonal receiver, as shown in [3] and by comparison of Figs. 4.12 and 3.13.

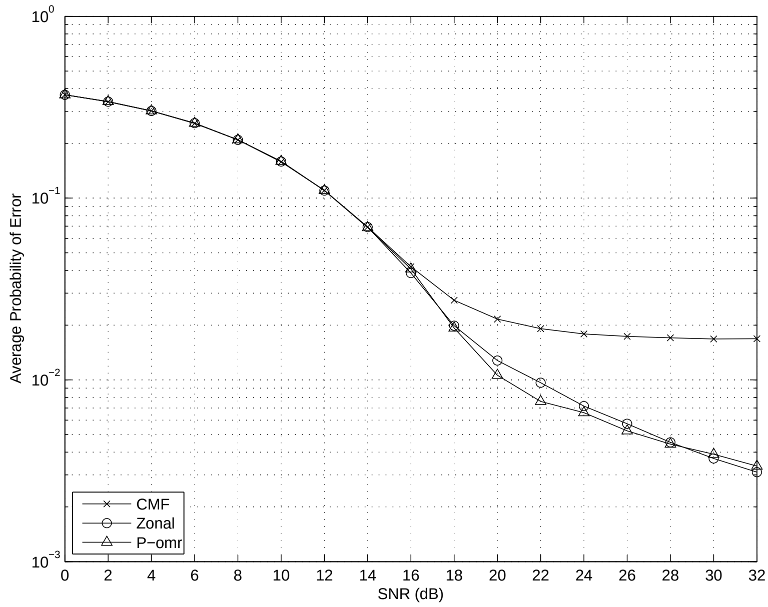

Fig. 4.13. The BER performance comparison of the CMF UWB receiver, the zonal UWB receiver and the p-omr in a free-space propagation channel.

be stored in look-up tables before the implementation. On the other hand, the nonlinear transform $g_{\mathrm{zonal}}(\cdot)$ in zonal receiver has a very simple structure, while the transform function $g_{\mathrm{pomr}}(\cdot)$ in the p-omr is relatively complicated. The advantages and disadvantages of the CMF UWB receiver, the zonal receiver, the p-omr and its enhanced version, the p-omatlr, are listed in Table 4.1.

4.8 Chapter Conclusion

It was shown that the MUI in IR UWB systems is impulsive and can be well modeled by a heavy-tailed distribution. In this chapter, the GG distribution was proposed to approximate the MUI in UWB systems. It was revealed that the GG distribution is an effective model for describing the MUI since the heaviness of the tail for the GG distribution can be controlled by a shape parameter and this shape parameter can be adjusted to accommodate different operating conditions. A receiver dubbed the p-omr was proposed based on the GG model and the likelihood ratio test. It was shown that with a properly selected shape parameter, the p-omr can always ourperform the CMF UWB receiver which is widely used in IR UWB systems, and the soft-limiting receiver which was proposed based on the Laplacian model of the MUI. An enhanced version of the p-omr, the p-omatlr, was proposed by adding an

TABLE 4.1
A SUMMARY OF SOME ADVANTAGES AND DISADVANTAGES OF UWB RECEIVERS, SOURCE: [3]

Receiver	Advantages	Disadvantages
CMF	optimal in absence of interference; less complex	inferior performance in low SIR; does not adapt to noise and interference conditions
Zonal	simple nonlinearity; very good performance	adapted thresholds use pre-simulated values stored in look-up table
p-omr	very good performance; transform function in the receiver can be obtained by theoretical calculation or excess *kurtosis* estimation	nonlinearity function more complex than the linear function in CMF
p-omatlr	performance always better than or equal to both CMF and p-omr with same complexity of nonlinearity	adaptation based on pre-simulated values

extra degree of freedom in the p-omr structure. It was illustrated that the p-omatlr can meet or surpass the performance of all of, the CMF receiver, the soft-limiting receiver and the p-omr. The parameter selection scheme for obtaining the shape parameter in the p-omr and p-omaltr was detailed in this chapter. It was revealed by simulation results that this parameter selection scheme is quite effective.

A new Rake receiver which adopts the p-omr or p-omatlr in each finger was proposed for signal detection in multipath fading channels. Theoretical analysis showed that this p-omr (p-omatlr) based Rake receiver can achieve larger SINR than the CMF based Rake receiver. The superiority of this new Rake receiver was also confirmed by simulation results. As the zonal receiver proposed in Chapter 3, the performance gain of the p-omr (p-omatlr) over the CMF is significant when MUI is the dominant disturbance in the channel.

Chapter 5

An Analysis of Coding Performance in Multiuser Impulse Radio UWB Systems[1]

Early studies of IR UWB systems used the repetition code for signaling, where each information bit is transmitted using several repetitive pulses [21]. It has been mentioned in Section 1.1 that the repetition code is a trivial channel coding scheme and not all the potentials are explored by systems using this channel code. Therefore, other channel codes have been suggested for IR UWB systems [12], [28], [29]. However, the results in these works either based on impractical transmission scenarios or have high computational complexity. It is worth mentioning that the key criteria in developing a framework to evaluate the performance of coded UWB systems can be described as follows; the adopted channel model should reflect practical UWB transmission scenarios and the analytical results should be computationally friendly.

As mentioned earlier, several transmitters should coexist viably in an UWB system. Even with an effective multiple access scheme (the DS technique, TH sequence technique, or a combination of both), the MUI caused by coexisting users due to asynchronous transmissions of different users as well as the multipath nature of UWB channels is difficult

[1] *A version of this chapter has been submitted to IEEE Transactions on Communications, and has been presented at IEEE Global Communications Conference (GLOBECOM), (2010); part of this chapter is based on a full paper published in IEEE Transactions on Communication, 58:1112-1120 and a full paper accepted for publication in IEEE Transactions on Wireless Communications.*

to eliminate. Also as mentioned in previous chapters, experimental evidences as well as theoretical considerations have suggested that the MUI in IR-UWB systems deviates from those conformable to the Gaussian model [11]–[14], [23]. The reason behind this has been revealed in Section 2.2.2. It has been shown in Chapters 3 and 4 that the non-Gaussian MUI in UWB systems exhibits impulsive nature and can be well modeled by heavy-tailed distributions with positive excess *kurtosis* [25, Ch.3] [26], [64]–[66]. It has also been shown in Chapter 4 that the generalized Gaussian distribution is an effective and convenient model for describing the impulsive noise and interference encountered in practical systems [25], [26], [95], with the Laplacian distribution being a special case. The Laplacian distribution captures the nature of impulsive noise (with a positive excess *kurtosis* 3), and has been proven to be valid for modeling the MUI in IR UWB systems [15], [95]. Moreover, the analysis based on this model is relatively simple and tractable as shown in the sequel.

In this chapter, we evaluate the coding performance of IR UWB systems in the presence of MUI, where the MUI is modeled by the Laplacian distribution; the validity of this model is also examined. The analytical methods provided by this chapter represent useful tools for predicting the performance of UWB systems when the dominant disturbance in the channel is caused by the transmission of coexisting UWB devices. As mentioned in Section 2.2.1, this scenario is commom in practice since the interference caused by other sources can be greatly reduced by choosing the system parameters properly. The remainder of this chapter is organized as follows. In Section 5.1, the system model is briefly discussed. Section 5.2 provides performance analysis of coded UWB systems in multipath fading channels. Numerical results based on the analytical methods provided by this chapter and corresponding discussions are given in Section 5.3.

5.1 System Model

We consider TH-BPSK UWB systems using a codebook with M codewords, where each codeword is of length N_s and can be represented by a vector $C_i = [c_{i,0}, \cdots, c_{i,N_\mathrm{s}-1}]$ $(i = 0, \cdots M-1)$. The results and analyses for UWB systems using PPM are similar. According to eq. (2.4), the signal of the *k*th user in a TH-UWB system can be expressed as [58]

$$s^{(k)}(t) = \sqrt{E_\mathrm{c}^{(k)}} \sum_{i=-\infty}^{+\infty} \sum_{m=0}^{N_\mathrm{s}-1} (2d_{i,m}^{(k)} - 1) p(t - c_{\mathrm{TH},m}^{(k)} T_\mathrm{c} - mT_\mathrm{f} - iT_\mathrm{cw}) \tag{5.1}$$

where $E_{\mathrm{c}}^{(k)}$ is the chip energy of the *k*th user. The indices of the codeword and the element (bit) within the codeword are denoted by i and m, respectively, and $d_{i,m}^{(k)}$ is the *m*th bit within the *i*th codeword of the *k*th user. Note that if the codeword C_n is transmitted by the *k*th user during the *i*th codeword block, we have $[d_{i,0}, \cdots, d_{i,N_{\mathrm{s}}-1}] = C_n$. Assuming that each codeword conveys n_{s} information bits and the same codebook is shared among all users in the system, the energy per information bit of the *k*th user is thus given by $E_{\mathrm{b}}^{(k)} = E_{\mathrm{c}}^{(k)} N_{\mathrm{s}}/n_{\mathrm{s}} = E_{\mathrm{c}}^{(k)}/R_{\mathrm{c}}$, where $R_{\mathrm{c}} = n_{\mathrm{s}}/N_{\mathrm{s}}$ is the code rate. The function $p(t)$ is the transmitted UWB pulse with unit energy as defined in Section 2.1.5. The codeword duration, T_{cw}, is divided into N_{s} frames, where one element (bit) in a codeword is transmitted per frame. The frame duration T_{f} is further divided into chips with duration T_{c}, where the position of the pulse within the frame depends on the TH sequence $\left\{c_{\mathrm{TH},m}^{(k)}\right\}$. Let $b_i^{(k)}$ denote the *i*th information bit of the *k*th user. For UWB systems with repetition coding, each information bit is repeatedly transmitted over N_{s} frames. Therefore, a length-N_{s} repetition code is formed by letting $d_{i,m}^{(k)} = b_i^{(k)}$ for $m = 0, \cdots, N_{\mathrm{s}} - 1$. For systems with other block coding schemes, every n_{s} information bits are grouped and encoded into a codeword of length N_{s}. It should be noted that the signal model given by eq. (5.1) also applies to systems with convolutional codes, since convolutional codes can be converted to block codes by the "tailing off" procedure, where zero bits are inserted at the end of a bit stream [70]. In this case, N_{s} is the length of the output bit stream of the encoder including the tailing off bits.

It has been mentioned in Section 2.1.6 that the IEEE 802.15.3a Task group recommended channel models for UWB transmission in 2002 [4]. However, the analyses based on these channel models are rather complicated because of the random arrival times of clusters and rays. Thus, we use a simplied channel model for analysis, where the CIR of the *k* user is given by [27]

$$h^{(k)}(t) = \sum_{l=0}^{L_{\mathrm{t}}-1} \alpha_l^{(k)} \delta(t - l\Delta) \tag{5.2}$$

where l is the multipath index and L_{t} is the total number of multipath components[2]. The RV $\alpha_l^{(k)} = p_l^{(k)} \beta_l^{(k)}$ is the fading coefficient of the *l*th multipath component where $p_l^{(k)}$ accounts for signal inversion due to reflection, assuming values of $\{+1, -1\}$ with equal probability, and $\beta_l^{(k)}$ reflects the fading amplitude associated with the *l*th multipath component. The

[2]We assume that the numbers of paths are the same for all the users in the system. However, generalization to different path numbers for different users is straightforward.

tap spacing Δ in this model can be chosen as $\Delta = 1/W$, where W is the bandwidth of the pulse used for signaling [27]. In this work, we consider the lognormal fading model adopted by [4], where the fading amplitude $\beta_l^{(k)} = |\alpha_l^{(k)}|$ is lognormally distributed with a standard deviation σ_{β_l}. The typical value of σ_{β_l} for indoor environments is usually between 3-5 dB [98]. An exponential decaying profile is adopted for the multipath fading channel where the power of the fading coefficient in the *l*th time bin can be written as [4]

$$\mathbb{E}\Big(\alpha_l^{(k)}\Big)^2 = \mathbb{E}\Big(\beta_l^{(k)}\Big)^2 = \Omega_0 e^{-\rho l}, \ \ l = 0, \cdots, L_{\rm t} - 1 \tag{5.3}$$

and Ω_0 is the average power of the first arriving multipath component. We normalize the power dispersion profile (PDP) of the channel, i.e., $\sum_{l=0}^{L_{\rm t}-1} \mathbb{E}\Big(\alpha_l^{(k)}\Big)^2 = \Omega_0 \frac{1-e^{-\rho L_{\rm t}}}{1-e^{-\rho}} = 1$. Therefore, the parameter Ω_0 is obtained as $\Omega_0 = \frac{1-e^{-\rho}}{1-e^{-\rho L_{\rm t}}}$. Moreover, we consider the quasi-static fading scenario where $\alpha_l^{(k)}$ is assumed to be constant during the transmission of a codeword (block). Interleaving is not considered here since it might cause significant delay in quasi-static fading scenarios [99]. We assume that the first user is the desired user, and the zeroth codeword of the desired user is to be recovered. Without loss of generality, the delay of the desired user can be assumed to be 0 at the receiver, while the relative time shift of the *k*th user T_k ($T_k \neq 1$) is assumed to be uniformly distributed in [0, $T_{\rm cw}$), where $T_{\rm cw}$ is the codeword duration. Based on the channel model described in eq. (5.2), the received signal can be written as [23]

$$r(t) = \sum_{l=0}^{L_{\rm t}-1} \alpha_l^{(1)} s^{(1)}(t - l\Delta) + \sum_{k=2}^{N_{\rm u}} \sum_{l=0}^{L_{\rm t}-1} \alpha_l^{(k)} s^{(k)}(t - T_k - l\Delta) + n(t) \tag{5.4}$$

where $n(t)$ is zero-mean AWGN, and $N_{\rm u}$ is the total number of users in the system. At the receiver, a Rake receiver with MRC is considered. Assume that the channel is perfectly known at the receiver and that the TH sequence of the first user is 0 for all the frames [11]. Therefore, the *m*th element within the zeroth codeword of the first user can be coherently detected and combined by employing the template $v(t) = \sum_{l=0}^{L_{\rm f}-1} \alpha_l^{(1)} p(t - mT_{\rm f} - l\Delta)$, where $L_{\rm f}$ is the number of Rake fingers. We consider the interference-limited case where the effect of the AWGN $n(t)$ can be ignored. Letting R_m denote the *m*th ($m = 0, \cdots, N_{\rm s} - 1$) sampled output of the Rake receiver for the desired signal (c.f. eq. (5.1)) and following a similar procedure as eqs. (3.18)-(3.20), we have

$$R_m = \int_{mT_\mathrm{f}}^{(m+1)T_\mathrm{f}} r(t)v(t)dt = R_m = S_m + I_m \tag{5.5a}$$

where S_m is the desired signal component given by

$$S_m = (2c_{0,m}^{(1)} - 1)\sqrt{E_\mathrm{c}^{(1)}} \sum_{l=0}^{L_\mathrm{f}-1} \left(\alpha_l^{(1)}\right)^2 \tag{5.5b}$$

and I_m is the MUI term in the *j*th frame of the zeroth codeword, which can be expressed as

$$\begin{aligned} I_m \;&= \sum_{l=0}^{L_\mathrm{f}-1} \alpha_l^{(1)} \sum_{k=2}^{N_\mathrm{u}} \sqrt{E_\mathrm{c}^{(k)}} \sum_{l_1=0}^{L_\mathrm{t}-1} \sum_{i_1=-\infty}^{\infty} \sum_{m_1=0}^{N_\mathrm{s}-1} \alpha_{l_1}^{(k)} (2d_{i_1,m_1}^{(k)} - 1) \\ \times &\int_{mT_\mathrm{f}+l\Delta}^{mT_\mathrm{f}+(l+1)\Delta} p(t - i_1 T_\mathrm{cw} - m_1 T_\mathrm{f} - c_{\mathrm{TH},m_1}^{(k)} T_\mathrm{c} - l_1\Delta - T_k) p(t - mT_\mathrm{f} - l\Delta)dt. \end{aligned} \tag{5.5c}$$

The mean of the MUI is $\mathbb{E}\left(I_m\right) = 0$. Given the fading coefficients $\left\{\alpha_l^{(1)}\right\}_{l=0}^{L_\mathrm{f}-1}$, the second moment of I_m is given by

$$\mathbb{E}\left(I_m{}^2 \middle| \left\{\alpha_l^{(1)}\right\}_{l=0}^{L_\mathrm{f}-1}\right) = \frac{\sum_{k=2}^{N_\mathrm{u}} E_\mathrm{c}^{(k)}}{T_\mathrm{f}} \int_{-\infty}^{\infty} R^2(t)dt \sum_{l=0}^{L_\mathrm{f}-1} \left(\alpha_l^{(1)}\right)^2 = \sigma_\mathrm{c}^2 \sum_{l=0}^{L_\mathrm{f}-1} \left(\alpha_l^{(1)}\right)^2 \tag{5.6a}$$

where

$$\sigma_\mathrm{c}^2 = \frac{1}{T_\mathrm{f}} \sum_{k=2}^{N_\mathrm{u}} E_\mathrm{c}^{(k)} \int_{-\infty}^{\infty} R^2(t)dt \tag{5.6b}$$

and $R(t)$ is the autocorrelation function of $p(t)$ defined by eq. (2.2). The derivation of eq. (5.6a) is given in Appendix B. Other denotations are defined at the beginning of this Section.

A complete description of the MUI PDF is difficult and unyielding, especially in multipath fading channels. Therefore, approximations are adopted. Here, conditioning on the fading coefficients of the desired user $\mathfrak{a}^{(1)} = \left\{\alpha_l^{(1)}\right\}_{l=0}^{L_\mathrm{f}-1}$, we examine the validity of two approximations for the MUI given by eq. (5.5c), the ubiquitous Gaussian PDF which has been widely used for noise modeling in wireless communication systems, and the Laplacian PDF which has been proved to be more accurate than the Gaussian PDF for modeling the UWB MUI under most practical circumstances [23]. It has been mentioned in Chapter 3

TABLE 5.1
SYSTEM PARAMTERS FOR CHAPTER 5

System Parameters					
Signals	τ_m	τ_p	T_c	T_f	N_h
	0.2877 ns	0.575 ns	1 ns	100 ns	10
Channel	L_t	ρ	σ_{β_l}	ν	
	10	0.043	4 dB	3	
Rake Receiver	L_f				
	5				

that an effective model for analyzing the interference in UWB networks was provided in [18], [74] where the spatial locations of the interferers are unknown and treated as complete random according to a homogeneous Poisson point process in a two-dimensional space $\mathcal{R}^2$ with a density λ [18], [74], [92]. Without loss of generality, the intended receiver can be assumed to locate at the origin of the two-dimensional plane, and the transmitter of the desired user is located at a distance R_0 from the origin. The network topology has been used in Chapter 3 and is plotted in Fig. 3.7. As in Chapter 3, two transmission scenarios are considered. The first scenario is the equal-power interferers scenario where we assume that the intended receiver acts as the "base station" of the network and coordinates the transmission of all the nodes within the coverage area. In this case, power control could be applied to all the nodes in the network [53] and the received powers of the interferers at the intended user, $E_c^{(k)}$, are the same for $k = 2, \cdots, N_\mathrm{u}$. The second scenario is for ad hoc UWB networks where no "base station" is provided. It was mentioned in Chapter 3 that the power of the interferers decay with the distance r according to k/r^ν for some constant k and the path-loss exponent ν [93]. Therefore, the received powers of the interferers at the intended receiver depend on their distances to the origin. The accuracies of the Gaussian and the Laplacian approximations are examined using the Kullback-Leibler (KL) divergence values obtained by Monte Carlo simulation [100]. For the first scenario, we use the parameters $E_c^{(k)} = 1$ $(k = 2, \cdots, N_\mathrm{u})$. In the second scenario, it should be noted that the distribution of the MUI given by eq. (5.5c) depends on the received powers $E_c^{(k)}(k = 2, \cdots, N_\mathrm{u})$ determined by the positions of the interfering nodes. Therefore, the KL divergences of the approximations in this case are RVs whose values are determined by a particular realization of the node

TABLE 5.2
KULLBACK-LEIBLER DIVERGENCE (IN NATS) FOR GAUSSIAN AND LAPLACIAN DISTRIBUTIONS

(a) Equal-power-interferers model

Kullback-Leibler	$N_{\mathrm{u}} = 5$	$N_{\mathrm{u}} = 10$	$N_{\mathrm{u}} = 15$	$N_{\mathrm{u}} = 20$
$\mathrm{D}_{\mathrm{KL}}\left(f_{\mathrm{MUI}} \vert\vert f_{\mathrm{G}}\right)$	0.133159	0.042569	0.024736	0.017767
$\mathrm{D}_{\mathrm{KL}}\left(f_{\mathrm{MUI}} \vert\vert f_{\mathrm{L}}\right)$	0.013439	0.006917	0.015738	0.021494

(b) Poisson field model

Kullback-Leibler	$\lambda = 0.1$	$\lambda = 0.3$	$\lambda = 0.5$
$E\left(\mathrm{D}_{\mathrm{KL}}\left(f_{\mathrm{MUI}} \vert\vert f_{\mathrm{G}}\right)\right)$	0.316111	0.221565	0.195440
$E\left(\mathrm{D}_{\mathrm{KL}}\left(f_{\mathrm{MUI}} \vert\vert f_{\mathrm{L}}\right)\right)$	0.083090	0.059661	0.049641

positions. In this scenario, we consider a 10 m $\times$ 10 m rectangular area where the interfering nodes distribute according to the Poisson process with different densities, and the KL divergences in this case are obtained by averaging over 1000 realizations of the positions of the interfering nodes. The signaling pulse used in the simulation is the second deviative of a Gaussian monocycle given by eq. (3.10), and the system parameters are given in Table 5.1. The simulated KL divergence values for the Gaussian and Laplacian distributions are given in Table 5.2 where the function $f_{\mathrm{MUI}}(x)$ denotes the simulated PDF of the UWB MUI, and the $f_{\mathrm{G}}(x)$ and $f_{\mathrm{L}}(x)$ denote the approximate Gaussian and Laplacian PDFs, respectively. It is seen in Table 5.2 that, for the equal-power interferers case, the Laplacian model works better than the Gaussian model till $N_{\mathrm{u}} = 15$. However, as the number of users increases, the CLT begins to work and the performance of the Gaussian model becomes better than the Laplacian model. However, in the second scenario, the Laplacian approximation works better than the Gaussian approximation even for $\lambda = 0.5\ \mathrm{m}^{-2}$ (i.e., there are 50 interferers in the 10 m $\times$ 10 m area on average). The reason behind this is that although the number of interferers is relatively large, the interferers which are close to the receiver contribute most of the interference power and the CLT does not converge quickly under such circumstances [25], [74]–[77]. Since most of the motivating applications of UWB devices operate in second scenario and the Laplacian approximation works well than the ubiquitous Gaussian model under such circumstances even with densely populated interfering nodes, it is reasonable to use the Laplacian distribution to model the UWB MUI given by eq. (5.5c) conditioning on the amplitudes of the desired user $\mathfrak{a}^{(1)}$. The PDF of the Laplacian distribution was given by eq. (4.16) as

$$f_{\mathrm{L}}(x) = \frac{1}{2b} \exp\left(-\frac{|x|}{b}\right) \tag{5.7}$$

with the first and second moments given by 0 and $2b^2$, respectively. Hence, when eq. (5.7) is used to model the MUI I_j conditioned on $\mathfrak{a}^{(1)}$, the parameter b can be obtained by matching the second moment of the MUI (c.f. eq. (5.6a)) with $2b^2$, i.e., conditioned on the fading coefficients, b can be expressed as

$$b = \sqrt{\mathbb{E}\left({I_m}^2 \middle| \left\{\alpha_l^{(1)}\right\}_{l=0}^{L_{\mathrm{f}}-1}\right)/2} = \sqrt{\frac{\sigma_{\mathrm{c}}^2}{2} \sum_{l=0}^{L_{\mathrm{f}}-1} \left(\alpha_l^{(1)}\right)^2} \tag{5.8}$$

where σ_c^2 is given by eq. (5.6b).

Note that $\sum_{l=0}^{L_{\mathrm{f}}-1} \left(\alpha_l^{(1)}\right)^2$ is an important term for evaluating the system performance, since both the desired signal component S_j (c.f. eq.(5.5b)) and the variance of the MUI (c.f. eq. (5.6a)) are closely related to it. For the time being, we drop the index 1 in the fading coefficients, with the implicit understanding that channel characteristics are the same for all the users in the same coverage area. As mentioned above, the fading amplitude $\beta_l = |\alpha_l|$ is lognormal distributed. Therefore, $x_l = \ln|\alpha_l| = \ln \beta_l$ is a normally distributed RV given by $x_l \sim \mathcal{N}(\mu_{x_l}, \sigma_{x_l}^2)$, where μ_{x_l} and $\sigma_{x_l}^2$ are the mean and variance of x_l, respectively. The moments of β_l can be expressed in terms of μ_{x_l} and σ_{x_l} as

$$\mathbb{E}(\beta_l^k) = \exp\left(\frac{2k\mu_{x_l} + k^2\sigma_{x_l}^2}{2}\right). \tag{5.9}$$

Let $\gamma = \sum_{l=0}^{L_{\mathrm{f}}-1} \alpha_l^2 = \sum_{l=0}^{L_{\mathrm{f}}-1} \beta_l^2$. The first and second moments of γ are given by

$$\mu_\gamma = \mathbb{E}(\gamma) = \sum_{l=0}^{L_{\mathrm{f}}-1} \mathbb{E}(\beta_l^2) = \sum_{l=0}^{L_{\mathrm{f}}-1} e^{2\mu_{x_l} + 2\sigma_{x_l}^2} \tag{5.10}$$

and

$$
\begin{aligned}
\mathbb{E}(\gamma^2) &= \sum_{l=0}^{L_\mathrm{f}-1} \mathbb{E}(\beta_l^4) + \sum_{l=0}^{L_\mathrm{f}-2} \sum_{l_1=l+1}^{L_\mathrm{f}-1} \mathbb{E}(\beta_l^2)\mathbb{E}(\beta_{l_1}^2) \\
&= \sum_{l=0}^{L_\mathrm{f}-1} e^{4\mu_{x_l}+8\sigma_{x_l}^2} + 2\sum_{l=0}^{L_\mathrm{f}-2} \sum_{l_1=l+1}^{L_\mathrm{f}-1} e^{2(\mu_{x_l}+\mu_{x_{l_1}})+2(\sigma_{x_l}^2+\sigma_{x_{l_1}}^2)} \qquad (5.11)
\end{aligned}
$$

respectively. Since β_l is lognormally distributed, the RV β_l^2 is also lognormally distributed. Although the distribution of $\gamma = \sum_{l=0}^{L_\mathrm{f}-1} \beta_l^2$ (which is a sum of independent lognormal RVs) is unknown, this sum can usually be approximated by another lognormal distributed RV [101].

5.2 Performance Analysis of Coded UWB Systems

We consider a soft-decision decoder where the receiver is followed by a decoder that forms the decision variables corresponding to each codeword according to the statistics given by eq. (5.5a) [27]. To be specific, the decoder forms the M metrics as

$$
\mathrm{CM}_i = \sum_{m=0}^{N_\mathrm{s}-1} (2c_{i,m}^{(1)} - 1)R_m, \ (i = 0, \cdots, M-1). \qquad (5.12)
$$

Without loss of generality, we assume the all-zero codeword C_0 is transmitted by the desired user. Therefore, correct decoding requires that the metric CM_0 exceeds all other metrics $\mathrm{CM}_i, (i = 1, \cdots, M-1)$. Let d denote the weight of the kth codeword. Thus, we have

$$
D_{0,k} = \mathrm{CM}_0 - \mathrm{CM}_k = 2dS_m - 2\sum_{m=1}^{d} I_m. \qquad (5.13)
$$

The pairwise error probability (PEP), which is the probability that the metric for a codeword with weight d is larger than that of the all-zero codeword ($\mathrm{CM}_k > \mathrm{CM}_0$), can be expressed as

$$
P_\mathrm{PEP}(d) = \mathrm{P_r}(D_{0,k} < 0) = \mathrm{P_r}\left(\sum_{m=1}^{d} I_m > dS_m\right) \qquad (5.14)
$$

where S_m is given by eq. (5.5b), and I_m is the MUI given by eq. (5.5c). It has been mentioned above that when conditioning on the fading coefficients $\mathfrak{a}^{(1)} = \left\{\alpha_l^{(1)}\right\}_{l=0}^{L_\mathrm{f}-1}$, I_m can be well modeled by the Laplacian distribution with the parameter b given by eq. (5.8).

Therefore, conditioning on the parameter $\gamma = \sum_{l=0}^{L_\mathrm{f}-1} \left(\alpha_l^{(1)}\right)^2$, the PEP given by eq. (5.14) depends on the distribution of the sum of identical independent distributed (i.i.d.) Laplacian noise. The PDF and CDF of this sum have been derived in [102]. Using these results, the conditional PEP can be rewritten as [103]

$$\begin{aligned} P_{\mathrm{PEP,con}}(d|\gamma) &= \mathrm{P_r}\left(\sum_{m=1}^{d} I_m > dS_m|\gamma\right) \\ &= \frac{1}{2} - \sum_{l=0}^{d-1} \frac{1}{2^{d+l}} \binom{d+l-1}{l} \left[1 - e^{-\frac{dS_m}{b}} E_{d-l-1}\left(\frac{dS_m}{b}\right)\right] \end{aligned} \tag{5.15}$$

where $E_k(x) = \sum_{m=0}^{k} \frac{x^m}{m!}$ is the incomplete exponential function [102], and b is the parameter in the Laplacian PDF used to model the MUI, which is given by eq. (5.8) conditioned on the fading coefficients. Substituting eqs. (5.5b) and (5.8) into (5.15) and conditioning on γ, the PEP can be expressed as

$$\begin{aligned} P_{\mathrm{PEP,con}}(d|\gamma) &= \frac{1}{2} - \sum_{l=0}^{d-1} \frac{1}{2^{(d+l)}} \binom{d+l-1}{l} \\ &\quad \times \left[1 - e^{-d\sqrt{\frac{2E_c^{(1)}}{\sigma_c^2}}\sqrt{\gamma}} E_{d-l-1}\left(d\sqrt{\frac{2E_c^{(1)}}{\sigma_c^2}}\sqrt{\gamma}\right)\right] \end{aligned} \tag{5.16}$$

where $E_\mathrm{c}^{(1)}$ is the chip energy of the desired user, as defined in Section 5.1.

It has been mentioned in the previous section that the RV γ can be approximated by a lognormal distributed RV. Using the Wilkinson approximation method [104] to obtain the approximate lognormal distribution of γ and letting $y = g(\gamma) = \ln(\sqrt{\gamma})$, y can be approximated by a normal distributed RV with PDF

$$f_y(y) = \frac{1}{\sqrt{2\pi}\sigma_y} e^{-(y-\mu_y)^2/(2\sigma_y^2)} \tag{5.17}$$

where μ_y and σ_y^2 are the mean and variance of y, respectively. These two parameters can be expressed in terms of the first and second moments of γ (c.f. eqs. (5.10) and (5.11)) as

$$\mu_y = \mathbb{E}(y) = \frac{1}{2}\ln\left(\frac{\mu_\gamma^2}{\sqrt{\mathbb{E}(\gamma^2)}}\right) \tag{5.18}$$

and

$$\sigma_y^2 = \ln\left(\frac{\mathbb{E}(\gamma^2)}{\mu_\gamma^2}\right). \tag{5.19}$$

Hence, the PEP in UWB multipath fading channels can be evaluated by averaging the conditional PEP given by eq. (5.16) over the PDF of y as

$$\begin{aligned} P_{\text{PEP}}(d) &= \int_\gamma \mathrm{P}_{\text{PEP,con}}(d|\gamma) f_\gamma(\gamma) d\gamma = \int_y \mathrm{P}_{\text{PEP,con}}(d|g^{(-1)}(y)) f_y(y) dy \\ &= \frac{1}{2} - \sum_{l=0}^{d-1} \frac{1}{2^{d+l}} \binom{d+l-1}{l} + \sum_{l=0}^{d-1} \frac{1}{2^{d+l}} \binom{d+l-1}{l} I_{\text{t}} \end{aligned} \tag{5.20a}$$

where

$$I_{\text{t}} = \frac{1}{\sqrt{\pi}} \int_{-\infty}^{\infty} e^{-d\sqrt{\frac{2E_c^{(1)}}{\sigma_c^2} e^{\sqrt{2}\sigma_y y + \mu_y}}} E_{d-l-1}\left(d\sqrt{\frac{2E_c^{(1)}}{\sigma_c^2} e^{\sqrt{2}\sigma_y y + \mu_y}}\right) e^{-y^2} dy. \tag{5.20b}$$

Several numerical techniques can be used to evaluate I_{t}. For instance, the value of integral $\int_{-\infty}^{+\infty} e^{x^2} f(x) dx$ can be approximated using Hermite-Gauss quadrature as

$$\int_{-\infty}^{+\infty} \exp(-x^2) f(x) dx = \sum_{i=1}^{n} w_i f(x_i) \tag{5.20c}$$

where x_i is the *i*th zero of the Hermite polynomial $H_n(x)$, and the associated weights w_i are given by $w_i = \frac{2^{n-1} n! \sqrt{\pi}}{n^2 [H_{n-1}(x_i)]^2}$ [105, (25.4.46)]. Therefore, I_{t} can be evaluated as

$$I_{\text{t}} = \frac{1}{\sqrt{\pi}} \sum_{i=1}^{n} w_i e^{-d\sqrt{\frac{2E_c^{(1)}}{\sigma_c^2} e^{\sqrt{2}\sigma_y y_i + \mu_y}}} E_{d-l-1}\left(d\sqrt{\frac{2E_c^{(1)}}{\sigma_c^2} e^{\sqrt{2}\sigma_y y_i + \mu_y}}\right). \tag{5.20d}$$

5.2.1 Codeword Error Probabilities

Upper Bounds

For codebooks consisting of only two codewords, e.g., the repetition code, the PEP given by eq. (5.20a) is both the codeword error probability and the bit error rate. However, if there are more than two codewords in the codebook, upper and lower bounds should be employed to assess the error performance. We first use the popular union bound to upper bound the codeword error probability as

$$P_{\text{CEP}} \leq P_{\text{ub,CEP}} = \sum_{d=d_{\min}}^{N_{\text{s}}} N_d P_{\text{PEP}}(d) \tag{5.21}$$

where $P_{\text{PEP}}(d)$ is the PEP given by eq. (5.20a), $d_{\min}$ is the minimum Hamming distance of the codebook, and N_d is the number of codewords with weight d in the codebook. Note that the union bound given by eq. (5.21) also applies to convolutional codes. The transfer function of convolutional codes can be expressed as

$$T(D, N) = \sum_{d=d_{\text{free}}}^{\infty} N_d N^{f(d)} D^d \tag{5.22}$$

where the exponent of D denotes the Hamming distance between the sequence of output bits compared to the all-zero sequence, N_d denotes the number of paths with Hamming distance d, the number of input bits 1 is denoted by the exponent of N, and d_{free} is the minimum free distance of the convolutional code. Note that eq. (5.20a) can also be used to calculate the PEP of a Viterbi decoder where the decoder incorrectly chooses a path identical to the all-zero path except in d positions [27]. Therefore, the union bound for convolutional codes has the same form as eq. (5.21). Assuming the "block" length of the output bit stream after tailing off is N_{s}, the union bound for the convolutional code can be calculated using eq. (5.21) where $d_{\min}$ in eq. (5.21) should be replaced by d_{free}, and N_{d} is given by the transfer function (c.f. eq. (5.22)).

It is well known that the union bound is valid for predicting the error rate performance in nonfading channels, especially for medium and large values of signal-to-interference ratio, as the error performance of soft-decoders is dominated by the minimum Hamming distance term as the SIR increases in unfaded scenarios [27], [106]. However, the union bound has been found to provide unsatisfactory results for quasi-static fading channels [99], [107]. The fundamental reason behind this is that the quasi-static fading channel can be viewed as an unfaded channel for which the instantaneous received SIR varies from one block to the next. The SIR value for a given frame can be quite low. Therefore, the union bound, which is known to diverge for low SIRs, although tight for moderate and large values of SIR, cannot always accurately evaluate the system performance in quasi-static fading channels. It will be shown in the sequel that the union bound in quasi-static fading channels, which is given by eq. (5.21), can easily become larger than unity. Improved upper bounds on the codeword and bit error probabilities have been proposed for quasi-static fading channels [99], [107]. The basic idea for deriving tighter bounds is based on the earlier work of Gallager [108], [109], where the bounding technique has the form

$$\begin{aligned} P_{\mathrm{gb}} &= \mathrm{P_r}(A|S_j \in \mathcal{R})\mathrm{P_r}(S_j \in \mathcal{R}) + \mathrm{P_r}(A|S_j \in \bar{\mathcal{R}})\mathrm{P_r}(S_j \in \bar{\mathcal{R}}) \\ &\leq \mathrm{P_r}(S_j \in \mathcal{R}) + \mathrm{P_r}(A|S_j \in \bar{\mathcal{R}})\mathrm{P_r}(S_j \in \bar{\mathcal{R}}) \end{aligned} \tag{5.23}$$

where A is the codeword error event, $\mathcal{R}$ can be seen as the region with low received SIR, and $\bar{\mathcal{R}}$ is its complement or high received SIR region. The union bound can be used in the high SIR region $\bar{\mathcal{R}}$ since it is known to converge for high received SIRs. One of the possible choices for $\mathcal{R}$ is to evalute the conditional union bound for all possible values of the channel gain, and then choose one for the codeword error probability when the union bound is greater than one (or 1/2 for the bit error rate) [99]. Based on this limiting-before-averaging approach, the improved bound for the codeword error probability in quasi-static fading channels is expressed as

$$P_{\mathrm{CEP}} \leq P_{\mathrm{gb,CEP}} = \int_{\gamma} \min \left[1, \sum_{d=d_{\min}}^{N_{\mathrm{s}}} N_d P_{\mathrm{PEP,con}}(d|\gamma) \right] f_{\gamma}(\gamma) d\gamma \tag{5.24}$$

where $P_{\mathrm{PEP,con}}(d|\gamma)$ is the conditional PEP given by eq. (5.16) and $f_{\gamma}(\gamma)$ is the PDF of the lognormally distributed RV $\gamma = \sum_{l=0}^{L_{\mathrm{f}}-1} \beta_l^2$ with the first and second moments given by eqs. (5.10) and (5.11), respectively. For block codes, N_d is the number of codes with Hamming distance d in the codebook, while for convolutional codes, N_d can be obtained in the transfer function given by eq. (5.22).

Lower Bound

A lower bound of the codeword error probability can be obtained by only considering the error event where the all-zero codeword is incorrectly decoded to a codeword with minimum Hamming distance, i.e.,

$$P_{\mathrm{CEP}} \geq P_{\mathrm{lb,CEP}} = P_{\mathrm{PEP}}(d_{\min}) \tag{5.25}$$

where $d_{\min}$ is the minimum Hamming distance of the codebook, and $P_{\mathrm{PEP}}(d)$ is given by eq. (5.20a). For convolutional codes, the lower bound of the "block" error probability can also be calculated by eq. (5.25), while d_{min} should be replace by the free distance d_{free} given in the transfer function (c.f. eq. (5.22)).

5.2.2 Bit Error Rate

Upper Bounds

In practice, it is also useful to know the bit error rate of the system. It is worth mentioning that the codeword error probability derived above is also the bit error probability for codes consisting of two codewords, e.g., the repetition code. For other codes, the bit error rate of the soft-decision decoder can be upper bounded by the union bound as [106], [110]

$$P_{\text{BER}} \leq P_{\text{ub,BER}} = \sum_{d=d_{\text{min}}}^{N_{\text{s}}} N_{d,\text{b}} P_{\text{PEP}}(d) \tag{5.26}$$

where $P_{\text{PEP}}(d)$ is the PEP that the all-zero codeword is incorrectly decoded to a codeword with weight d given by eq. (5.20a). For block codes, $N_{d,\text{b}}$ can be written as $N_{d,\text{b}} = N_d \delta_d / n_{\text{s}}$, where N_d is the number of codewords with Hamming distance d in the codebook, δ_d is the average number of nonzero information bits associated with a codeword of weight d, and n_{s} is the number of information bits that are encoded into a codeword [110, eq. (3)]. The union bound for the bit error rate of convolutional codes can also be expressed in terms of the PEP in similar fashion as eq. (5.26). Taking the derivative of the transfer function (c.f. (5.22)) with respect to N and setting $N = 1$, we have

$$\left. \frac{dT(D,N)}{dN} \right|_{N=1} = \sum_{d=d_{\text{free}}}^{N_{\text{s}}} N_d f(d) D^d. \tag{5.27}$$

Note in eq. (5.27) that, for paths separated from the all-zero path in d positions, the number of the corresponding information bit errors is given by $N_d f(d)$ [27], [70]. Therefore, letting $N_{d,\text{b}} = N_d f(d)$, eq. (5.26) can also be used to calculate the union bound for the bit error rate of convolutional codes, where N_d and $f(d)$ are the convolutional code parameters seen in the transfer function given by eq. (5.22).

It has been mentioned that the union bound provides an unsatisfactory upper bound in quasi-static fading channels, especially for small and medium SIR. Therefore, we here provide the improved Gallager bound for the bit error performance evaluation as we did for the codeword error performance assessment. In similar fashion as eq. (5.24), the Gallenger bound for the bit error rate can be expressed as [99]

$$P_{\text{BER}} \leq P_{\text{gb,BER}} = \int_{\gamma} \min\left[\frac{1}{2}, \sum_{d=d_{\min}}^{N_{\text{s}}} \text{N}_{d,\text{b}} P_{\text{PEP,con}}(d|\gamma)\right] f_{\gamma}(\gamma) d\gamma \tag{5.28}$$

where $P_{\text{PEP,con}}(d|\gamma)$ is the conditional PEP given by eq. (5.16), and $f_{\gamma}(\gamma)$ is the PDF of the lognormally distributed RV $\gamma = \sum_{l=0}^{L_{\text{f}}-1} \beta_l^2$ with the first and second moments given by eqs. (5.10) and (5.11), respectively. The parameter $N_{d,\text{b}} = N_d \delta_d / n_{\text{s}}$ for block codes, where the parameters N_d, δ_d and n_{s} can be obtained from the codebook. For convolutional codes, $N_{d,\text{b}} = N_d f(d)$ where N_d and $f(d)$ are the parameters given by eq. (5.22).

Lower Bound

The lower bound of the bit error rate can be obtained in similar fashion as eq. (5.25) by considering only the error event that the all-zero codeword is incorrectly decoded to a codeword with minimal Hamming distance, i.e.,

$$P_{\text{BER}} \geq P_{\text{lb,BER}} = \tilde{\text{N}}_{d,\text{b}} P_{\text{PEP}}(d_{\min}) \tag{5.29}$$

where $P_{\text{PEP}}(d_{\min})$ is the PEP given by eq. (5.20a) and $\tilde{\text{N}}_{d,\text{b}} = \delta_{d_{\min}}/m$ for block codes. Eq. (5.29) can also be used to provide a lower bound for the bit error rate for convolutional codes by replacing $d_{\min}$ with d_{free}, and expressing $\tilde{\text{N}}_{d,\text{b}}$ as $f(d_{\text{free}})$, where d_{free} and $f(d)$ are given in eq. (5.22).

5.3 Numerical Results and Discussion

In this section, analytical methods provided above are used to evaluate codeword and bit error rates of the soft-decision decoder. Simulation results are also provided. The performance of the repetition code, which was widely used in the early studies of UWB systems, and the superorthogonal code [70] are evaluated and compared. For the superorthogonal code, the transfer function is given by

$$T_{\text{so}} = \frac{NW^{k+2}(1-W)}{1-W\left[1+N(1+W^{k-3}-2W^{k-2})\right]} \tag{5.30}$$

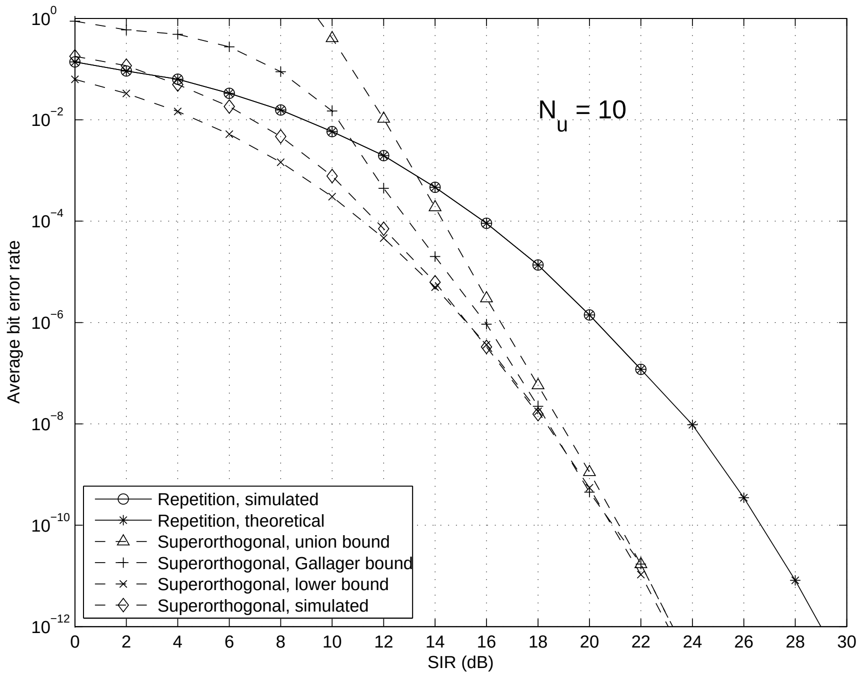

Fig. 5.1. The average BER in multipath fading UWB channels, when $N_\mathrm{u} = 10$ and a Rake receiver with 10 fingers is used.

where $W = D^{2^{k-3}}$ and k is the constraint length of the superorthogonal code [70, eq. (5.43)]. To provide fair comparison, the same code rate $R_\mathrm{c} = 1/2$ is used for both the repetition code and the superorthogonal code, where the constraint length of the superorthogonal code with $R_\mathrm{c} = 1/2$ is given by $k = 3$. The signaling pulse used in simulation is given by eq. (3.10), and the system parameters are given in Table 5.1. We assume equal-power interferers and the SIR is defined as $\mathrm{SIR} = E_b^{(1)}/\sigma_c^2 \sum_{k=2}^{N_\mathrm{u}-1} E_b^{(k)}$, where $E_b^{(1)}$ and $E_b^{(k)}$ are the bit energy of the desired user and the interfering user, respectively, and σ_c^2 is given by eq. (5.6b)

Fig. 5.1 shows the BER performance for both codes when there are 10 users (9 interfering users) in the system, and the number of Rake fingers is $L_\mathrm{f} = 5$. For the repetition code, since there are only two codewords in the codebook, the PEP, $P_\mathrm{PEP}(d)$, which can be calculated by eq. (5.20a), is both the codeword and bit error rate. As for the superorthogonal code, the union bound and the improved Gallager bound, which can be calculated by eqs. (5.26) and (5.28), respectively, are provided for upper bounding the bit error rate. The lower bound given by eq. (5.29) is also plotted. Simulation results are presented for small and moderate SIR values. It is seen in Fig. 5.1 that the analytical results comply well with

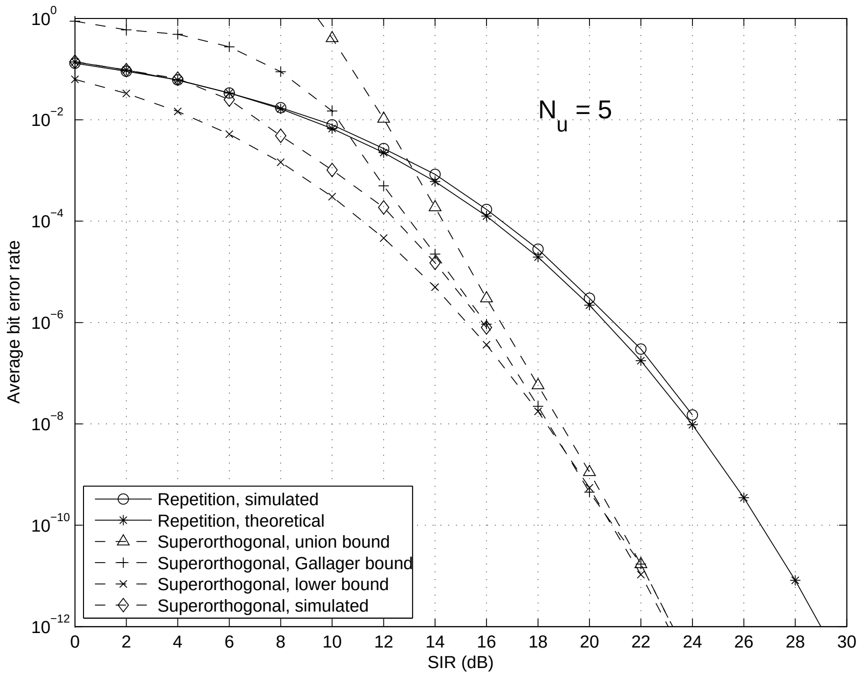

Fig. 5.2. The average BER in multipath fading UWB channels, when $N_{\mathrm{u}} = 5$ and a Rake receiver with 10 fingers is used.

the Monte Carlo simulation results for the repetition code, i.e., the analysis provided in Section 5.2 are reliable and the Laplacian model is accurate for approximating the MUI under such operating conditions which has been shown in Table 5.2. Note also that the union bound is loose for evaluating the error performance for small and medium SIR values, as expected. However, it becomes tight for relatively large values of the SIR. Meanwhile, the Gallager bound performs better for upper bounding the bit error probabilities. It provides 1.3 dB improvement over the union bound at the error rate level of 10^{-4}. Note also that, the superorthogonal code provides significant performance gains over the simple repetition code without requiring extra bandwidth, although the Viterbi decoding process might add complications to the receiver structure. Note that at the error rate level 10^{-4}, the difference in performance between the two codes is approximately 4.4 dB.

Figs. 5.2 and 5.3 show the bit error rate performance of both codes for the same operating condition as in Fig. 5.1 when there are 5 users (9 interfering users) and 15 users (14 interfering users) in the system, respectively. As mentioned above, for the repetition code, the bit error rate is also the PEP, $P_{\mathrm{PEP}}(d)$, which can be calculated by eq. (5.20a). It is seen in both figures that there are some discrepancies between the theoretical and simulated

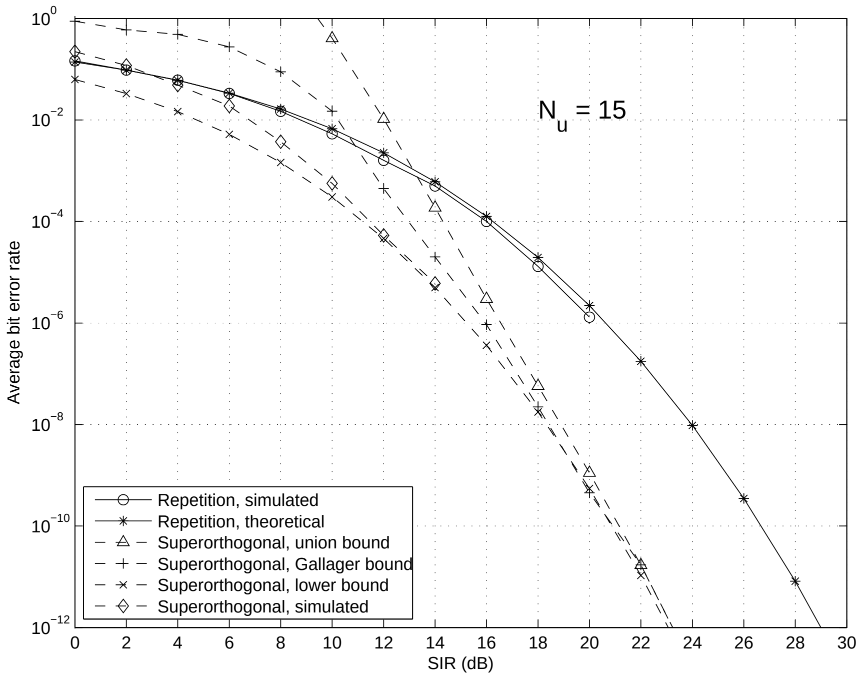

Fig. 5.3. The average BER in multipath fading UWB channels, when $N_{\rm u} = 15$ and a Rake receiver with 10 fingers is used.

results for medium and large values of the SIR. The reason behind this is that the Laplacian model does not describe the distribution of the MUI as well as the case with $N_{\rm u} = 10$. This behavior can be predicted by the values of the KL divergence shown in Table 5.2. However, the analytical results given in Section 5.2 can still provide reasonable prediction of the coding performance, e.g, at the error rate level 10^{-6}, the SIR difference between the simulated and analytical results is only 0.16 dB for $N_{\rm u} = 15$. As for the superorthogonal code, the union bound and the improved Gallager bound are calculated by eqs. (5.26) and (5.28), respectively, and the lower bound is given by eq. (5.29). Simulation results are also presented for small and medium values of the SIR. It is revealed that as in the $N_{\rm u} = 10$ case, the union bound and the lower bound can provide tight bounds for large SIR values, and the Gallager bound can improve the performance of the union bound.

5.4 Chapter Conclusion

In this chapter, we have developed an analytical framework for assessing the coding performance of IR UWB systems. Unlike previous works on this subject, this framework adopts a more accurate model for the disturbance, and a channel model which can describe the practical UWB transmission scenario is considered. Based on this framework, analytical results were provided to assess codeword and bit error probabilities of soft-decision decoders in the presence of MUI, when a Rake receiver with MRC is adopted for signal reception. It was shown by simulation results that the analytical methods provided in this chapter are computationally friendly and can accurately predict the coding performance of IR UWB systems. Note that these analytical tools are useful especially when the performance evaluation of coded UWB systems based on simulation is time-consuming or even impossible. Furthermore, the coding performance of other communication systems with disturbances that share statistical similarities with the UWB MUI can also be predicted by the analytical results provided in this chapter.

Chapter 6

Sequence Designs for Narrowband Interference Mitigation in Impulse Radio UWB Systems[1]

It has been mentioned earlier that the huge bandwidth brings unique advantages to UWB, which include 1) high data rates; 2) low probability of interception; 3) accurate position location and ranging, just to name a few [2]. On the other hand, the large bandwidth also brings challenges to UWB system deployment. The UWB band overlaps with several frequency bands already allocated to established narrowband (NB) services. Therefore, the successful deployment of UWB systems requires that UWB devices contend and coexist with serives already operating in the dedicated band.

As mentioned in Section 2.2.5, several NB suppression techniques have been borrowed from those used in CDMA SS systems [40]–[42]. However, these techniques are used to reduce the effect of NB interference on UWB devices. Note that the mutual interference should be as low as possible to ensure that UWB and NB services can coexist viable in the same coverage area. Therefore, the effect of IR UWB signals on NB services should also be minimized. It has also been mentioned in Section 2.2.5 that an effective approach to suppress the mutual interference between UWB and NB systems is to shape the spectrum of UWB signals and create frequency nulls at NB service dedicated bands, and this can

[1] *A version of this chapter has been accepted as a full paper for publication in IEEE Transactions on Communications, and to be presented at IEEE International Conference on Communications (IEEE ICC), (2011).*

be done efficiently by designing DS or TH sequence in UWB signals. In [32], [33], the authors developed several techniques for designing the DS or TH sequence for IR UWB systems to mitigate NB interference in certain bands. However, another problem arises. Inherently, direct and TH sequences are PN codes. They are used to introduce an element of unpredictability or pseudorandomness in each of the transmitted signals that is only known to the desired receiver but not to intended or unintended listeners, by maintaining desired properties for SS signals, e.g, LPI and low MUI [27]. The DS and the TH sequence designs proposed in [32], [33] have been shown to enhance the BER performance of UWB systems in the presence of NB interference, however, the desired properties of SS signals might be lost through the alteration of these sequences. Motivated by the need to suppress the NB interference while maintaining the desired properties provided by the PN code, it is reasonable to use both DS and TH sequence in an UWB signal, where one of them is used to shape the signal spectrum and reduce the mutual interference between NB and UWB systems, while the other uses a PN code to preserve desired properties of SS signals [111]–[113]. In this chapter, this UWB signal structure is considered; both the DS design where a PN code is used as the TH sequence, and the TH sequence design where a PN code is adopted as the DS, are examined [2]. It will be shown in the sequel that these designs can greatly suppress the mutual interference between NB and UWB systems, which clears a crucial hurdle for UWB device deployment. These sequence designs can adapt to the spectral occupancy state of current channels; this information can be provided by cognitive radio or a priori knowledge of the spectrum usage in the network.

The remainder of this chapter is organized as follows. In Section 6.1, the system model used in this chapter is briefly discussed. Section 6.2 proposes the DS design, while the TH sequence design is given in Section 6.3. Numerical results showing the effects of these designs and discussion of the results are provided in Section 6.4.

---

[2] The DS and TH sequence design problems considered in [32], [33] and other relevant literatures are special cases of those examined by this work. For example, the DS design examined in [33] is a special case of that considered by this work, where the PN TH sequence adopted by the signal structure used in this paper is replaced by an all-zeros TH sequence. As for the TH sequence design problem dealt with in [32], it can be considered as a special case of that studied by this work, where the PN DS code applied to the signal structure used by this work is replaced by an all-ones DS in [32].

6.1 System Model and Problem Formulation

In this chapter, we consider binary modulation where the transmitted signal can be expressed as [19]

$$s_{\mathrm{u}}(t) = \sqrt{E_{\mathrm{u}}} \sum_i b(t - iT_{\mathrm{b}}; d_i), \quad d_i \in \{0, 1\} \tag{6.1}$$

where E_{u} is the energy per information bit for the UWB system, d_i is the ith information bit, and T_{b} is the bit duration and $b(t, d_i)$ is a unit-energy waveform used to transmit information bit d_i. We consider a BPSK signal. The analysis and results are similar for PPM signals. As mentioned above, we use both DS and TH sequence in a UWB signal. The IR UWB signal structures with DS and TH multiple access schemes were given by eqs. (2.4) and (2.5), respectively. Therefore, $b(t)$ can be given as [3] [22]

$$b(t; d_i) = (2d_i - 1) \sum_{k=0}^{N_{\mathrm{s}}-1} c_{\mathrm{DS},k} p(t - kT_{\mathrm{f}} - c_{\mathrm{TH},k} T_{\mathrm{c}}) \tag{6.2}$$

where all the system parameters are the same as defined in Section 3.1. We assume here that $p(t)$ is the transmitted UWB pulse with energy $1/\sqrt{N_{\mathrm{s}}}$ to ensure that $b(t, d_i)$ has unit-energy. As mentioned above, we consider an UWB system where each user is assigned a pair of DS and TH sequence, where one of them is a PN code and the other is used to shape the UWB signal spectrum according to the PN code and the spectral occupancy information in the current network. The DS and the TH sequence are represented as $\{c_{\mathrm{DS},k}\}_{k=0}^{N_{\mathrm{s}}-1}$ and $\{c_{\mathrm{TH},k}\}_{k=0}^{N_{\mathrm{s}}-1}$, respectively, where the DS is a bipolar sequence with $c_{\mathrm{DS},k} \in \{+1, -1\}$, and the component of the TH sequence $c_{\mathrm{TH},k} \in \{0, \cdots, N_{\mathrm{h}} - 1\}$.

As mentioned in previous chapters, the propagation channel for UWB signals is frequency-selective. The UWB CIR has been written by eq. (2.6) as

$$h_{\mathrm{u}}(t) = \sum_{l=0}^{L_{\mathrm{t}}-1} \alpha_{\mathrm{u},l} \delta(t - \tau_{\mathrm{u},l}) \tag{6.3}$$

where all the channel parameters are the same as defined in Section 2.1.6. In the sequel, let $\mathbf{h} = (\alpha_{\mathrm{u},0}, \cdots, \alpha_{\mathrm{u},L_{\mathrm{t}}-1})$ and $\mathbf{t} = (t_{\mathrm{u},0}, \cdots, t_{\mathrm{u},L_{\mathrm{t}}-1})$ denote the random vectors representing the gains and delays of the multipath components of an UWB channel.

[3] We here drop the user index k in eqs. (2.4) and (2.5) since we will focus on the effect of NB interference on UWB systems in this chapter, where only one UWB device transmits and the MUI is absent.

For NB interferers, the signals can be approximated by sinusoidal tones as [19], [20] [4]

$$s_n(t) = \sqrt{2E_n}\cos(2\pi f_n t + \theta_n) \tag{6.4}$$

where $s_n(t)$ is the signal and E_n is the transmitted power of the *n*th NB interferer. The parameters f_n and θ_n denote the carrier frequency and the phase of the *n*th NB interferer. For NB signals, it is reasonable to consider flat fading propagation channels, where the CIR for the *n*th interferer can be given by

$$h_n(t) = \alpha_n \delta(t - \tau_n) \tag{6.5}$$

where α_n and τ_n are the channel gain and delay for the *n*th NB user, respectively. We assume Rayleigh fading for NB signals. To emphasize the effect of NB interference, a single-user UWB system is considered. Assuming that there are N_n NB interferers in the channel, the signal at the UWB receiver can be expressed as [19]

$$r(t) = \sqrt{E_\mathrm{u}} \sum_i r_\mathrm{u}(t - iT_b; d_i) + \sum_{n=1}^{N_\mathrm{n}} \sqrt{E_n} r_n(t) + n(t) \tag{6.6a}$$

where

$$r_\mathrm{u}(t; d_i) = b_\mathrm{u}(t; d_i) * h_\mathrm{u}(t) = \sum_{l=0}^{L_\mathrm{t}-1} \alpha_{\mathrm{u},l} b(t - \tau_{\mathrm{u},l}; d_i) \tag{6.6b}$$

is the received waveform of the *i*th UWB information bit,

$$r_n(t) = s_n(t) * h_n(t) = \alpha_n s_n(t - \tau_n) \tag{6.6c}$$

is the interfering signal from the *n*th NB user, $n(t)$ is AWGN with two-sided PSD of $N_0/2$ and $*$ denotes convolution. We consider Rake reception with perfect channel information at the receiver, where the signal template $v(t; \mathbf{h}, \mathbf{t}) = r_\mathrm{u}(t; 0) - r_\mathrm{u}(t; 1)$ is adopted for coherent detection [5]. Assuming that the zeroth UWB information bit d_0 is to be detected

[4] This approximation is valid when the NB bandwidth is much smaller than the bit rate of UWB systems, as shown in [19].

[5] We here assume that the Rake receiver correlates the received signal with a signal template matched to all of the received paths. However, the analysis provided in this chapter is also valid when only a subset of the received paths are correlated and combined, i.e., the number of the Rake fingers L_f is less than that of the total resolvable multipaths, L_t. For the scenario where $L_\mathrm{f} \leq L_\mathrm{t}$, we only need to replace L_t in the subsequent analysis by L_f.

and perfect synchronization can be achieved, the sampled output of the Rake receiver is given by [19] [6]

$$R = 2\sqrt{E_{\mathrm{u}}}\sum_{l=0}^{L_{\mathrm{t}}-1}\alpha_{\mathrm{u},l}^2 + \sum_{n=1}^{N_{\mathrm{n}}}\alpha_n\sqrt{2E_n}|H(f_n;\mathbf{h},\mathbf{t})|\cos\phi_n + N \tag{6.7}$$

where $H(f;\mathbf{h},\mathbf{t})$ is the transfer function of the MF for a UWB signal propagating through a channel with the gain vector $\mathbf{h} = (h_{\mathrm{u},0},\cdots,h_{\mathrm{u},L_{\mathrm{t}}-1})$ and the delay vector $\mathbf{t} = (t_{\mathrm{u},0},\cdots,t_{\mathrm{u},L_{\mathrm{t}}-1})$ (c.f. eq. (6.3)). The RV N represents the zero-mean AWGN term with variance

$$\mathrm{var}(N) = \frac{N_0}{2}\int_{-\infty}^{\infty} v^2(t;\mathbf{h},\mathbf{t})dt = 2N_0\sum_{l=0}^{L_{\mathrm{t}}-1}\alpha_{\mathrm{u},l}^2. \tag{6.8}$$

In eq. (6.7), α_n is the channel gain of the *n*th NB interferer, and $\phi_n \in [0,2\pi)$ is the random phase term absorbing all of the signal phase θ_n, the phase of the transfer function $H(f;\mathbf{h},\mathbf{t})$ and the phase distortion caused by the delay of the *n*th NB interferer. The MF is matched to the received UWB bit waveform and its transfer function is the Fourier transform (FT) of the template $v(t;\mathbf{h},\mathbf{t})$ given by

$$H(f;\mathbf{h},\mathbf{t}) = \mathcal{F}_{v(t;\mathbf{h},\mathbf{t})}(f) = \mathcal{F}_{(r_{\mathrm{u}}(t;0)-r_{\mathrm{u}}(t;1))}(f) \tag{6.9}$$

where $\mathcal{F}_g(f)$ denotes the Fourier transform of function $g(t)$ defined as

$$\mathcal{F}_g(f) = \int_{-\infty}^{\infty} g(t)\exp(-j2\pi ft)dt. \tag{6.10}$$

In particular, it has been shown in [19] that $|H(f;\mathbf{h},\mathbf{t})|$ can be separated into two components

$$|H(f;\mathbf{h},\mathbf{t})| = |H_0(f)||H_{\mathrm{u}}(f;\mathbf{h},\mathbf{t})| \tag{6.11}$$

where $H_0(f) = \mathcal{F}_{b(t;0)-b(t;1)}(f)$ depends on the UWB signal structure and the second component

$$H_{\mathrm{u}}(f;\mathbf{h},\mathbf{t}) = \mathcal{F}(h_{\mathrm{u}}(t)) = \sum_{l=0}^{L-1}\alpha_{\mathrm{u},l}e^{-j2\pi f\tau_{\mathrm{u},l}} \tag{6.12}$$

is the Fourier transform of the UWB CIR and reflects current UWB channel conditions. Note that $H_0(f)$ is the transfer function of UWB MF for AWGN and flat-fading channels

[6]To emphasize the effect of NB interference, we ignore here other interference caused by the UWB multipath fading channel, e.g., the intersymbol interference (ISI) and interchip interference (ICI).

[19]. Consider an UWB signal given by eq. (6.2); $|H_0(f)|$ is given by

$$|H_0(f)| = 2|P(f)| \left| \sum_{k=0}^{N_\mathrm{s}-1} c_{\mathrm{DS},k} \exp\left(j2\pi f(mT_\mathrm{f} + c_{\mathrm{TH},k}T_\mathrm{c})\right) \right| \tag{6.13}$$

where $P(f)$ is the Fourier transform of the UWB pulse $p(t)$.

Since we assume that NB signals propagate through Rayleigh fading channels and the phase distortions $\{\phi_n\}_{n=1}^{N_\mathrm{n}}$ in eq. (6.7) are uniformly distributed in $[0, 2\pi)$, the interference term in eq. (6.7), which includes NB interference and AWGN, is Gaussian distributed conditioned on the CIR [7]. Therefore, the BER of the Rake receiver conditioned on the CIR is given as

$$P_{e|\mathbf{h},\mathbf{t}} = \mathcal{Q}(\sqrt{2\mathrm{SINR}_\mathrm{con}}) \tag{6.14}$$

where $\mathcal{Q}(\cdot)$ is the well-known $\mathcal{Q}$-function defined as

$$\mathcal{Q}(x) = \frac{1}{\sqrt{2\pi}} \int_x^\infty \exp(-\frac{y^2}{2})dy \tag{6.15}$$

and $\mathrm{SINR}_\mathrm{con}$ is the SINR at the output of the Rake receiver conditioned on the UWB CIR. This conditional SINR can be expressed as [19]

$$\mathrm{SINR}_\mathrm{con} = \frac{\mathrm{S}(\mathbf{h})}{\frac{N_0}{E_\mathrm{u}} + \sum_{n=1}^{N_\mathrm{n}} \frac{E_n}{2CT_\mathrm{b}} \cdot \frac{|H_0(f_n)|^2 |H_\mathrm{u}(f_n;\mathbf{h},\mathbf{t})|^2}{\mathrm{S}(\mathbf{h})}} \tag{6.16}$$

where $\mathrm{S}(\mathbf{h}) = \sum_{l=0}^{L-1} \alpha_{\mathrm{u},l}^2$, and $C = E_\mathrm{u}/T_\mathrm{b}$ denotes the useful receiver power of the UWB signal [19]. For BER performance analysis, the conditional BER $P_{e|\mathbf{h},\mathbf{t}}$ needs to be averaged over the random vectors $\mathbf{h}$ and $\mathbf{t}$, which involves weighting the conditional BER by positive quantities [8]. Hence, improving the BER performance of UWB devices in the presence of NB signals is equivalent to enhancing the conditional SINR given by eq. (6.16). Note that the only term in eq. (6.16) that can be affected by the UWB signal structure is $|H_0(f_n)|^2$ in the denominator. Therefore, to improve UWB system performance in the presence of NB

[7]The NB signals have a full duty cycle. Therefore, at the UWB MF receiver, the NB interference is present at every UWB frame. Therefore, different from the MUI discussed in previous chapters, the NB interference converges quickly to a Gaussian RV according to the CLT conditioned on the CIR.

[8]For detailed BER performance analysis, which requires averaging the conditional BER $P_{e|\mathbf{h},\mathbf{t}}$, over the distributions of random vectors $\mathbf{h}$ and $\mathbf{t}$, see [19], [20]. In [18], the authors provided a more comprehensive discussion on the BER performance of UWB systems in the presence of NB interference by considering a heterogeneous interfering network where the interfering nodes are spatially scattered according to a Poisson field.

services, the DS and the TH sequence should be designed to make the function $|H_0(f)|^2$ as small as possible at f_i $(i = 1, \cdots, N_\mathrm{n})$, i.e., they need to inherently create notch frequencies in $H_0(f)$ at bands where NB services operate. Moreover, note that the magnitude response of the MF is identical to the transmitted signal spectrum [27]. Hence, the DS and the TH sequence designs also reduce the power transmitted by UWB signals at the dedicated NB locations, and the interference caused by UWB devices to NB services is subsequently reduced.

6.2 Direct Sequence Design

In this section, we assume that a PN code is used as the TH sequence for the desired UWB user (c.f. eq. (6.2)) and this PN code is known by the UWB device. A DS design will be proposed based on this TH sequence and the spectral occupancy state of the current channel. In the sequel, we denote the DS by a vector $C_\mathrm{DS} = (c_{\mathrm{DS},0}, \cdots, c_{\mathrm{DS},N_\mathrm{s}-1})$, and the TH sequence by a vector $C_\mathrm{TH} = (c_{\mathrm{TH},0}, \cdots, c_{\mathrm{TH},N_\mathrm{s}-1})$. We also assume that these two sequences are independent of the symbol epoch, which implies that short codes are being considered. Therefore, the DS and the TH sequence can be fully described by C_DS and C_TH, respectively. The following denotations are also used. If A is a matrix, the transpose of A is denoted by A^T and the Hermitian adjoint of A is given by A^*, where $A^* = \bar{A}^T$ and $\bar{A}$ is the element-wise conjugate of matrix A.

As mentioned above, to enhance the performance of UWB systems in the presence of NB interference, the conditional SINR at the output of Rake receiver should be maximized. If there are N_n NB users with carrier frequencies $\{f_1, \cdots, f_{N_\mathrm{n}}\}$ coexisting with an UWB user, the conditional SINR is given by eq. (6.16). It should be mentioned that, for a typical NB carrier frequency, the statistic $H_\mathrm{u}(f_n, \mathbf{h}, \mathbf{t})$ is usually independent of the carrier frequency f_n [19]. Therefore, we may be able to interpret the NB interference related term in the denominator of eq. (6.16) as

$$\frac{H_\mathrm{u}(f_n, \mathbf{h}, \mathbf{t})|^2}{2CT_\mathrm{b}\mathrm{S}(\mathbf{h})} \sum_{n=1}^{N_\mathrm{n}} E_n |H_0(f_n)|^2. \tag{6.17}$$

Based on eq. (6.17), maximizing the SINR value in eq. (6.16) is equivalent to minimizing $\sum_{n=1}^{N_\mathrm{n}} E_n |H_0(f_n)|^2$, where $|H_0(f)|$ is given by eq. (6.13). Again, this means notch frequencies should be created in $|H_0(f)|$ at the dedicated NB locations. Let $p_{k,n} = \exp(j2\pi f_n(kT_\text{f} + c_{\text{TH},k}T_\text{c}))$ and $V_{p,n} = (p_{0,n}, \cdots, p_{N_\text{s}-1,n})$. The objective function can be expressed as

$$\begin{aligned}\sum_{n=1}^{N_\text{n}} E_n|H_0(f_n)|^2 &= C_\text{DS}^* \left(\sum_{n=1}^{N_\text{n}} E_n V_{p,n} V_{p,n}^*\right) C_\text{DS} \\ &= C_\text{DS}^* Q_\text{DS} C_\text{DS} \qquad (6.18\text{a})\end{aligned}$$

where C_DS is the length-N_s DS sequence with ± 1 components, and

$$Q_\text{DS} = \sum_{n=1}^{N_\text{n}} E_n V_{p,n} V_{p,n}^*. \qquad (6.18\text{b})$$

Note that eq. (6.18a) is a quadratic function of $c_{\text{DS},k}$ ($m = 0, \cdots, N_\text{s} - 1$), where $c_{\text{DS},k} \in \{-1, +1\}$ are the components of C_DS. In the sequel, we use $\mathcal{I}_\text{DS}^{N_\text{s}}$ to denote the set of vectors whose component is either +1 or -1, i.e., all the vectors in $\mathcal{I}_\text{DS}^{N_\text{s}}$ can potentially be used as the DS. Minimizing eq. (6.18a) is an optimization problem which can be solved by quadratic integer programming [114]. However, this is a NP hard problem [115]. The search for the optimal solution might be time-consuming for practical systems, which is undesired for low-cost, simple-structured UWB devices. Therefore, we resort to another approach to find a suboptimal solution with low computational complexity. We first relax the integer constraint on the components of C_DS [114], and the optimization problem becomes

$$\begin{aligned}&\text{minimize} \quad C_\text{DS}^* Q_\text{DS} C_\text{DS} \\ &\text{s.t.} \qquad\quad C_\text{DS}^* C_\text{DS} = N_\text{s}\end{aligned} \qquad (6.19)$$

where Q_DS given by eq.(6.18b) is a Hermitian matrix. It is useful to recall the Rayleigh-Ritz Theorem from [116, p. 176].

Theorem 6.1 (Rayleigh-Ritz). Let A denote a $n \times n$ Hermitian matrix, and let the eigenvalues of A be ordered as $\lambda_1 \leq \cdots \leq \lambda_n$. Then,

$$\lambda_1 x^* x \leq x^* A x \leq \lambda_n x^* x \quad \text{for all} \quad x \in \mathcal{C}^n \qquad (6.20)$$

where $\mathcal{C}^n$ is the vector space of complex vectors with length n. The first equality in eq.

(6.20) can be achieved by choosing x as the eigenvector of A corresponding to the smallest eigenvalue λ_1, and the second equality can be obtained by choosing x as the eigenvector of A corresponding to the largest eigenvalue λ_n.

The proof of Theorem 1 is provided in [116, p. 176]. Since Q_{DS} is a Hermitian matrix, it has N_{s} orthogonal eigenvectors. We denote the eigenvalues of Q_{DS} by $\lambda_1, \cdots, \lambda_{N_{\mathrm{s}}}$ where $\lambda_1 \leq \cdots \leq \lambda_{N_{\mathrm{s}}}$ and the corresponding eigenvectors as $q_1, \cdots, q_{N_{\mathrm{s}}}$ with norm $\sqrt{N_{\mathrm{s}}}$ [9]. According to Theorem 1, $x = q_1$ minimizes the expression $x^* Q_{\mathrm{DS}} x$ among all the length-N_{s} norm-$\sqrt{N_{\mathrm{s}}}$ complex vectors with a minimum $\lambda_1 N_{\mathrm{s}}$. Therefore, if $q_1 \in \mathcal{I}_{\mathrm{DS}}^{N_{\mathrm{s}}}$, i.e., the component of q_1 is either +1 or -1 and q_1 is a candidate for the DS, we can choose DS as $C_{\mathrm{DS}} = q_1$ so that the quadratic form $C_{\mathrm{DS}}^* Q_{\mathrm{DS}} C_{\mathrm{DS}}$ is minimized subject to the condition $C_{\mathrm{DS}}^* C_{\mathrm{DS}} = N_{\mathrm{s}}$ (c.f. eq. (6.19)). However, it should be noted that, generally, the component of q_1 can be any complex number and it cannot be used as the DS directly. Observe that the quadratic function $x^* Q_{\mathrm{DS}} x$ is smooth. Therefore, it is intuitive and reasonable to choose C_{DS} as a vector in $\mathcal{I}_{\mathrm{DS}}^{N_{\mathrm{s}}}$ which has the smallest Euclidean distance from q_1, since this C_{DS} gives the expression $C_{\mathrm{DS}}^* Q_{\mathrm{DS}} C_{\mathrm{DS}}$ a value close to the minimum $q_1^* Q_{\mathrm{DS}} q_1 = \lambda_1 N_{\mathrm{s}}$ [117]. Assuming that the eigenvector q_1 can be written as $q_1 = (q_{10}, \cdots, q_{1 N_{\mathrm{s}}-1})$, the distance between q_1 and C_{DS} is given by

$$D = \sqrt{\sum_{k=0}^{N_{\mathrm{s}}-1} (c_{\mathrm{DS},k} - q_{1k})^2} \tag{6.21}$$

where $c_{\mathrm{DS},k}$ is the kth component of C_{DS}. The DS with the smallest Euclidean distance from q_1 can be chosen by minimizing each term in the summation on the right side of eq. (6.21), i.e., if q_{1k} is on the left side of the complex plane, $c_{\mathrm{DS},k}$ is set to be -1; otherwise, $c_{\mathrm{DS},k} = +1$. To simplify the denotations, we represent the procedure of transfering a vector $V = (v_0, \cdots, v_{n-1}) \in \mathcal{C}^n$ to its closest vector $\tilde{V} = (\tilde{v}_0, \cdots, \tilde{v}_{n-1}) \in \mathcal{I}_{\mathrm{DS}}^n$ by $\mathrm{Int}_{\mathrm{DS,app}}(\cdot)$. This procedure can be expressed mathematically as

$$\mathrm{Int}_{\mathrm{DS,app}}(V) = \tilde{V}, \text{ where } \tilde{v}_k = \mathrm{sign}(\mathrm{real}(v_k)) \text{ for } k = \{0, \cdots, n-1\}. \tag{6.22}$$

Therefore, if the eigenvector $q_1 \notin \mathcal{I}_{\mathrm{DS}}^{N_{\mathrm{s}}}$, we choose the DS as $C_{\mathrm{DS}} = \mathrm{Int}_{\mathrm{DS,app}}(q_1)$. Intuitively, the basic idea behind our DS design is to find the eigenvector of Q_{DS} corresponding

[9] Note that the norm of C_{DS} is $\sqrt{N_{\mathrm{s}}}$. We set the norm of the eigenvectors to be the same as that of C_{DS} in order to make the selection of the DS code convenient, as shown in the sequel.

to the smallest eigenvalue. If this eigenvector is in $\mathcal{I}_{\mathrm{DS}}^{N_{\mathrm{s}}}$ and can be used as the DS directly, we choose the DS to be this eigenvector. Otherwise, a vector in $\mathcal{I}_{\mathrm{DS}}^{N_{\mathrm{s}}}$ with the smallest Euclidean distance from the eigenvector will be selected.

In the design procedure described above, we consider the simplest case where the smallest eigenvalue has only one corresponding eigenvector. However, the most common scenario in practical systems is that the smallest eigenvalue of Q_{DS} has algebraic multiplicity $m > 1$. The reason behind this is revealed by eq. (6.18b). Note that Q_{DS} is a summation of N_{n} rank-1 positive semidefinite matrices $V_{p,n}V_{p,n}^*$ $(n = 1, \cdots, N_{\mathrm{n}})$, and the weights associated with the summands, E_n $(n = 1, \cdots, N_{\mathrm{n}})$, are all positive. Therefore, Q_{DS} is a $N_{\mathrm{s}} \times N_{\mathrm{s}}$ matrix which is also positive semidefinite, and its rank satisfies the condition $\mathrm{rank}(Q_{\mathrm{DS}}) \leq N_{\mathrm{n}}$. In practical scenarios, the number of targeted NB frequency bands is usually smaller than the number of frames per bit, i.e., $N_{\mathrm{n}} \leq N_{\mathrm{s}}$. Under such circumstances, the smallest eigenvalue of Q_{DS} is 0 and the multiplicity of this zero eigenvalue is the dimension of the nullspace of Q_{DS}, which is given by $N_{\mathrm{s}} - \mathrm{rank}(Q_{\mathrm{DS}})$. As for the DS design problem, care must be taken to cope with this scenario. Denote the multiplicity of the smallest eigenvalue by m $(m \geq 1)$ and the corresponding m norm-$\sqrt{N_{\mathrm{s}}}$ orthogonal eigenvectors by $\{q_1, \cdots, q_m\}$. In this case, any linear combination of these m eigenvectors, $x = c_1 q_1 + \cdots + c_m q_m$ with $c_1^2 + \cdots + c_m^2 = 1$ and $c_i \geq 0$ [10], is also an eigenvector of Q_{DS} corresponding to the smallest eigenvalue λ_1, and we have

$$\begin{aligned} x^* Q_{\mathrm{DS}} x &= (c_1 q_1 + \cdots + c_m q_m)^* Q_{\mathrm{DS}} (c_1 q_1 + \cdots + c_m q_m) \\ &= (c_1^2 + \cdots + c_m^2) \lambda_1 N_{\mathrm{s}} = \lambda_1 N_{\mathrm{s}} \end{aligned} \tag{6.23}$$

which gives the minimum among all the length-N_{s} norm-$\sqrt{N_{\mathrm{s}}}$ complex vectors. Therefore, following the basic idea of our DS design as mentioned above, we have to find a linear combination of $\{q_1, \cdots, q_m\}$ such that the resulting vector $x = c_1 q_i + \cdots + c_m q_m \in \mathcal{I}_{\mathrm{DS}}^{N_{\mathrm{s}}}$. Then, $C_{\mathrm{DS}} = x$ solves the optimization problem given by eq. (6.19). If it is not possible to find such weights, we have to traverse through all possible weight vectors $(c_1, \cdots, c_m)$ satisfying the conditions $c_1^2 + \cdots + c_m^2 = 1$ and $c_i \geq 0$. For each vector $x = c_1 q_i + \cdots + c_m q_m$, the corresponding vector in $\mathcal{I}_{\mathrm{DS}}^{N_{\mathrm{s}}}$ is calculated as $\tilde{x} = \mathrm{Int}_{\mathrm{DS,app}}(x)$. For all the resulting $\tilde{x}$, the vector rendering the smallest value for $\tilde{x}^* Q_{\mathrm{DS}} \tilde{x}$ is chosen to be C_{DS}. However, this search-

[10] We put the constraint $c_1^2 + \cdots + c_m^2 = 1$ on the weights of the eigenvectors to assure that $||x|| = \sqrt{N_{\mathrm{s}}}$, which makes the selection of the DS code convenient.

ing process increases the computational complexity and is time-consuming. Therefore, a simplified approach is adopted here. Instead of considering all the linear combinations of the eigenvectors corresponding to the smallest eigenvalue, the searching process described above will only be performed on the eigenvectors $\{q_1, \cdots, q_m\}$. Hence, the algorithm can be described as follows:

Direct Sequence Design Algorithm

1. Obtain the matrix $Q_{\mathrm{DS}} = \sum_{n=1}^{N_\mathrm{n}} E_n V_{p,n} V_{p,n}^*$ where $V_{p,n} = (p_{0,n}, \cdots, p_{N_\mathrm{s}-1,n})$ and $p_{k,n} = \exp\left(j2\pi f_n(kT_\mathrm{f} + c_{\mathrm{TH},k}T_\mathrm{c})\right)$.

2. Find the smallest eigenvalue λ_1 of the matrix Q_{DS}. If this eigenvalue has multiplicity of m $(m \geq 1)$, find the corresponding eigenvectors $\{q_1, \cdots, q_m\}$, and set the norms of these vectors to $\sqrt{N_\mathrm{s}}$.

3. If any of these eigenvectors is in the set $\mathcal{I}_{\mathrm{DS}}^{N_\mathrm{s}}$, the search is over and the DS is chosen to be this eigenvector [11].

4. If the condition in Step 3) fails, for each eigenvector q_i $(i = 1, \cdots, m)$, find a vector $\tilde{q}_i \in \mathcal{I}_{\mathrm{DS}}^{N_\mathrm{s}}$ that has the smallest Euclidean distance to q_i, i.e., $\tilde{q}_i = \mathrm{Int}_{\mathrm{DS,app}}(q_i)$ where $\mathrm{Int}_{\mathrm{DS,app}}(\cdot)$ is given by eq. (6.22).

5. Calculate $\tilde{q}_i^* Q_{\mathrm{DS}} \tilde{q}_i$ for $i = 1, \cdots, m$, choose the vector that renders the smallest value and set C_{DS} to be this vector.

Discussion

Note that if there are multiple NB interferers in the network, the powers of the NB interferers, E_n $(n = 1, \cdots, N_\mathrm{n})$, should be known to decide the objective function given by eq. (6.19). However, this information is not always available or accurate at the UWB device where the DS is selected. Note in eq. (6.19) that E_n can also be viewed as a weight that

[11] If there are multiple eigenvectors in $\mathcal{I}_{\mathrm{DS}}^{N_\mathrm{s}}$, we can choose any one of them as C_{DS} without loss of optimality.

is put on the *n*th NB user in the interference suppression process, viz., the larger E_n is, the more emphasis is put on suppressing the interference caused by the *n*th NB user. Therefore, if the power of coexisting NB services is not known at the UWB device, E_n does not need to be the accurate value of the interferer's power and it can be chosen according to other information. For example, a priori knowledge of the spectral occupancy condition in the current network can be utilized to determine E_n, i.e., larger E_n is selected for the over-crowded frequency band where higher NB power is expected and stronger NB suppression is desired.

6.3 Time-Hopping Sequence Design

In this section, we assume that a PN code is used as the DS for the desired UWB user, and this PN sequence is known by the UWB device. A TH sequence design will be proposed based on the DS and the spectrum occupation information in the UWB victim link. The TH sequence design is more complicated than the DS design, since it is observed in eq. (6.13) that the TH sequence related terms in $|H_0(f)|$ appear as arguments of exponential functions. However, if there is only one coexisiting NB interferer, the TH sequence design has similarity to the DS design in the previous section. Consider the conditional SINR given by eq. (6.16) for the single NB interferer case. It is noted that there is only one term in the summation in the denominator. Hence, maximizing the conditional SINR is equivalent to minimizing $|H_0(f_1)|^2$ through the TH sequence design. According to eq. (6.13), the objective function $|H_0(f_1)|^2$ can be rewritten as

$$|H_0(f_1)|^2 = \left| \sum_{k=0}^{N_\mathrm{s}-1} e^{j2\pi f_1 c_{\mathrm{TH},k} T_\mathrm{c}} c_{\mathrm{DS},k} e^{j2\pi f_1 k T_\mathrm{f}} \right|^2 . \tag{6.24}$$

Here, we introduce a new vector $C_{\mathrm{TH,e}} = (c^e_{\mathrm{TH},0}, \cdots, c^e_{\mathrm{TH},N_\mathrm{s}-1})$, where $c^e_{\mathrm{TH},k} = \exp(j2\pi f_1 c_{\mathrm{TH},k} T_\mathrm{c})$ $(m = 0, \cdots, N_\mathrm{s}-1)$. Letting $p_{k,1} = c_{\mathrm{DS},k} \exp(j2\pi f_1 k T_\mathrm{f})$ and $V_{p,1} = (p_{0,1}, \cdots, p_{N_\mathrm{s}-1,1})$, eq. (6.24) can be expressed as

$$|H_0(f_1)|^2 = C^*_{\mathrm{TH,e}} (V_{p,1} V^*_{p,1}) C_{\mathrm{TH,e}} = C^*_{\mathrm{TH,e}} Q_{\mathrm{TH}} C_{\mathrm{TH,e}} \tag{6.25a}$$

where

$$Q_{\mathrm{TH}} = V_{p,1} V^*_{p,1}. \tag{6.25b}$$

Comparing eq. (6.25a) with the objective function of the DS design problem given by eq. (6.18a), we notice that TH sequence design can be stated in a similar fashion as the DS design (c.f. eq. (6.19)), where C_{DS} in eq. (6.19) is replaced by $C_{\mathrm{TH,e}}$. It should also be mentioned that the vectors C_{DS} and $C_{\mathrm{TH,e}}$ also show resemblance since their components assume discrete values. The component of C_{DS} assumes value from $\{+1, -1\}$ and the component of $C_{\mathrm{TH,e}}$, which is given by $c_k^{\mathrm{TH,e}} = \exp(j2\pi f_1 c_{\mathrm{TH},k} T_c)$ for $c_{\mathrm{TH},k} \in \{0, \cdots, N_{\mathrm{h}} - 1\}$, has at most N_h discrete values. We denote the set containing these discrete values by $\mathcal{D} = \{\mathrm{d}_0, \cdots, \mathrm{d}_{N_{\mathrm{h}}-1}\}$ where $\mathrm{d}_k = \exp(j2\pi f_1 k T_c)$ [12], and use $\mathcal{I}_{\mathrm{TH}}^{N_{\mathrm{s}}}$ to represent the set of length-N_{s} norm-$\sqrt{N_{\mathrm{s}}}$ vectors whose components assume values in the set $\mathcal{D}$. Note that $\mathcal{I}_{\mathrm{TH}}^{N_{\mathrm{s}}}$ is the feasible set for $C_{\mathrm{TH,e}}$; i.e., all the vectors in $\mathcal{I}_{\mathrm{TH}}^{N_{\mathrm{s}}}$ can be potentially used as $C_{\mathrm{TH,e}}$.

Based on these observations, it is intuitive to design the TH sequence by following a similar procedure to that used for designing the DS, as stated in the previous section. However, instead of finding the TH sequence directly, a new sequence, $C_{\mathrm{TH,e}}$, whose components are exponential functions of the original TH sequence, will be searched first, and the corresponding TH sequence can be determined accordingly [13]. The design procedure can be described as follows. We first find the smallest eigenvalue of $Q_{\mathrm{TH}} = V_{p,1} V_{p,1}^*$. Assume that the multiplicity of this eigenvalue is $m \geq 1$ and denote the corresponding norm-$\sqrt{N_{\mathrm{s}}}$ eigenvectors by $\{q_1, \cdots, q_m\}$. If any of these eigenvectors belongs to the set $\mathcal{I}_{\mathrm{TH}}^{N_{\mathrm{s}}}$, this eigenvector can be used directly as $C_{\mathrm{TH,e}}$ and the objective function $|H_0(f_1)|^2 = C_{\mathrm{TH,e}}^* Q_{\mathrm{TH}} C_{\mathrm{TH,e}}$ is minimized [14]. If none of the eigenvectors is in $\mathcal{I}_{\mathrm{TH}}^{N_{\mathrm{s}}}$, we follow a similar procedure as in the DS design case. For each eigenvector q_i ($i = 1, \cdots, m$), we find a vector $\tilde{q}_i \in \mathcal{I}_{\mathrm{TH}}^{N_{\mathrm{s}}}$ which has the smallest Euclidean distance to q_i. Letting $q_i = (q_{i0}, \cdots, q_{iN_{\mathrm{s}}-1})$ and $\tilde{q}_i = (\tilde{q}_{i0}, \cdots, \tilde{q}_{iN_{\mathrm{s}}-1})$, the distance between q_i and $\tilde{q}_i$ is given by

$$D(q_i, \tilde{q}_i) = \sqrt{\sum_{k=0}^{N_{\mathrm{s}}-1} (q_{ik} - \tilde{q}_{ik})^2}. \tag{6.26}$$

Note that q_{ik} can be any point in the complex plane, while $\tilde{q}_{ik}$ assumes discrete values in

[12] These discrete values can be represented as points on the unit circle in the complex plane. There might be repeated values in $\mathcal{D} = \{\mathrm{d}_0, \cdots, \mathrm{d}_{N_{\mathrm{h}}-1}\}$, depending on the product $f_1 T_{\mathrm{c}}$.

[13] The TH sequence C_{TH} might not be uniquely determined by $C_{\mathrm{TH,e}}$, since the components of $C_{\mathrm{TH,e}}$ and C_{TH} follow the relationship $c_k^{\mathrm{TH,e}} = \exp(j2\pi f_1 c_{\mathrm{TH},k} T_{\mathrm{c}})$, which is not necessarily a one-to-one function. The solution to this problem is provided in the sequel.

[14] If there are more than one eigenvector in $\mathcal{I}_{\mathrm{TH}}^{N_{\mathrm{s}}}$, $C_{\mathrm{TH,e}}$ can be chosen to be any one of them without loss of optimality.

$\mathcal{D} = \{d_0, \cdots, d_{N_\mathrm{h}-1}\}$ which contains at most N_h points on the unit circle of the complex plane. Let $\mathrm{Arg}(x) \in [-\pi, \pi)$ denote the principal argument of a complex number x. According to eq. (6.26), the vector $\tilde{q}_i \in \mathcal{I}_{\mathrm{TH}}^{N_\mathrm{s}}$ with the smallest Euclidean distance from q_i can be chosen by minimizing each term in the summation on the right side of eq. (6.26), i.e., its component $\tilde{q}_{ik}$ can be chosen as d_j so that among all the values in $\mathcal{D}$, $|\mathrm{Arg}(q_{ik} - \mathrm{d}_j)|$ gives the minimum. To simplify the notations, for any complex N_s-vector $V = (v_0, \cdots, v_{n-1})$, we denote the procedure of finding a vector $\tilde{V} = (\tilde{v}_0, \cdots, \tilde{v}_{n-1}) \in \mathcal{I}_{\mathrm{TH}}^{n}$ which has the smallest Euclidean distance from V, by $\mathrm{Int}_{\mathrm{TH,app}}(\cdot)$. This procedure can be expressed mathematically as

$$\begin{aligned} \tilde{V} &= \mathrm{Int}_{\mathrm{TH,app}}(V) \\ \text{where } \tilde{v_k} &= \mathrm{d}_j = \exp(j2\pi f_1 j T_c), \ \text{ if } \ j = \mathop{\arg\min}_{j\in\{0,\cdots,N_\mathrm{h}-1\}} |\mathrm{Arg}(v_k - \mathrm{d}_j)| \ \ k = 0, \cdots, n-1. \end{aligned} \tag{6.27}$$

Therefore, for each eigenvector q_i, its corresponding vector $\tilde{q}_i = \mathrm{Int}_{\mathrm{TH,app}}(q_i)$ is calculated. These new vectors have all their components in $\mathcal{D}$ and are candidates for $C_{\mathrm{TH,e}}$. Among these m vectors, we choose the one which gives $\tilde{q}_i^* Q_{\mathrm{TH}} \tilde{q}_i$ the smallest value and set $C_{\mathrm{TH,e}} = \tilde{q}_i$. This value for $C_{\mathrm{TH,e}}$ is supposed to give the objective function in eq. (6.25a) a value close to the minimum. The corresponding TH sequence can then be determined accordingly. In summary, the TH sequence design algorithm can be described as follows:

Time-Hopping Sequence Design Algorithm

1. Find the smallest eigenvalue of $Q_{\mathrm{TH}} = V_{p,1}^* V_{p,1}$ and the corresponding eigenvectors $\{q_1, \cdots, q_m\}$ $(m \geq 1)$.
2. If any of the eigenvectors is in $\mathcal{I}_{\mathrm{TH}}^{N_\mathrm{s}}$, i.e., all the components of the vector belong to the set $\mathcal{D}$, the search is over and $C_{\mathrm{TH,e}}$ is set to be this eigenvector.
3. If the condition in Step 2) fails, for each eigenvector q_i, find a sequence $\tilde{q}_i = \mathrm{Int}_{\mathrm{TH,app}}(q_i)$ where $\mathrm{Int}_{\mathrm{TH,app}}(\cdot)$ is given by eq. (6.27). Calculate $\tilde{q}_i^* Q_{\mathrm{TH}} \tilde{q}_i$ for $i = 1, \cdots, m$, choose the vector rendering the smallest result and set $C_{\mathrm{TH,e}}$ to this vector.

4. Find the TH sequence C_{TH} based on $C_{\mathrm{TH,e}}$ according to their relationship, i.e., if the kth component of $C_{\mathrm{TH,e}}$, $c^{e}_{\mathrm{TH},k} = \exp(j2\pi f_1 c_{\mathrm{TH},k} T_{\mathrm{c}}) = \mathrm{d}_j$, the kth component of the TH sequence, $c_{\mathrm{TH},k} = j$ [15].

6.4 Numerical Results and Discussion

In this section, simulation results are presented to illustrate the UWB system performance enhancement provided by the DS and the TH sequence designs given in prevous sections. We consider a second derivative of the Gaussian monocycle with energy $1/\sqrt{N_{\mathrm{s}}}$, which is given by (c.f. eq. (3.10))

$$p(t) = \sqrt{\frac{8}{3N_{\mathrm{s}}\tau_p}} \left[1 - 4\pi \left(\frac{t}{\tau_p}\right)^2\right] e^{-2\pi(\frac{t}{\tau_p})^2} \tag{6.28}$$

for signal transmission. The values of the system parameters (c.f. eq. (6.2)) used in the simulation for this chapter are given in Table 6.1. To show the effects of the DS and the TH sequence designs on the BER performance of UWB systems, we consider multipath fading propagation channels where Rake reception is adopted for signal recovery. The CM1 channel model suggested by [4] is considered. The SNR is defined as

$$\mathrm{SNR} = \frac{E_{\mathrm{u}}}{N_0} \tag{6.29}$$

where E_{u} is the energy per information bit for UWB systems, and the SIR is defined as

$$\mathrm{SIR} = \frac{C}{E_{\mathrm{n,tot}}} \tag{6.30}$$

where $C = E_{\mathrm{u}}/T_{\mathrm{b}}$ is the useful power transmitted by the UWB device, and $E_{\mathrm{n,tot}}$ is the total transmitted power of the NB interferers.

[15] The function $\exp(j2\pi f_1 c_{\mathrm{TH},k} T_{\mathrm{c}})$ is not necessarily injective for $c_{\mathrm{TH},k} \in \{0, \cdots, N_{\mathrm{h}} - 1\}$. Therefore, there might be more than one $c_{\mathrm{TH},k}$ that gives $c^{e}_{\mathrm{TH},k} = \exp(j2\pi f_1 c_{\mathrm{TH},k} T_{\mathrm{c}}) = \mathrm{d}_j$. In this case, any one of these values can be chosen for $c_{\mathrm{TH},k}$ without loss of performance.

TABLE 6.1
SYSTEM PARAMETERS FOR CHAPTER 6

Parameter	Value	Parameter	Value
N_{h}	16	N_{s}	16
τ_p	0.5 ns	T_{c}	1 ns
T_{f}	$T_{\mathrm{c}}N_{\mathrm{h}} = 16$ ns	T_{b}	$N_{\mathrm{s}}T_{\mathrm{f}} = 256$ ns

6.4.1 Direct Sequence Design

We first examine the impact of the DS design on an UWB system. In this case, a PN code is used as the TH sequence for the desired user. We randomly choose the TH sequence as $\mathrm{C_{TH}} = [8, 9, 15, 7, 5, 5, 12, 10, 4, 1, 8, 6, 14, 13, 12, 4]$ and assume that this sequence is known by the UWB device where the DS design is performed [16].

A Simple Illustration

Before we examine the effect of the DS design in practical systems, an example will be used here to illustrate how the design improves the performance of UWB system in the presence of NB interferers. Consider a case where the carrier frequence of the NB service is extremely low, e.g., f_1 = 1 KHz. Therefore, for a typical UWB device with system parameter given in Table 6.1, the NB signal shows itself as a flat line during the bit duration of the UWB pulse (c.f. Fig. 6.1). Therefore, at the UWB receiver, when the received signal is matched to the UWB pulse train propagating through the *l*th path, the NB interference component can be expressed as

$$\begin{aligned}
&\alpha_{\mathrm{u},l} \int_{iT_{\mathrm{b}}}^{(i+1)T_{\mathrm{b}}} \sqrt{E_n} r_n(t) b(t - iT_{\mathrm{b}} - \tau_{\mathrm{u},l}, d_i) dt \\
&= \alpha_{\mathrm{u},l}\sqrt{E_n} \int_{iT_{\mathrm{b}}}^{(i+1)T_{\mathrm{b}}} b(t - iT_{\mathrm{b}} - \tau_{\mathrm{u},l}, d_i) dt \\
&= \alpha_{\mathrm{u},l}\sqrt{E_n}(2d_i - 1) \int_0^{T_{\mathrm{b}}} p(t) dt \sum_{k=0}^{N_{\mathrm{s}}-1} c_{\mathrm{DS},k}. \qquad (6.31)
\end{aligned}$$

[16] In practical systems, the TH sequence should be a PN code with good Hamming correlation [118] instead of a random sequence used here. However, the DS design works effectively no matter what kind of code the TH sequence assumes. Therefore, a random sequence is used here as the TH sequence for illustration purposes. For the same reason, a random sequence will be used as the DS when the TH design is examined in the sequel.

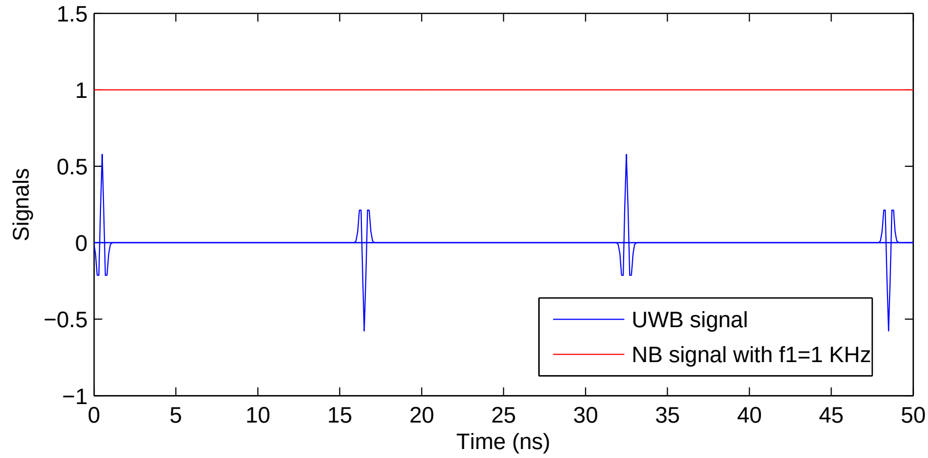

Fig. 6.1. An example of received NB and UWB signals when the carrier frequency of the NB device is $f_1 = 1$ KHz, and the system parameters for the UWB device is given by Table 6.1.

In this case, the DS generated by the DS design is given as

$$C_{\text{DS}} = [1, -1, 1, 1, -1, 1, 1, -1, 1, -1, -1, -1, 1, -1, 1, -1]. \tag{6.32}$$

Note that the summation of all the elements in C_{DS}, which appears on the right side of eq. (6.31), is zero. Therefore, the NB interference component equals zero, i.e., the NB interference in the UWB system is eliminated.

DS Design for Practical Systems

Consider here two scenarios where there is only one NB interferer and there are multiple NB interferers with different carrier frequencies in the channel. For both scenarios, the total transmitted power of the NB interferers is given by $E_{n,\text{tot}}$. For the first case, we assume the carrier frequency of the NB service is $f_1 = 2.412$ GHz, while in the second scenario, the carrier frequencies of the NB interferers are given as $f_1 = 2.402$ GHz, $f_2 = 2.412$ GHz and $f_3 = 2.420$ GHz. Furthermore in the second scenario, to illustrate how the power distribution of the NB services affects the NB interference suppression process, we consider two situations where the powers of these three NB interferers are given as $(0.33E_{n,\text{tot}}, 0.33E_{n,\text{tot}}, 0.33E_{n,\text{tot}})$ and $(0.8E_{n,\text{tot}}, 0.1E_{n,\text{tot}}, 0.1E_{n,\text{tot}})$, respectively.

The DS selected for these scenarios are given in Table 6.2. Fig. 6.2 shows the normalized transfer function $H_0(f)/\sqrt{T_b}$ of an UWB system with and without the DS chosen by

TABLE 6.2
THE DS SELECTED BY THE DS DESIGN

NB carrier frequencies (GHz)	NB powers ($\times E_{n,\mathrm{tot}}$)	Selected Direct Sequence
2.412	1	$[1, -1, 1, -1, 1, 1, -1, -1,$ $-1, 1, -1, -1, -1, -1, 1, -1]$
$(2.402, 2.412, 2.420)$	$(0.33, 0.33, 0.33)$	$[1, -1, -1, -1, 1, 1, -1, -1,$ $1, -1, -1, -1, 1, 1, 1, 1]$
$(2.402, 2.412, 2.420)$	$(0.8, 0.1, 0.1)$	$[-1, 1, 1, -1, -1, -1, 1, 1,$ $-1, 1, -1, -1, -1, 1, -1, 1]$

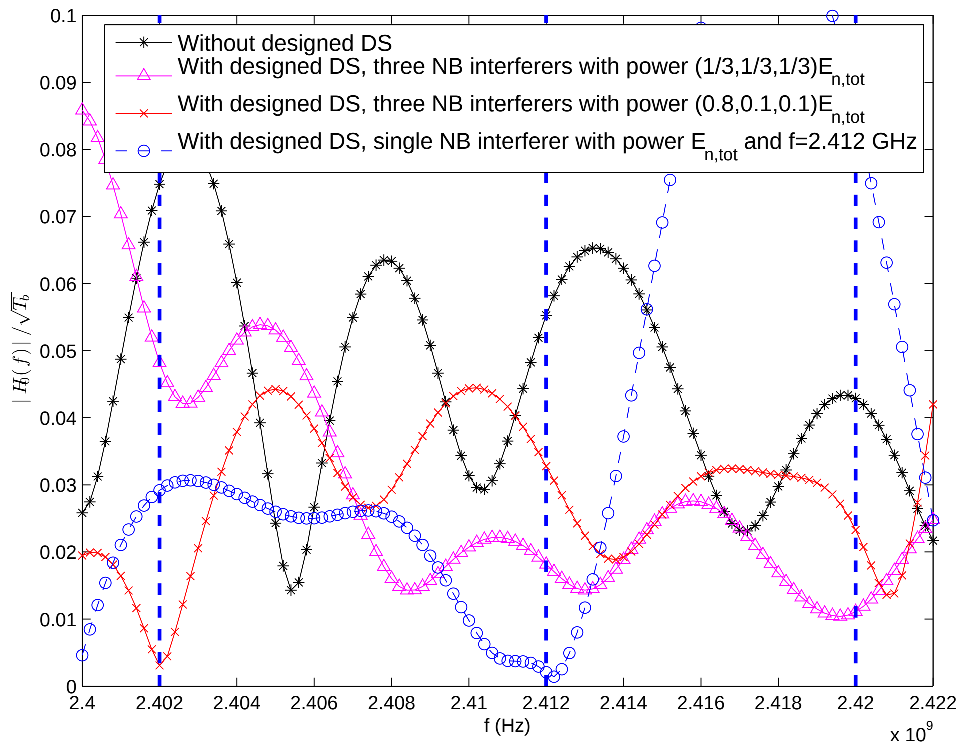

Fig. 6.2. The normalized transfer function $H_0(f)/\sqrt{T_b}$ of an UWB system with and without the designed DS around the carrier frequencies of the NB interferers.

the algorithm in Section 6.2. It is seen in Fig. 6.2 that the DS design creates notch frequencies at the targeted NB service bands. Note also that the effect of the DS design on the

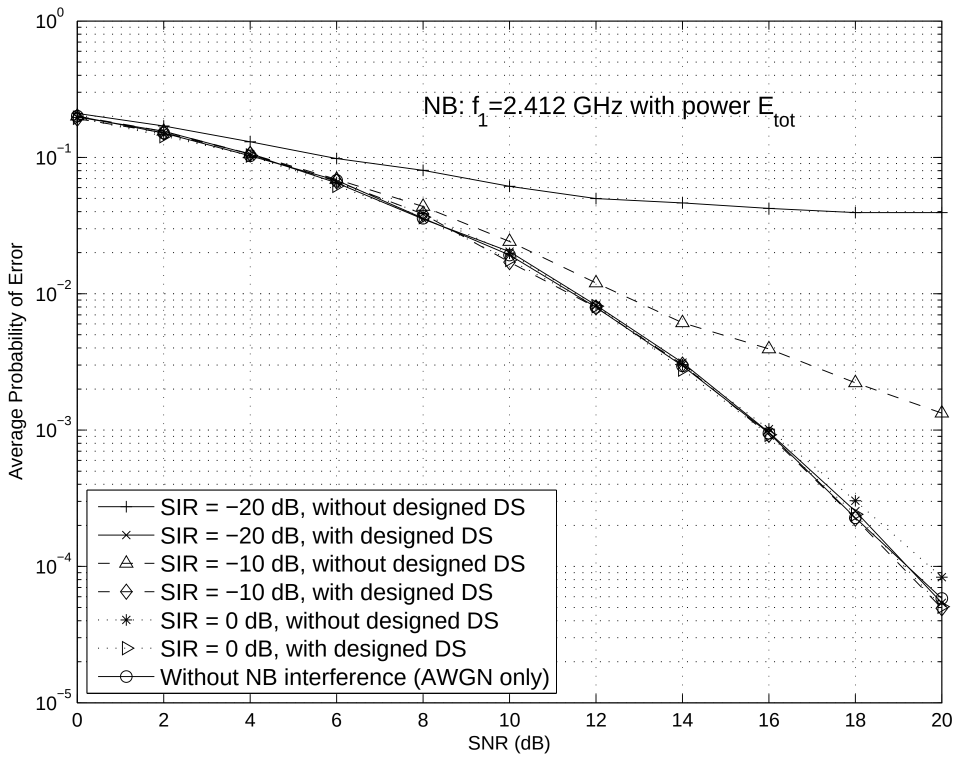

Fig. 6.3. The BER of an UWB system with and without the designed DS, when there is only one NB interferer with $f_1 = 2.412$ GHz and transmitted power $E_{\mathrm{n,tot}}$ in the system; the case where NB interference is absent is also plotted for comparison.

signal spectrum depends on the power distribution among different NB services [17]. Observe that more emphasis is put on suppressing the NB service with relatively large power, so that the total interference caused by NB signals is reduced. Note also that, compared to the multiple NB interferers case, the DS design algorithm performs better when there is only one interferer in the system, since all the efforts are put on suppressing the NB service at this particular band and a deep notch is thus created. On the other hand, since the magnitude response of the MF is identical to the transmitted UWB signal, low frequency responses of the MF at the NB carrier frequencies also mean that low power is carried by UWB signals at these bands. Therefore, when the designed DS is applied to UWB signals, the NB system performance in the presence of UWB signals is also enhanced since the UWB interference to the NB systems is highly reduced.

Fig. 6.3 shows the BER curves of an UWB system with and without the DS chosen by

[17]The single NB interferer case can be interpreted as the multiple NB interferers case with power $(0, E_{n,\mathrm{tot}}, 0)$.

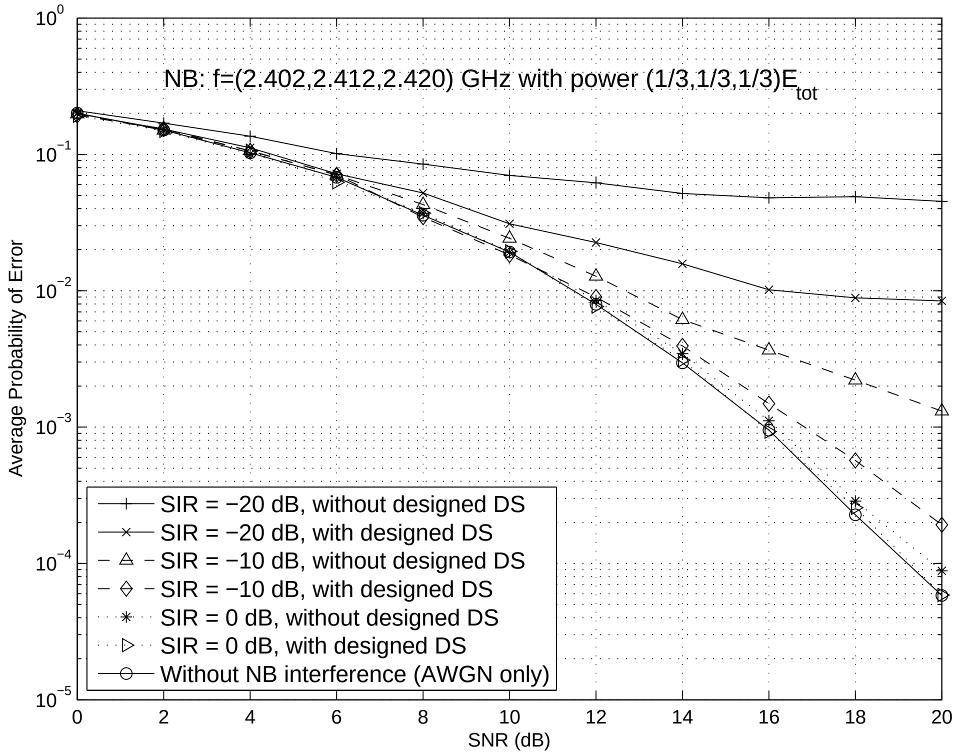

Fig. 6.4. The BER of an UWB system with and without the designed DS, when there are three NB interferers with different carrier frequencies in the system; the case where NB interference is absent is also plotted for comparison.

the algorithm in Section 6.2, when there is only one NB interferer with carrier frequency $f_1 = 2.412$ GHz in the UWB victim link. For comparison, the BER curve of an UWB system where the NB interference is absent and the signals are only corrupted by AWGN is also plotted. It is shown that the DS design algorithm can highly enhance the BER performance of UWB systems, and the enhancement is significant when the NB interference in the channel is strong. Note that for all the SIR values, the DS design algorithm can almost eliminate the NB interference, since the BER curves of UWB systems with the designed DS are graphically coincident with that for the case where the NB interference is absent. Fig. 6.4 shows the BER curves of an UWB system with and without the designed DS when there are three NB interferers in the victim UWB link. The carrier frequencies of the NB interferers are $f_1 = 2.402$ GHz, $f_2 = 2.412$ GHz and $f_3 = 2.420$ GHz and the power distribution is given by $(E_{n,\mathrm{tot}}/3, E_{n,\mathrm{tot}}/3, E_{n,\mathrm{tot}}/3)$. Note that the DS design algorithm also enhances the BER performance of UWB systems when multiple NB interferers are present. However, the performance enhancement is not as significant as the single NB

TABLE 6.3
THE TH SEQUENCE SELECTED BY THE TH SEQUENCE DESIGN

NB carrier frequencies (GHz)	NB powers ($\times E_{n,\mathrm{tot}}$)	Selected TH Sequence
2.412	1	$[4, 3, 8, 1, 0, 5, 4, 14, 13, 12, 5, 10, 9, 2, 7, 0]$

interferer case. Note that for SIR = -20 dB, the NB interference can not be eliminated by the DS design and the BER curve of an UWB system with the designed DS still reaches an error floor at 8.5×10^{-3} for practical SNR values.

6.4.2 Time-Hopping Sequence Design

In this part, we examine the effect of the TH sequence design given in Section 6.3. We assume a PN code is used as the DS for the desired UWB user. This DS is randomly chosen as $\mathrm{C_{DS}} = [1, 1, -1, 1, 1, -1, -1, 1, 1, 1, -1, 1, 1, -1, 1, -1]$ and assumed to be known by the UWB device where the TH sequence design is implemented. The TH sequence selected by the TH sequence design is given in Table 6.3. Note that the TH sequence design algorithm in Section 6.3 can only cope with the single NB interferer case. Therefore, we assume that there is only one NB interferer with carrier frequency $f_1 = 2.412$ GHz in the victim UWB link. Fig. 6.5 shows the normalized transfer function $H_0(f)/\sqrt{T_\mathrm{b}}$ of an UWB system with and without the TH sequence chosen by the algorithm in Section 6.3. It is seen in Fig. 6.5 that the TH sequence design creates a notch frequency at the targeted NB service band. Therefore, the mutual interference between UWB and NB systems can be highly reduced when the designed TH sequence is applied to UWB signals.

Fig. 6.6 shows the BER performance of an UWB system with and without the designed TH sequence when there is only one interferer with a carrier frequency $f_1 = 2.412$ GHz and power $E_{\mathrm{n,tot}}$ in the UWB victim link. It is seen in Fig. 6.6 that, for all SIR values, the BER curve of the UWB system with the designed TH sequence has almost the same performance as that in a channel where the NB interference is absent, viz., the TH sequence design can almost eliminate the NB interference for the single interferer case, at least for the condition we are examining. However, for the multiple interferers case, the TH design becomes complicated and might not be suitable for low-cost, simple-structured UWB systems.

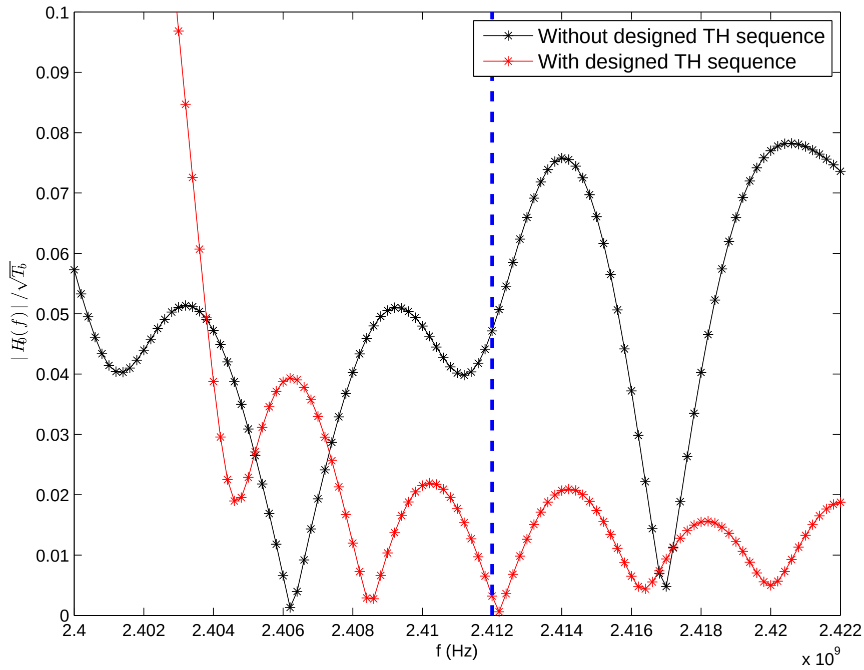

Fig. 6.5. The normalized transfer function $H_0(f)/\sqrt{T_b}$ of an UWB system with and without the designed TH sequence around the carrier frequency of the NB interferer.

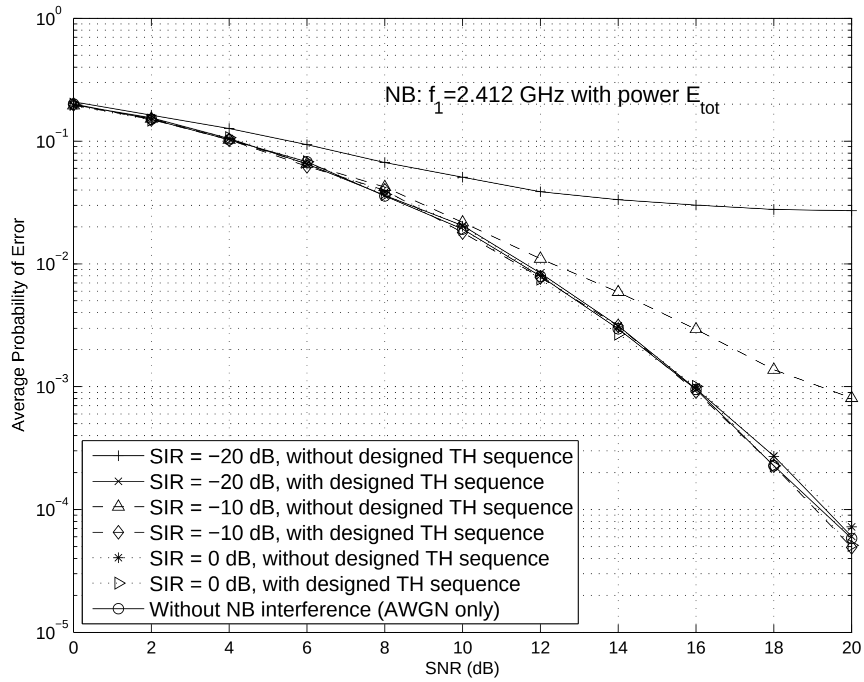

Fig. 6.6. The BER of an UWB system with and without the designed TH sequence, when there is only one interferer in the system; the case where NB interference is absent is also plotted for comparison.

6.5 Chapter Conclusion

Sequence code designs were proposed for IR UWB systems to cope with the coexistence problem between UWB and NB devices. An UWB signal structure with both DS and TH sequence was suggested, where one of them is used to shape the signal spectrum and reduce the mutual interference between NB and UWB systems and the other uses a PN code to preserve desired properties of SS signals. With this signal structure, a DS design was proposed when a PN code was used as the TH sequence, and a TH sequence design was also proposed when the DS assumes a PN code. It was shown that these sequence code designs are flexible in practical systems; they can efficiently create frequency nulls in the UWB spectrum so that the power transmitted by UWB signals are minimized in NB dedicated bands. Simulation results illustrated that the mutual interference between NB and UWB systems was significantly suppressed and the performance of IR UWB systems was greatly enhanced by adopting these sequence designs in UWB systems. Moreover, it was also shown that these code designs have low computational complexity. Therefore, they can be used to solve the coexistence problem effectively without complicating the UWB system structure extensively.

Chapter 7

Conclusions and Future Work

This chapter summarizes the contributions of the thesis and suggests some topics for future research.

7.1 Concluding Remarks

In this thesis, we focused on the performance evaluation and system designs of IR UWB systems in presence of MUI and NB interference. New system designs have been proposed to reduce the effect of interference and enhance the performance of UWB devices. A summary of our contributions is given as follows.

In Chapter 3, we first studied the MUI in IR UWB systems; the qualitative nature of the MUI PDF was observed, i.e., the correlator output amplitude can be binned into zones where the sent bit can be distinguished with high reliability and zones where the sent bit is essentially indistinguishable. A novel UWB receiver structure, named the zonal UWB receiver, was thus proposed based on the qualitative nature and the optimal, minimum probability of error, decision rule. This zonal receiver structure effectively erases the correlator output whenever the partial decision based on this sample becomes highly unreliable. A thorough mathematical analysis of this receiver design was also given in Chapter 3. It was established that the bounds defining the zones for the zonal receiver can be determined by certain system parameters which can be estimated in real-time, and bounds adapted to current operating conditions can be chosen from a look-up table according to these estimated parameters. It was also established that the CMF is just a special case of the zonal structure, and the zonal receiver can be adapted to provide no loss of optimality even in pure AWGN environments where the CMF is optimal. Simulation results in Chapter 3 showed that this zonal UWB receiver structure can always outperform the CMF UWB receiver, and the performance gain is significant in interference-limited scenarios. A Rake receiver adopting the zonal receiver structure in the fingers was also proposed for UWB signal detection in multipath fading channels, where this new Rake structure was shown to outperform the CMF based Rake receiver. More generally still, the zonal receiver approach can be applied to systems for which a plurality of correlations need to be performed in a receiver and better performance can be achieved by erasing or weighting the unreliable correlator output samples.

Experimental evidences as well as theoretical considerations have suggested that the MUI in IR UWB deviates from those conformable to a Gaussian model, and can be well described by heavy-tailed distributions. In Chapter 4, we used a generalized Gaussian distribution to model the MUI in UWB systems. It was shown in Chapter 4 that the generalized Gaussian distribution is a superior candidate for modeling the UWB MUI, since it can accurately model the MUI in almost all scenarios. Corresponding mathematical analysis was conducted thoroughly for this model, and a detailed method was provided to accommodate different UWB transmission scenarios by adjusting parameters in the generalized Gaussian distribution. A novel UWB receiver structure, dubbed the p-omr, was proposed in the Chapter 4 based on this model of the MUI. By adding another degree of freedom to the receiver design, an enhanced version of p-omr, the p-omatlr was also proposed. Thorough analysis and design studies for these novel receivers were conducted in Chapter 4; the entire receiver structure was specified, and an effective channel state estimator was also specified to obtain current channel information and generate updated parameters for the signal recovery. Mathematical analysis and theoretical results showed that these novel receivers have better BER performance than the CMF, which is widely used in IR UWB systems, and the performance gains are significant especially when the MUI is strong in the channel. A Rake receiver structure adopting p-omr or p-omatlr in each finger was also proposed in Chapter 4, and it was shown that this new Rake receiver can highly enhance the performance of the CMF based Rake receiver.

The repetition code is widely adopted in early studies of IR UWB systems. However, the repetition code is a trivial channel coding scheme, and not all potentials are explored by this channel code. Using other channel codes in IR UWB systems and providing performance analysis of such systems are thus motivated. In Chapter 5, an analytical framework for assessing the performance of coding in IR-UWB systems was developed. Analytical results were provided to assess codeword and bit error probabilities of soft-decision decoders in IR UWB system with the presence of the MUI, where a Rake receiver with MRC is adopted for signal reception in lognormal multipath fading UWB channels. Unlike previous works on this subject, a more accurate model other than the Gaussian model is adopted for the MUI. The analytical methods provided by Chapter 5 were shown to provide reliable prediction of error rate performance for coded UWB systems, and they are useful especially for the cases where performance evaluation based on simulation is time-consuming or impossible. The results have been derived for both block and convolutional codes, and can be applied to other communication systems where impulsive noise is present.

The UWB band overlaps with several frequency bands already allocated to established NB services. Successful deployment of UWB systems requires that UWB devices contend and coexist with these NB services. Therefore, the mutual interference between UWB and NB devices in the same coverage area should be minimized. In Chapter 6, direct and TH sequence designs which are adaptive to current channel conditions were proposed for IR UWB systems to cope with this coexistence problem. These designs shape the UWB signal spectrum and create spectral nulls at bands where NB services operate. Therefore, mutual interference between UWB and NB systems can be greatly reduced. It was shown in Chapter 6 that the BER performance of UWB systems is greatly enhanced, and the impact of UWB interference in NB systems is significantly decreased when the sequences generated by the sequence designs are adopted by UWB signals. It was also shown that these sequence designs have low computational complexities and can be easily implemented in low-cost, simple-structured UWB devices. With these sequence designs, the integrity of both UWB and NB systems are highly enhanced.

7.2 Directions for Future Reseach

In this thesis, we studied the interference in IR UWB systems and proposed system designs to reduce the impact of interference on the system performance. The research done in this thesis has opened some areas for future research.

In Chapter 5, a framework was developed to evaluate the performance of the soft-decision decoder in IR UWB systems. It has been mentioned that the MUI in IR UWB is impulsive and heavy-tailed. In [87], the authors mentioned that the hard-decision decoder can offer substantial improvement over the linear correlation receiver for impulsive noise channel over certain range of SNRs. Therefore, the performance of the hard-decision decoder in IR UWB systems with MUI is an interesting topic and worth investigation. Moreover, since the ambient noise is modeled by the Laplacian distribution, the soft-decision decoder is not optimum, and the optimum maximum likelihood detector based on the LRT is expected to enhance the performance of the soft-decision decoder. The performance of this optimum detector is worth investigation.

Furthermore, we have proposed several sequence designs for suppressing the mutual interference between UWB and NB services, where the NB signals are represented by sinusoidal tones. However, this approximation is only valid when the NB bandwidth is much smaller than the bit rate of UWB systems. Therefore, for those NB systems with relatively large bandwidth coexisting with low-data-rate UWB systems, some assumptions in Chapter 6 should be re-evaluated since the bandwidth of the NB service might become an issue. The sequence designs under such circumstances can be based on those provided in Chapter 6, and this topic can be considered as a future research direction.

In addition, the DS designs proposed in Chapter 6 are based on the premise that the elements of the DS assume values in $\{+1, -1\}$. However, it has been shown in [72] that this constraint might be relaxed. Note also in Chapter 6 that, when there is only one NB carrier frequency in the channel, the effect of the NB interference on UWB systems can be totally eliminated. However, when there is more than one carrier frequency in the channel, there is room for further improvement of the DS designs; this improvement might be achieved by relaxing the constraint on the direct sequence. This topic can be investigated as a future research. Moreover, the TH sequence design proposed in Chapter 6 can only handle the scenario where there is only one NB carrier frequency in the channel. This TH sequence design can be extended to the case where there is more than one NB interferer operating with UWB devices; and this is also an interesting topic for future research.

References

[1] FCC First Report and Order: In the matter of Revision of Part 15 of the Commission's Rule Regarding Ultra-Wideband Transmission Systems, FCC 02-48, Apr. 2002.

[2] L. Yang and G. B. Giannakis, "Ultra-wideband communications: An idea whose time has come," *IEEE Signal Process. Mag.*, pp. 26–54, Nov. 2004.

[3] N. C. Beaulieu and D. J. Young, "Designing time-hopping ultra-wide bandwidth receivers for multi-user interference environments," *Proc. IEEE*, pp. 255–284, Feb. 2009.

[4] J. R. Foerster, "Channel modeling sub-committee report (final)," 2003, IEEE P802.15-02/490r1-SG3a, Feb. 2003.

[5] M. D. Benedetto, T. Kaiser, A. F. Molisch, I. Oppermann, C. Politano, and E. D. Porcino, *UWB Communication Systems: A Comprehensive Overview*. Hindawi: EURASIP, 2006.

[6] S. Wood and A. Roberto, *Essentials of UWB*. Cambridge University Press, 2008.

[7] D. Cassioli, M. Z. Win, and A. F. Molisch, "Performance of low-complexity Rake reception in a realistic UWB channel," in *Proc. IEEE Int. Conf. on Commun. (ICC 2002)*, 2002, pp. 763–767.

[8] F. Ramlrez-Mireles, "On the performance of ultra-wide-band signals in Gaussian noise and dense multipath," *IEEE Trans. Veh. Techn.*, vol. 50(1), pp. 244–249, Jan. 2001.

[9] J. Zhang, R. Kennedy, and T. Abhayapala, "Performance of Rake reception for ultra wideband signals in a lognormal-fading channel," in *Proc. International Workshop on Ultra Wideband Systems (IWUWBS 2003)*, 2003, pp. 5–9.

[10] J. A. Gubner and K. Hao, "A computable formula for the average bit error probability as a function of window size for the IEEE 802.15.3a UWB channel model," *IEEE Trans. Microwave Theory Tech.*, vol. 54, pp. 1762–1768, Apr. 2006.

[11] G. Durisi and S. Benedetto, "Performance evaluation of TH-PPM UWB systems in the presence of multiuser interference," *IEEE Commun. Lett.*, vol. 7, pp. 224–226, May 2003.

[12] A. R. Forouzan, M. Nasiri-Kenari, and J. A. Salehi, "Performance analysis of time-hopping spread-spectrum multiple-access systems: uncoded and coded schemes," *IEEE Trans. Wireless Commun.*, vol. 1, pp. 671–681, Oct. 2002.

[13] B. Hu and N. C. Beaulieu, "Accurate performance evaluation of time-hopping and direct-sequence UWB systems in multi-user interference," *IEEE Trans. Commun.*, vol. 53, pp. 1053–1062, Jun. 2005.

[14] M. Sabattini, E. Masry, and L. B. Milstein, "A non-Gaussian approach to the performance analysis of UWB TH-BPPM systems," in *Proc. IEEE Conf. on Ultra Wideband Systems and Technologies (UWBST 2003)*, 2003, pp. 52–55.

[15] N. C. Beaulieu and B. Hu, "Soft-limiting receiver structures for time-hopping UWB in multiple-access interference," *IEEE Trans. Veh. Technol.*, vol. 57, pp. 801–818, Mar. 2008.

[16] N. C. Beaulieu and S. Niranjayan, "New UWB receiver designs based on a Gaussian-Laplacian noise-plus-MAI model," in *Proc. IEEE Int. Conf. on Commun. (ICC 2007)*, 2007, pp. 4128–4133.

[17] S. Niranjayan and N. C. Beaulieu, "A myriad filter detector for UWB multiuser communications," in *Proc. IEEE Int. Conf. on Commun. (ICC 2008)*, 2008, pp. 3918–3922.

[18] P. Pinto, A. Giorgetti, M. Z. Win, and M. Chiani, "A stochastic geometry approach to coexistence in heterogeneous wireless networks," *IEEE J. Sel. Areas Commun*, vol. 27, pp. 1268–1282, Sept. 2009.

[19] A. Giorgetti, M. Chiani, and M. Z. Win, "The effect of narrowband interference on wideband wireless communication systems," *IEEE Trans. Commun.*, vol. 53, pp. 2139–2149, Dec. 2005.

[20] M. Chiani and A. Giorgetti, "Coexistence between UWB and narrow-band wireless communication systems," *Proc. IEEE*, vol. 97, pp. 231–254, Feb. 2009.

[21] R. A. Scholtz, "Multiple access with time-hopping impulse modulation," in *Proc. Military Communications Conf. (MILCOM 1993)*, vol. 2, 1993, pp. 447–450.

[22] M. Hussain, "Principles of space-time array processing for ultrawide-band impulse radar and radio communications," *IEEE Trans. Veh. Technol.*, vol. 51, pp. 393–403, May 2002.

[23] H. Shao and N. C. Beaulieu, "An analytical method for calculating the bit error rate performance of Rake reception in UWB multipath fading channels," *IEEE Trans. Commun.*, vol. 58, pp. 1112–1120, Apr. 2010.

[24] M. Z. Win and R. A. Scholtz, "On the robustness of ultra-wide bandwidth signals in dense multipath environments," *IEEE Commun. Lett.*, vol. 2, pp. 51–53, Feb. 1998.

[25] S. A. Kassam, *Signal Detection in Non-Gaussian Noise*. Springer-Verlag, 1988.

[26] S. M. Kay, *Fundamentals of Statistical Signal Processing: Detection Theory*. Englewood Cliffs: Prentice Hall, 1998.

[27] J. G. Proakis, *Digital Communications*. New York: McGraw-Hill, 1995.

[28] H. R. Ahmadi and M. Nasiri-Kenari, "Performance analysis of time-hopping ultra-wideband systems in multipath fading channels (uncoded and coded schemes)," in *Proc. 13th IEEE International Symp. Personal, Indoor Mobile Radio Commun. (PIMRC 2002)*, 2002, pp. 1694–1698.

[29] Z. Ahmadian and L. Lampe, "Performance Analysis of the IEEE 802.15.4a UWB System," *IEEE Trans. Commun.*, vol. 57, pp. 1474 –1485, May 2009.

[30] N. C. Beaulieu and B. Hu, “On determining a best pulse shape for multiple access ultra-wideband communication systems,” *IEEE Trans. Wireless Commun.*, vol. 7, pp. 3589 –3596, Sept. 2008.

[31] N. C. Beaulieu and B. Hu, “A pulse design paradigm for ultra-wideband communication systems,” *IEEE Trans. Wireless Commun.*, vol. 5, pp. 1274–1278, Jun. 2006.

[32] L. Piazzo and J. Romme, “Spectrum control by means of the TH code in UWB systems,” in *Proc. IEEE Vehicular Technology Conference (VTC 2003)*, 2003, pp. 1649–1653.

[33] A. Giorgetti, M. Chiani, D. Dardari, R. Piesiewicz, and G. Bruck, “The cognitive radio paradigm for ultra-wideband systems: The European project EUWB,” in *Proc. IEEE International Conference on Ultra-Wideband (ICUWB 2008)*, 2008, pp. 169–172.

[34] M. M. Hämäläinen, R. Tesi, J. Iinatti, and V. Hovinen, “On the performance comparison of different UWB data modulation schemes in AWGN channel in the presence of jamming,” in *Proc. IEEE Radio and Wireless Conf. (RAWCON 2002)*, 2002, pp. 83 – 86.

[35] M. M. Hämäläinen, V. Hovinen, R. Tesi, J. Iinatti, and M. Latva-aho, “On the UWB system coexistence with GSM900, UMTS/WCDMA, and GPS,” *IEEE J. Sel. Areas Commun.*, vol. 20, pp. 1712 – 1721, Dec. 2002.

[36] B. Hu and N. C. Beaulieu, “Performance of an ultra-wideband communication system in the presence of narrowband BPSK- and QPSK-modulated OFDM interference,” *IEEE Trans. Commun.*, vol. 54, pp. 1720 –1724, Oct. 2006.

[37] L. Milstein, “Interference rejection techniques in spread spectrum communications,” *Proc. IEEE*, vol. 76, pp. 657 –671, Jun. 1988.

[38] L. A. Rusch and H. V. Poor, “Narrowband interference suppression in CDMA spread spectrum communications,” *IEEE Trans. Commun.*, vol. 42, pp. 1969 –1979, Feb./Mar./Apr. 1994.

[39] H. V. Poor and X. Wang, "Code-aided interference suppression for DS/CDMA communications. I. Interference suppression capability," *IEEE Trans. Commun.*, vol. 45, pp. 1101–1111, Sept. 1997.

[40] J. Wang and W. T. Tung, "Narrowband interference suppression in time-hopping impulse radio ultra-wideband communications," *IEEE Trans. Commun.*, vol. 54, pp. 1057–1067, Jun. 2006.

[41] B. Gaffney and A. Fagan, "Adaptive nonlinear narrow band interference rejection in ternary DS-UWB," in *Proc. IEEE Int. Conf. on Commun. (ICC 2006)*, 2006, pp. 3146 –3150.

[42] I. Bergel, E. Fishler, and H. Messer, "Narrowband interference suppression in time-hopping impulse-radio systems," in *Proc. IEEE Conf. on Ultra Wide-band Systems and Technologies (UWBST 2002)*, 2002, pp. 303–307.

[43] M. Z. Win and R. A. Scholtz, "Impulse radio: how it works," *IEEE Commun. Lett.*, vol. 2, pp. 36 –38, Feb. 1998.

[44] G. F. Ross and K. W. Robbins, *Base-band radiation and reception system*, June 12 1973, U.S. Patent 3,739,392.

[45] S. Verd*ú*, "Wireless bandwidth in the making," *IEEE Commun. Mag.*, vol. 38, pp. 53–58, 2000.

[46] Assessment of Ultra-Wideband (UWB) Technology, OSD/DARPA, Ultra-Wideband Radar Review Panel, R-6280, Jul. 13, 1990.

[47] C. E. Shannon, "A mathematical theory of communication," *Bell System Tech. J.*, vol. 27, pp. 379–423,623–656, Jul., Oct., 1948.

[48] A. Batra *et al.*, "Multi-band OFDM physical layer proposal for IEEE 802.15 task group 3a," IEEE 802.15-04/0493r1, Sept. 2004.

[49] I. Oppermann, L. Stoica, A. Rabbachin, Z. Shelby, and J. Haapola, "UWB wireless sensor networks: UWEN - a practical example," *IEEE Commun. Mag.*, pp. S27–S32, Dec. 2004.

[50] J. G. Proakis and M. Salehi, *Communication System Engineering*. Prentice-Hall, Englewood Cliffs, NJ, USA, 2004.

[51] J. R. Foerster, "The performance of a direct-sequence spread ultra wideband system in the presence of multipath, narowband interference, and multiuser interference," in *Proc. IEEE Conf. on Ultra Wide-band Systems and Technologies (UWBST 2002)*, 2002, pp. 245–250.

[52] A. A. M. Saleh and R. A. Valenzuela, "A statistical model for indoor multipath propagation," *IEEE J. Sel. Areas Commun.*, vol. SAC-5, pp. 128–137, Feb. 1987.

[53] D. Tse and P. Viswanath, *Fundamentals of Wireless Communication*. Cambridge University Press, 2005.

[54] S. Verdú, "Minimum probability of error for asynchronous Gaussian multiple-access channels," *IEEE Trans. Inform. Theory*, vol. IT-14, pp. 85–96, Jan. 1986.

[55] Y. C. Yoon and R. Kohno, "Optimum multi-user detection in ultra-wideband (uwb) multiple-access communication systems," in *Proc. IEEE Int. Conf. on Commun. (ICC 2002)*, 2002, pp. 812 – 816.

[56] M. B. Pursely, "Performance evaluation for phase-coded spread-spectrum multiple-access communication - Part I: System analysis," *IEEE Trans. Commun.*, vol. COM-25, pp. 795–799, Aug. 1977.

[57] D. E. Borth and M. B. Pursely, "Analysis of direct-sequence spread-spectrum multiple-access communication over rician fading channels," *IEEE Trans. Commun.*, vol. COM-27, pp. 1566–1577, Oct. 1979.

[58] M. Z. Win and R. A. Scholtz, "Ultra-wide bandwidth time-hopping spread-spectrum impulse radio for wireless multiple-access communications," *IEEE Trans. Commun.*, vol. 48, pp. 679–691, Apr. 2000.

[59] A. Taha and K. M. Chugg, "A theoretical study on the effects of interference on UWB multiple access impulse radio," in *Proc. Asilomar Conf. Signals, Systems and Computers*, Nov. 2002, pp. 728–732.

[60] J. Cheng and N. C. Beaulieu, “Accurate DS-CDMA bit-error probability calculation in Rayleigh fading,” *IEEE Trans. Wireless Commun.*, vol. 1, pp. 3–15, Jan. 2002.

[61] G. Durisi and G. Romano, “On the validity of Gaussian approximation to characterize the multiuser capacity of UWB TH-PPM,” in *Proc. IEEE Conf. on Ultra Wideband Systems and Technologies (UWBST 2003)*, 2003, pp. 157–161.

[62] N. C. Beaulieu and I. Hosseini, “On the PDF of multiple access interference in time-hopping UWB systems,” in *Proc. XXIX General Assembly of the Union of Radio Science International (URSI 2008)*, Aug. 2008.

[63] M. Z. Win, G. Chrisikos, and N. R. Sollenberger, “Performance of Rake reception in dense multipath channels: implications of spreading bandwidth and selection diversity order,” *IEEE J. Sel. Areas Commun.*, pp. 1516–1525, Aug. 2000.

[64] J. Ilow and D. Hatzinakos, “Analytic alpha-stable noise modeling in a Poisson field of interferers or scatterers,” *IEEE Trans. Signal Process.*, vol. 46, pp. 1601–1611, Jun. 1998.

[65] G. R. Arce, *Nonlinear Signal Processing*. New Jersey: Wiley, 2005.

[66] S. Buzzi, E. Conte, and M. Lops, “Optimum detection over Rayleigh-fading, dispersive channels, with non-Gaussian noise,” *IEEE Trans. Commun.*, vol. 45, pp. 1061–1069, Sept. 1997.

[67] N. C. Beaulieu and B. Hu, “A soft-limiting receiver structure for time-hopping UWB in multiple access interference,” in *Proc. IEEE International Symposium on Spread Spectrum Techniques and Application (ISSSTA 2006)*, 2006, pp. 417–421.

[68] Y. Dhibi and T. Kaiser, “On the impulsiveness of multiuser interferences in TH-PPM-UWB systems,” *IEEE Trans. Signal Process.*, vol. 54, pp. 2853 –2857, Jul. 2006.

[69] T. Erseghe, V. Cellini, and G. Dona, “On UWB impulse radio receivers derived by modeling MAI as a Gaussian mixture process,” *IEEE Trans. Wireless Commun.*, vol. 7, pp. 2388 –2396, Jun. 2008.

[70] A. J. Viterbi, *CDMA: Principles of Spread Spectrum Communication*. Addison Wesley Longman, Inc, 1995, 7th printing.

[71] IEEE 802.15.4a-2007, "Part 15.4: Wireless Medium Access Control (MAC) and Physical Layer (PHY) Specifications for Low-Rate Wireless Personal Area Networks (WPANs); Amendment 1: Add Alternate PHYs," Mar. 2007.

[72] L. Yang and G. B. Giannakis, "Digital-carrier multi-band user codes for baseband UWB multiple access," in *Proc. IEEE Conference on Ultra-Wideband Systems and Technologies (UWBST 2003)*, Nov. 2003, pp. 334 – 338.

[73] A. Papoulis and P. S. U. Pillai, *Random Variables and Stochastic Processes 4th ed.* Boston, MA: McGraw-Hill, 2002.

[74] M. Z. Win, P. C. Pinto, and L. A. Shepp, "A mathematical theory of network interference and its applications," *Proc. IEEE*, vol. 97, pp. 205 –230, Feb. 2009.

[75] E. J. Wegman, S. C. Schwartz, and J. B. Thomas, *Topics in Non-Gaussian Signal Processing*. New York: Springer, 1989.

[76] M. Chiani, "Analytical distribution of linearly modulated cochannel interferers," *IEEE Trans. Commun.*, vol. 45, pp. 73 –79, Jan. 1997.

[77] A. Giorgetti and M. Chiani, "Influence of fading on the Gaussian approximation for BPSK and QPSK with asynchronous cochannel interference," *IEEE Trans. Wireless Commun.*, vol. 4, pp. 384 – 389, Mar. 2005.

[78] H. Shao and N. C. Beaulieu, "A novel zonal UWB receiver structure with improved performance in multiple access interference," in *Proc. IEEE Global Commun. Conf. (GLOBECOM 2007)*, 2007, pp. 4118–4123.

[79] H. Shao and N. C. Beaulieu, "A novel zonal UWB receiver with superior performance," *IEEE Trans. Commun.*, vol. 57, pp. 1197–1206, Apr. 2009.

[80] N. C. Beaulieu and C. Leung, "On the performance of three suboptimal detection schemes for binary signaling," *IEEE Trans. Commun.*, vol. 33, pp. 241–245, Mar. 1985.

[81] G. Samorodnitsky, *Stable Non-Gaussian Random Processes: Stochastic Models with Infinite Variance*. Chapman & Hall, 1994.

[82] H. L. van Trees, *Detection, Estimation, and Modulation Theory*. Wiley-Interscience, Inc., 2001.

[83] K. L. Blackard, T. S. Rappaport, and C. W. Bostian, "Measurements and models of radio frequency impulsive noise for indoor wireless communications," *IEEE J. Sel. Areas Commun.*, vol. 11, pp. 991–1001, Sept. 1993.

[84] T. K. Blankenship, D. M. Kriztman, and T. S. Rappaport, "Measurements and simulation of radio frequency impulsive noise in hospitals and clinics," in *Proc. IEEE Vehicular Technology Conference (VTC 1997)*, vol. 3, Apr.-Jul. 1997, pp. 1942 – 1946.

[85] D. Middleton, "Man-made noise in urban environments and transportation systems: models and measurements," *IEEE Trans. Veh. Technol.*, vol. 22, pp. 148 – 157, Nov. 1973.

[86] D. Middleton, "Non-Gaussian noise models in signal processing for telecommunications: new methods an results for class A and class B noise models," *IEEE Trans. Inf. Theory*, vol. 45, pp. 1129 –1149, May 1999.

[87] B. Aazhang and H. V. Poor, "Performance of DS/SSMA communications in impulsive channels - II: Hard-limiting correlation receivers," *IEEE Trans. Commun.*, vol. 36, pp. 88–97, Jan. 1988.

[88] D. G. Brennan, "Linear diversity combining techniques," *Proc. IRE*, vol. 47, pp. 1075–1102, Jun. 1959.

[89] S. Im and E. J. Powers, "An algorithm for estimating signal-to-noise ratio of UWB signals," *IEEE Trans. Veh. Technol.*, vol. 54, pp. 1905 – 1908, Sept. 2005.

[90] Y. Chen and N. C. Beaulieu, "SNR Estimation Methods for UWB Systems," *IEEE Trans. Wireless Commun.*, vol. 6, pp. 3836 –3845, Oct. 2007.

[91] Y. Chen, N. C. Beaulieu, and H. Shao, "SNR and SIR estimation for multiuser UWB IR systems with TH-BPSK," *IEEE Signal Process. Lett.*, vol. 17, pp. 465 – 468, May 2010.

[92] J. Kingman, *Poisson Processes*. Oxford University Press, 1993.

[93] A. Goldsmith, *Wireless Communications*. Cambridge University Press: New York, 2005.

[94] H. Shao and N. C. Beaulieu, “Analysis of a novel p-order metric UWB receiver structure with improved performance in multiple access interference,” in *Proc. IEEE Global Commun. Conf. (GLOBECOM 2007)*, 2007, pp. 4112–4117.

[95] N. C. Beaulieu, H. Shao, and J. Fiorina, “P-order metric UWB receiver structures with superior performance,” *IEEE Trans. Commun.*, vol. 56, pp. 1666–1676, Oct. 2008.

[96] M. Schwartz and L. Shaw, *Signal Processing: Discrete Spectral Analysis, Detection, and Estimation*. New York: McGraw-Hill, 1975.

[97] H. Mathis, Ph. D. Thesis*, Nonlinear functions for blind separation and equalization,*. Swiss Federal Institute of Technology, Zrich, Nov. 2001.

[98] H. Hashemi, “The indoor radio propagation channel,” *Proc. IEEE*, vol. 81, pp. 943 –968, Jul 1993.

[99] E. Malkamaki and H. Leib, “Evaluating the performance of convolutional codes over block fading channels,” *IEEE Trans. Inf. Theory*, vol. 45, pp. 1643–1646, Jul. 1999.

[100] T. M. Cover and J. A. Thomas, *Elements of Information Theory, 2nd ed.* Wiley-Interscience, 2006.

[101] N. C. Beaulieu, A. A. Abu-Dayya, and P. J. McLane, “Estimating the distribution of a sum of independent lognormal random variables,” *IEEE Trans. Commn.*, vol. 43, pp. 2869–2873, Dec. 1995.

[102] R. J. Marks, G. L. Wise, D. G. Haldeman, and J. L. Whited, “Detection in Laplace noise,” *IEEE Trans. Aerosp. Electron. Syst.*, vol. AES-14, pp. 866–872, Nov. 1978.

[103] H. Shao and N. C. Beaulieu, “Block coding for impulsive Laplacian noise,” in *Proc. IEEE Int. Conf. on Commun. (ICC 2010)*, 2010, pp. 1–6.

[104] S. C. Schwartz and Y. S. Yeh, “On the distribution function and moments of power sums with lognormal components,” *Bell Syst. Tech. J.*, vol. 61, pp. 1441–1462, Sept. 1982.

[105] M. Abramowitz and I. A. Stegun, *Handbook of mathematical functions: with formulas, graphs, and mathematical tables, 9th printing*. New York: Dover Publications, Inc., 1965.

[106] G. C. Clark and J. B. Cain, *Error-Correction Coding for Digital Communications*. Plenum Press: New York, 1981.

[107] H. Bouzekri and S. Miller, "Distance spectra and performance bounds of space-time trellis codes over quasistatic fading channels," *IEEE Trans. Inf. Theory*, vol. 50, pp. 1820–1831, Aug. 2004.

[108] R. Gallager, *Low-Density Parity-Check Codes*. Cambridge, MA: MIT Press, 1963.

[109] R. Gallager, "A simple derivation of the coding theorem and some applications," *IEEE Trans. Inf. Theory*, vol. 11, pp. 3–18, Jan. 1965.

[110] M. P. C. Fossorier, S. Lin, and D. Rhee, "Bit-error probability for maximum-likelihood decoding of linear block codes and related soft-decision decoding methods," *IEEE Trans. Inf. Theory*, vol. 44, pp. 3083–3090, Nov. 1998.

[111] H. Shao and N. C. Beaulieu, "A time-hopping sequence design for narrowband interference suppression in impulse radio UWB systems," to be presented at *IEEE Int. Conf. on Commun. (ICC 2011)*, Kyoto, Japan, Jun. 2011.

[112] H. Shao and N. C. Beaulieu, "A direct sequence design for narrowband interference mitigation in impulse radio UWB systems," submitted to *IEEE Global Commun. Conf. (GLOBECOM 2011)*, Houston, Texas, USA, Dec. 2011.

[113] H. Shao and N. C. Beaulieu, "Direct sequence and time-hopping sequence designs for narrowband interference mitigation in impulse radio UWB systems," to appear in *IEEE Trans. Commun.*.

[114] O. V. Volkovich and V. Roshchin, "Models and methods of solution of quadratic integer programming problems," *Translated from KibernetiKa*, no. 3, pp. 1–15, May-June 1987.

[115] A. Beck and M. Teboulle, "Global optimality conditions for quadratic optimization problems with binary constraints," *SIAM Journal on Optimization*, vol. 11, pp. 179–188, 2000.

[116] R. Horn and C. R. Johnson, *Matrix Analysis*. Cambridge University Press, 1985.

[117] C. Wang, M. Ma, R. Ying, and Y. Yang, "Narrowband interference mitigation in DS-UWB systems," *IEEE Signal Process. Lett.*, vol. 17, pp. 429–432, May 2010.

[118] M. K. Simon, J. K. Omura, R. A. Scholtz, and B. K. Levitt, *Spread Spectrum Communications Handbook, revised ed.* New York: McGraw-Hill, 1994.

Appendix A

Proof of Eqs. (4.9) and (4.10)

In this section, a proof of eqs. (4.9) and (4.10), which are the expressions for the second and fourth moments of the MUI component in a single UWB frame, respectively, is provided.

Note that the expression for I_m is given by eq. (4.3) as

$$I_m = \sum_{k=2}^{N_\mathrm{u}} \sqrt{\frac{E_\mathrm{b}}{N_\mathrm{s}}} A_k \left(2d^{(k)}_{\lfloor (m+m_k)/N_\mathrm{s} \rfloor} - 1\right) R\left(a_k - c^{(k)}_{\mathrm{TH},m+m_k} T_\mathrm{c}\right) \tag{A-1}$$

where N_u is the number of users in the system, E_b is the bit energy of the UWB signal and A_k is the channel attenuation of the *k*th user. The RV $d^{(k)}_{\lfloor (m+m_k)/N_\mathrm{s} \rfloor}$ represents the information bit transmitted by the *k*th user, assuming values in $\{+1, -1\}$ with equal probability, m_k is the value of the transmission time difference, $T_1 - T_k$, measured in durations of one frame time rounded to the nearest integer, a_k is the fractional part which is uniformly distributed in $[-T_\mathrm{f}/2, T_\mathrm{f}/2)$, and $c^{(k)}_{\mathrm{TH},m+m_k}$ is the TH sequence of the *k*th user which takes integer values in the range $[0, \cdots, N_\mathrm{h}]$ with equal probability. Let $C^{(k)}_{\mathrm{TH}} = (c^{(k)}_{\mathrm{TH},0}, \cdots, c^{(k)}_{\mathrm{TH},N_\mathrm{s}-1})$ denote the vector representing the TH sequence of the *k*th user. Therefore, assuming that signals from different users are independent, the second moment of I_m conditioned on a_k and $C^{(k)}_{\mathrm{TH}}$ $(k = 2, \cdots, N_\mathrm{u})$ can be expressed as

$$\mathbb{E}\left(I_m^2 | \left\{a_k, C^{(k)}_{\mathrm{TH}}\right\}_{k=2}^{N_\mathrm{u}}\right) = \sum_{k=2}^{N_\mathrm{u}-1} \frac{E_\mathrm{b}}{N_\mathrm{s}} A_k^2 R^2 \left(a_k - c^{(k)}_{\mathrm{TH},m+m_k} T_\mathrm{c}\right) \tag{A-2}$$

Note that $c^{(k)}_{\mathrm{TH},m+m_k}$ assumes values in $\{0, \cdots, N_\mathrm{h}\}$ with equal probability. Therefore, the second moment of I_m conditioned on a_k can be obtained by averaging eq. (A-2) over the

PDF of $c_{\mathrm{TH},m+m_k}^{(k)}$ as

$$\mathbb{E}\left(I_m^2|\left\{a_k\right\}_{k=2}^{N_\mathrm{u}}\right)=\frac{1}{N_\mathrm{h}}\sum_{h=0}^{N_\mathrm{h}}\sum_{k=2}^{N_\mathrm{u}-1}\frac{E_\mathrm{b}}{N_\mathrm{s}}A_k^2R^2\left(a_k-hT_\mathrm{c}\right). \tag{A-3}$$

The RV a_k can be further averaged out as

$$\mathbb{E}\left(I_m^2\right)=\frac{1}{N_\mathrm{h}}\sum_{h=0}^{N_\mathrm{h}}\sum_{k=2}^{N_\mathrm{u}-1}\frac{E_\mathrm{b}}{N_\mathrm{s}}A_k^2\frac{1}{T_\mathrm{f}}\int_{-T_\mathrm{f}/2}^{T_\mathrm{f}/2}R^2\left(a_k-hT_\mathrm{c}\right)da_k \tag{A-4}$$

since a_k is uniformly distribution in $[-T_\mathrm{f}/2, T_\mathrm{f}/2)$.

Note that the duration of the UWB pulse $p(t)$ is τ_p, thus, the support of the autocorrelation function $R(x)$ is $[-\tau_p, \tau_p)$. Letting $x = a_k - hT_\mathrm{c}$, the term for a particular value of h in eq. (A-4) can be rewritten as

$$\int_{-T_f/2}^{T_f/2}R^2(a_k-hT_\mathrm{c})d\alpha_k=\int_{-T_f/2-hT_\mathrm{c}}^{T_f/2-hT_\mathrm{c}}R^2(x)dx. \tag{A-5}$$

With the assumption $N_hT_\mathrm{c} < T_\mathrm{f}/2 - 2\tau_p$ [58], the region of the integration at the right side of eq. (A-5) is an interval covering the support of the integrand. Thus, we can extend the integration region to $(-\infty, +\infty)$ without changing the integral, and the term for a particular h can be rewritten as $\int_{-\infty}^{+\infty} R^2(x)dx$. Note that these terms for all the possible values of h are the same. Thus, eq. (A-4) can be expressed as eq. (4.9). The derivation of eq. (4.10) can be obtained by following a same procedure. The conditional fourth moment of I_m can be expressed as

$$\begin{aligned}
\mathbb{E}\left(I_m^4|\left\{a_k, C_{\mathrm{TH}}^{(k)}\right\}_{k=2}^{N_\mathrm{u}}\right) &= \sum_{k=2}^{N_\mathrm{u}}\left(\frac{E_\mathrm{b}}{N_\mathrm{s}}\right)^2A_k^4R^4\left(a_k-c_{\mathrm{TH},m+m_k}^{(k)}T_\mathrm{c}\right)\\
&+\sum_{k=2}^{N_\mathrm{u}-1}\sum_{k_1=k+1}^{N_\mathrm{u}}A_k^2A_{k_1}^2\left(\frac{E_\mathrm{b}}{N_\mathrm{s}}\right)^2R^2\left(a_k-c_{\mathrm{TH},m+m_k}^{(k)}T_\mathrm{c}\right)R^2\left(a_{k_1}-c_{\mathrm{TH},m+m_{k_1}}^{(k_1)}T_\mathrm{c}\right)\\
&+\sum_{k=2}^{N_\mathrm{u}}\sum_{k_1\neq k}^{N_\mathrm{u}}A_kA_{k_1}^3\mathbb{E}\left(\left(2d_{\lfloor(m+m_k)/N_\mathrm{s}\rfloor}^{(k)}-1\right)\left(2d_{\lfloor(m+m_{k_1})/N_\mathrm{s}\rfloor}^{(k_1)}-1\right)^3\right)\left(\frac{E_\mathrm{b}}{N_\mathrm{s}}\right)^2\\
&\times R\left(a_k-c_{\mathrm{TH},m+m_k}^{(k)}T_\mathrm{c}\right)R^3\left(a_{k_1}-c_{\mathrm{TH},m+m_{k_1}}^{(k_1)}T_\mathrm{c}\right).
\end{aligned} \tag{A-6}$$

Since we assume that the information sent by different users are independent and the $d_i^{(k)}$ assumes values in $\{0, 1\}$ with equal probability, the last double summation on the right side of eq.(A-6) equals zero. Therefore, assuming that the TH sequences assigned to different users are independent, $c_{\mathrm{TH},m+m_k}^{(k)}$ and $c_{\mathrm{TH},m+m_{k_1}}^{(k_1)}$ can be averaged out from eq. (A-6) and the conditional fourth moment of I_m can be expressed as

$$\begin{aligned}\mathbb{E}\left(I_m^4 |\left\{a_k\right\}_{k=2}^{N_\mathrm{u}}\right) = {} & \frac{1}{N_\mathrm{h}} \sum_{h=0}^{N_\mathrm{h}-1} \sum_{k=2}^{N_\mathrm{u}} \left(\frac{E_\mathrm{b}}{N_\mathrm{s}}\right)^2 A_k^4 R^4\left(a_k - hT_\mathrm{c}\right) \\ & + \sum_{k=2}^{N_\mathrm{u}-1} \sum_{k_1=k+1}^{N_\mathrm{u}} A_k^2 A_{k_1}^2 \left(\frac{E_\mathrm{b}}{N_\mathrm{s}}\right)^2 \frac{1}{N_\mathrm{h}^2} \sum_{h=0}^{N_\mathrm{h}-1} R^2\left(a_k - hT_\mathrm{c}\right) \sum_{h_1=0}^{N_\mathrm{h}-1} R^2\left(a_{k_1} - h_1 T_\mathrm{c}\right).\end{aligned} \tag{A-7}$$

Note that a_k $(k = 2, \cdots, N_\mathrm{u})$ are independent and uniformly distributed in $[-T_\mathrm{f}/2, T_\mathrm{f}/2)$. Therefore, the fourth moment of I_m can be obtained by averaging eq. (A-7) over the PDF of a_k as

$$\begin{aligned}\mathbb{E}\left(I_m^4 |\left\{a_k\right\}_{k=2}^{N_\mathrm{u}}\right) = {} & \frac{1}{N_\mathrm{h}} \sum_{h=0}^{N_\mathrm{h}-1} \sum_{k=2}^{N_\mathrm{u}} \left(\frac{E_\mathrm{b}}{N_\mathrm{s}}\right)^2 A_k^4 \frac{1}{T_\mathrm{f}} \int_{a_k=-T_\mathrm{f}/2}^{T_\mathrm{f}/2} R^4\left(a_k - hT_\mathrm{c}\right) da_k \\ & + \sum_{k=2}^{N_\mathrm{u}-1} \sum_{k_1=k+1}^{N_\mathrm{u}} A_k^2 A_{k_1}^2 \left(\frac{E_\mathrm{b}}{N_\mathrm{s}}\right)^2 \frac{1}{N_\mathrm{h}^2} \sum_{h=0}^{N_\mathrm{h}-1} \frac{1}{T_\mathrm{f}^2} \int_{a_k=-T_\mathrm{f}/2}^{T_\mathrm{f}/2} R^2\left(a_k - hT_\mathrm{c}\right) da_k \\ & \times \sum_{h_1=0}^{N_\mathrm{h}-1} \int_{a_{k_1}=-T_\mathrm{f}/2}^{T_\mathrm{f}/2} R^2\left(a_{k_1} - h_1 T_\mathrm{c}\right) da_{k_1}.\end{aligned} \tag{A-8}$$

Using eq. (A-5) and adopting the assumption $N_h T_\mathrm{c} < T_\mathrm{f}/2 - 2\tau_p$ [58], eq. (A-8) can be further simplified as eq. (4.10).

Appendix B

Proof of Eq. (5.6a)

In this section, a proof of eq. (5.6a), which is the expression for the second moment of the MUI component in a single UWB frame when UWB signals propagate through multipath fading channels, is provided.

Note that the MUI component in a frame when UWB signals propagate through multipath fading channels can be mathematically expressed as (c.f. eq. (5.5c))

$$I_m = \sum_{l=0}^{L_{\mathrm{f}}-1} \alpha_l^{(1)} \sum_{k=2}^{N_{\mathrm{u}}} \sqrt{E_{\mathrm{c}}^{(k)}} \sum_{l_1=0}^{L_{\mathrm{t}}-1} I_{l_1,l,m}^{(k)} \tag{B-1}$$

where

$$\begin{aligned} I_{l_1,l,m}^{(k)} &= \sum_{i_1=-\infty}^{\infty} \sum_{m_1=0}^{N_{\mathrm{s}}-1} \alpha_{l_1}^{(k)} (2d_{i_1,m_1}^{(k)} - 1) \\ &\times \int_{mT_{\mathrm{f}}+l\Delta}^{mT_{\mathrm{f}}+(l+1)\Delta} p(t - i_1 T_{\mathrm{cw}} - m_1 T_{\mathrm{f}} - c_{\mathrm{TH},m_1}^{(k)} T_{\mathrm{c}} - l_1\Delta - T_k) p(t - mT_{\mathrm{f}} - l\Delta) dt. \end{aligned} \tag{B-2}$$

We here use $R(x)$ to denote the autocorrelation function of $p(t)$ (c.f. eq. (2.2)). Then we have

$$\begin{aligned} I_{l_1,l,m}^{(k)} &= \sum_{i_1=-\infty}^{\infty} \sum_{m_1=0}^{N_{\mathrm{s}}-1} \alpha_{l_1}^{(k)} (2d_{i_1,m_1}^{(k)} - 1) \\ &\times R(i_1 T_{\mathrm{cw}} + (m_1 - m) T_{\mathrm{f}} + c_{\mathrm{TH},m_1}^{(k)} T_{\mathrm{c}} + (l_1 - l)\Delta + T_k) \end{aligned} \tag{B-3}$$

As mentioned previously, the amplitudes $\left\{\alpha_l^{(k)}\right\}_{l=0}^{L_{\mathrm{t}}-1}$ all have zero means, and the interfering information bit $d^{(k)}_{i_1,m_1}$ assumes value from $\{+1,-1\}$ with equal probability. Thus, the PDF of $I^{(k)}_{l_1,l,m}$ is symmetric about the point 0, and its mean is zero. According to eq. (B-4), the MUI I_m also has zero mean. Let $m_d = i_1 N_{\mathrm{s}} + m_1$. Since $T_{\mathrm{cw}} = N_{\mathrm{s}} T_{\mathrm{f}}$ (c.f. Section 5.1), eq. (B-4) can be rewritten as

$$I^{(k)}_{l_1,l,m} = \sum_{m_d=-\infty}^{\infty} \alpha^{(k)}_{l_1}(2c^{(k)}_{m_d} - 1) R\left((m_d - m)T_{\mathrm{f}} + c^{(k)}_{\mathrm{TH},m_1} T_{\mathrm{c}} + (l_1 - l)\Delta + T_k\right) \quad \text{(B-4)}$$

where $c^{(k)}_{m_d} = d^{(k)}_{i_1,m_i}$. We denote the time shift $(l_1-l)\Delta+T_k$ in the argument of the function $R(\cdot)$ on the right side of eq. (B-4) by $\tau_{l_1,l,k}$, and model $\tau_{l_1,l,k}$ as [58]

$$\tau_{l_1,l,k} = (l_1 - l)\Delta + \tau_k = m_k T_{\mathrm{f}} + a_k \quad \text{(B-5)}$$

where m_k is the value of the time shift of the *k*th user rounded to the nearest frame time, and a_k is the fractional part in the rounding process, which is uniformly distributed in $[-\frac{T_{\mathrm{f}}}{2}, \frac{T_{\mathrm{f}}}{2})$. Thus, the argument of the function $R(\cdot)$ in (B-4) can be rewritten as $(m_d + m_k - m)T_{\mathrm{f}} + c^{(k)}_{\mathrm{TH},m_1} T_{\mathrm{c}} + a_k$. Since the autocorrelation function $R(t)$ is non-zero for $t \in [-\tau_{\mathrm{p}}, \tau_{\mathrm{p}})$, and the assumption $N_h T_c < T_f/2 - 2\tau_{\mathrm{p}}$ is adopted, there is only one non-zero term in the summation on the right side of eq. (B-4), where the frame index m_d satisfies the condition $m_d + m_k - m = 0$. Therefore, eq. (B-4) can be rewritten as

$$I^{(k)}_{l_1,l,m} = \alpha^{(k)}_{l_1}(2c^{(k)}_{m-m_k} - 1) R\left(c^{(k)}_{\mathrm{TH},m_1} T_{\mathrm{c}} + a_k\right). \quad \text{(B-6)}$$

Substituting eq. (B-6) into (B-1), I_m can be rewritten as

$$I_m = \sum_{l=0}^{L_{\mathrm{f}}-1} \alpha^{(1)}_l \sum_{k=2}^{N_{\mathrm{u}}} \sqrt{E^{(k)}_{\mathrm{c}}} \sum_{l_1=0}^{L_{\mathrm{t}}-1} \alpha^{(k)}_{l_1}(2c^{(k)}_{m-m_k} - 1) R\left(c^{(k)}_{\mathrm{TH},m_1} T_{\mathrm{c}} + a_k\right). \quad \text{(B-7)}$$

Assuming that the interference originating from different users and different paths are independent, we have

$$\begin{aligned}
&\mathbb{E}\left(I_m{}^2 \middle| \left\{\alpha^{(1)}_l\right\}_{l=0}^{L_{\mathrm{f}}-1}, \left\{a_k, C^{(k)}_{\mathrm{TH}}\right\}_{k=2}^{N_{\mathrm{u}}}\right) \\
&\quad = \sum_{l=0}^{L_{\mathrm{f}}-1} \left(\alpha^{(1)}_l\right)^2 \sum_{k=2}^{N_{\mathrm{u}}} E^{(k)}_{\mathrm{c}} \sum_{l_1=0}^{L_{\mathrm{t}}-1} \mathbb{E}\left(\left(\alpha^{(k)}_{l_1}\right)^2\right) R^2\left(c^{(k)}_{\mathrm{TH},m_1} T_{\mathrm{c}} + a_k\right). \quad \text{(B-8)}
\end{aligned}$$

Note that $c_{\mathrm{TH},m_1}^{(k)}$ assumes values in $\{0, \cdots, N_{\mathrm{h}} - 1\}$ with equal probability, and a_k is uniformly distributed in $[-T_{\mathrm{f}}/2, T_{\mathrm{f}}/2)$. Therefore, these RVs can be averaged out by following a similar procedure as given in Appendix A. Moreover, since we normalize the power dispersion profile of the channel, i.e., $\sum_{l=0}^{L_{\mathrm{t}}-1} \mathbb{E}\left(\alpha_l^{(k)}\right)^2 = 1$ for the analysis in Chapter 5 (c.f. Section 5.1), eq. (B-8) can be rewritten as eq. (5.6a).